STRUCTURAL AND FUNCTIONAL CHARACTERIZATION OF CHAPERONES IN FE-S CLUSTER BIOGENESIS AND REGULATION

Puglisi, Rita

Awarding institution:
King's College London

STRUCTURAL AND FUNCTIONAL CHARACTERIZATION OF CHAPERONES IN FE-S CLUSTER BIOGENESIS AND REGULATION

Rita Puglisi

Doctor of Philosophy

2017

"Human beings would not even begin to search for something of which they knew nothing or for something which they thought was wholly beyond them. Only the sense that they can arrive at an answer leads them to take the first step. This is what normally happens in scientific research. When scientists, following their intuition, set out in search of the logical and verifiable explanation of a phenomenon, they are confident from the first that they will find an answer, and they do not give up in the face of setbacks. They do not judge their original intuition useless simply because they have not reached their goal; rightly enough they will say that they have not yet found a satisfactory answer. The same must be equally true of the search for truth when it comes to the ultimate questions.

The search for truth, even when it concerns a finite reality of the world or of man, is never-ending, but always points beyond to something higher than the immediate object of study, to the questions which give access to Mystery" (JP II, Fides et Ratio)

ABSTRACT

Dysfunctions in Fe-S protein biogenesis and mitochondrial iron accumulation in heart and neurones are part of the phenotype of a genetic neurodegenerative disease called Friedreich's ataxia. This pathology is caused by the deficiency of a mitochondrial protein, frataxin, highly conserved throughout species and currently thought to be a regulator of Fe-S cluster biosynthesis. The study of the mechanism of Fe-S cluster assembly in mitochondria is important to provide insights and valuable information potentially relevant for the study of iron-storage diseases. The biogenesis of iron sulfur clusters involves a complex molecular machine with macromolecular structures containing multiple subunits with specific functions. The high level of conservation of the components suggests the bacterial system as excellent model because of its inherent lower complexity. *Isc* is one of the operons that encodes proteins responsible for Fe-S cluster biogenesis in bacteria, including the desulfurase IscS, the scaffold protein IscU on which the Fe-S cluster is assembled, the two chaperones HscA and HscB, the trascription regulator IscR, a ferredoxin and two other proteins called IscA and YfhJ, whose role is still unclear. The function of the chaperones HscA and HscB is thought to assist the transfer of the cluster from the scaffold protein to the final acceptors.

The main objective of this project was to get new evidence to understand the functions of the chaperones and the mechanisms by which they are involved in Fe-S cluster biogenesis and regulation through the application of structural biology and biochemistry. In particular, I focused on the structural and functional characterization of co-chaperone HscB and the analysis of its interactions with other members of the machinery through NMR and other biophysical techniques. My main findings are that HscB has an unprecedently reported interaction with IscS and that this interaction slows down cluster formation explaining a large plethora of evidence.

These findings provide an entirely new perspective to the comprehension of the role of HscB and propose this protein as partner of central components of the Isc machine.

TABLE OF CONTENTS

TABLE OF FIGURES AND TABLES

TABLE OF BOXES

ABBREVIATIONS

This is a list of the useful abbreviations I used in my thesis:

Aco2	Aconitase2
ATP/ADP	Adenosine triphosphate/Adenosine diphosphate
BMRD	Biological Magnetic Resonance Database
BS^3	Bis[sulfosuccinimidyl]suberate
CD	Circular Dichroism
DMA	Dimethyl adipimidate
DP	Differential power
DTT	Dithiothreitol
EDTA	Ethylenediaminetetraacetic acid
FdX	Ferredoxin
FID	Free Induction Decay,
FPLC	Fast Protein Liquid Chromatography
FRDA	Friedreich Ataxia
GST	Glutathione S-Transferase
HADDOCK	High Ambiguity Driven biomolecular DOCKing
HSQC	Heteronuclear Single Quantum Correlation
IPTG	Isopropyl β-D-1-thiogalactopyranoside
ISC	Iron Sulfur Cluster
ITC	Isothermal Titration Calorimetry
LB	Luria-Bertani medium
LED	Light-emitting diode
MESG	2-amino-6-mercapto-7-methylpurine riboside
MST	MicroScale Thermophoresis
NHS	N-hydroxysuccinimide
Ni-NTA	Ni-nitrilotriacetic acid
NMR	Nuclear Magnetic Resonance

OD	Optical Density
PBS	Phosphate-buffered saline
PCR	Polymerase Chain Reaction
PDB	Protein Data Bank
PLP	Pyridoxal phosphate
PNP	Purine Nucleoside Phosphorylase
RF	Radio Frequency
ROS	Reactive Oxygen Species
SDS PAGE	Sodium Dodecyl Sulfate Polyacrylamide Gel Electrophoresis
SEC	Size Exclusion Chromatography
TCEP	Tris(2-carboxyethyl)phosphine
TEV	Tobacco Etch Virus
Tris	Tris(hydroxymethyl)aminomethane
TROSY	Transverse Relaxation Optimized SpectroscopY

AKNOWLEDGEMENTS

I would like to thank all of those who have helped in the realisation of this work.

First of all to my supervisor Prof. Annalisa Pastore. Thank you not only for the scientific contribution, for sharing your knowledge with me and for the financial contribution, but even more for the encouragement, the help, the guidance and the friendship.

Thanks to Dr. Steve Martin for the insights and for giving me access to the biophysics facilities of the MRC institute.

In particular I'm grateful to Salvatore Adinolfi for the support in science and in developing my confidence and self-belief.

For the technical support, I would like to thank Laura Masino, Joeff Kelly, Beppe Nicastro and Cesira De Chiara.

A special thank to Robert Yan and Alessandro Sicorello for the stimulating discussions.

I'm grateful to Caterina Alfano, Domenico Sanfelice, Tommaso Vannocci, Pierandrea Temussi, Angela Corvino, Serena Faggiano, Matija Popovic, Masooma Rasheed, Elsa Zacco, Giulia Milordini, Havva Yalinca and all the people of the Pastore's group because it is not only a source of good advice and collaboration, but overall of friendship.

My apologies to the others who I have not mentioned by name, I am indebted to you for the many ways you helped me.

Finally, I would especially like to thank my family and all my friends for the constant support. Without their love nothing of this would have been possible.

INTRODUCTION

Iron is an essential element for life. The survival of prokaryotic and eukaryotic organisms depends on it and both the lack and an excess of free iron lead the cell to death. Free iron is toxic and at the same time a deficiency of iron is deleterious to cells because it is required as a constituent of functional groups. (Hentze, Muckenthaler et al. 2004). A tight regulation of iron metabolism is thus demanded. Determining its homeostasis and how its cellular forms are regulated in amount and allocation is of particular importance for understanding how these mechanisms can be at time so compromised to cause pathological conditions, such as metabolic and neurodegenerative diseases.

Important prosthetic groups containing iron are Fe-S clusters which are present both in prokaryotes and eukaryotes. They are formed under the control of complex machineries highly conserved through species (Cowan 2009). These machines were discovered several years ago and little is still known about how the Fe-S cluster biosynthesis works and how its malfunctioning is related to disease.

In bacteria, the genes responsible for cluster biogenesis are mostly grouped in three distinct operons (named *nif*, *suf* and *isc*) (Jacobson, Cash et al. 1989, Lill and Kispal 2000, Py, Moreau et al. 2011). The *isc* operon contains genes encoding for eight proteins each of them with a close orthologue in eukaryotes (Tokumoto and Takahashi 2001). These proteins include a desulfurase, IscS, which is able to convert cysteine into alanine and liberate sulfur, a scaffold protein, IscU, on which the cluster is assembled, the two chaperones HscA and HscB, though to assist the trasfer of the cluster to an apo-acceptor, a ferredoxin and three other proteins for which little is known. Even if some reports attempeted to provide information on the role of specific components, a clear picture of how the whole machine works is still missing.

The study of the simpler bacterial model system may help to understand also how iron is correlated to human diseases. Some imbalance or damage of the Isc components in human may cause serious neurodegenerative diseases such as the hereditary Friedreich's ataxia (Puccio and Koenig 2000). This pathology is caused by the deficiency of a mitochondrial protein, frataxin, extremely conserved throughout species. It takes part in the Fe-S cluster machinery and currently it is thought to act as a regulator of the enzymatic activity of the desulfurase IscS even though, in bacteria, it is not encoded by the isc operon (Pandolfo and Pastore 2009).

An intriguing issue is that of better understanding the mechanism of Fe-S cluster biosynthesis. Adding a new tessera to this complicated puzzle was the main purpose of my PhD project.

I first dissected the machinery by investigating on the simpler bacterial system with a biochemical approach. I studied the kinetic of cluster assembly *in vitro* in the presence of the desulfurase IscS and scaffold IscU and observing the effect that chaperones HscA and HscB have on it.

However, the comprehension of the mechanism of Fe-S cluster formation could be achieved only with the structurally and functionally characterization of the components of the machinery and the study of their mutual interactions. I started by exploring the role of the co-chaperone HscB. With the help of several different biochemical assays and biophysical techniques (as pull-down assays, size exclusion chromatography, crosslinking, NMR relaxation measurements, ITC and MST) I documented a previously undetected weak interaction between the chaperone HscB and the desulfurase IscS, one of the two main players of the machine. The surfaces of interaction were then obtained using HSQC and cross saturation NMR experiments and validated with the mutagenesis of residues involved.

In my thesis, I present the work I carried out during my PhD course at King's College London. It is divided in chapters which describe biochemical, biophysical and structural approaches depending on the studies performed.

During my studies, I had the possibility to use several different techniques and to learn about their employability in the investigation of molecular basis of neurodegenerative diseases (Prischi and Pastore 2016). For each of them I explain the main principles and characteristics in boxes.

In the conclusive chapter I show the reasons why the existence of a complex between HscB and IscS adds a completely new perspective to the comprehension of the Isc machinery and HscB can be supposed to be one of the main players in the mechanism of Fe-S clusters formation.

All these finding have also been described in a paper published in Frontiers in Molecualar Biosciences in September 2016 (Puglisi, Yan et al. 2016).

1. IRON-SULFUR CLUSTERS

Iron is ubiquitous in the environment and in biology. Eukaryotic cells (and most prokaryotic organisms) require iron for survival and proliferation, as a constituent of hemoproteins, iron-sulfur (Fe-S) proteins and other proteins that use iron in functional groups to carry out essential housekeeping functions for cellular metabolism. Cellular iron deficiency arrests cell growth and leads to cell death (Hentze, Muckenthaler et al. 2004).

The biological importance of iron is largely attributable to its chemical properties: it is involved in one-electron oxidation-reduction reactions with transition between its ferric and ferrous states. However, the same chemical property explains why an excess of free and reactive iron is toxic. In the cytoplasm, a significant fraction of iron is reduced and can participate in “Fenton-type” redox chemistry. Ferrous iron reacts with hydrogen peroxide (H_2O_2) or lipid peroxides to generate ferric iron, OH^-, and the highly reactive hydroxyl radical (HO•) or lipid radicals such as LO• and LOO•. Ferric ion is then reduced back to Fe^{2+} by another molecule of hydrogen peroxide, forming a hydroperoxyl radical (HOO•) and proton. Iron behaves thus as a catalyst, meaning that very low quantities of free iron can be toxic. Radicals produced damage lipid membranes, proteins, and nucleic acids (Hentze, Muckenthaler et al. 2004, Jang and Imlay 2010).

$$Fe^{2+} + H_2O_2 \rightarrow Fe^{3+} + OH^- + HO\cdot$$

$$Fe^{3+} + H_2O_2 \rightarrow Fe^{2+} + HOO\cdot + H^+$$

Since both cellular iron overload and iron deficiency cause cell death, the levels of reactive iron must be carefully controlled and limited (Hentze, Muckenthaler et al. 2004).

Biological iron–sulfur (Fe-S) clusters were identified about 50 years ago as acid-labile prosthetic groups contained within a class of electron carrier proteins called ferredoxins (Frazzon and Dean 2003). They are widely distributed in nature and can

be found in anaerobic, aerobic and photosynthetic bacteria, fungi, plants and mammals (Cowan 2009). Most known Fe-S proteins of a eukaryotic cell are located in the mitochondria, but some also exist outside of them. Finally, at least one Fe-S protein, the endonuclease Ntg2p, has been localized to the cell nucleus (Lill and Kispal 2000).

Since their discovery, Fe-S clusters have been considered ideal agents of electron transfer because of their versatile electronic properties (Beinert, Holm et al. 1997). Many different proteins that contain these clusters have been described with different functionality (Johnson 1998).

Fe-S clusters are now known to have roles in controlling protein structure and in enzyme active sites (see for instance aconitase), to act as environmental sensors (as in FNR), to serve as modulators of gene regulation (IRP and SoxR), and to participate in radical generation (Beinert, Holm et al. 1997). Such functional diversity almost reflects the chemical versatility of iron and sulfur, leading to the suggestion that prebiotic iron-sulfur complexes could have played an important role in the emergence of life on earth. The importance of Fe-S clusters is furthermore underlined by their involvement in three major processes required to sustain life on earth: nitrogen fixation, photosynthesis and respiration (Frazzon and Dean 2003).

1.1 Structure and function

The most common Fe-S clusters found in nature are [2Fe–2S] and [4Fe–4S] clusters and these are usually coordinated to proteins by cysteine ligands. However, biological Fe-S clusters of higher nuclearity have been discovered, and not all are attached to their protein partners through cysteines. Despite the apparent diversity in the overall structure, reactivity, electronic properties and polypeptide environments, polynuclear Fe-S clusters are all constructed from [2Fe–2S] rhombs (Frazzon and Dean 2003). For example two [2Fe-2S] units may be converted to the cubane [4Fe-4S]. Cuboidal cluster [3Fe-4S] is considerably less stable. It has been assembled from [4Fe-4S] via loss of one iron atom and it could be converted to

linear [2Fe-2S] or cubane [4Fe-4S] (Beinert, Holm et al. 1997). In addition, not all Fe-S proteins contain clusters with Fe as the only metal: the nitrogenase MoFe protein for example, contains a cluster which has a [7Fe–9S–Mo] core (Frazzon and Dean 2003).

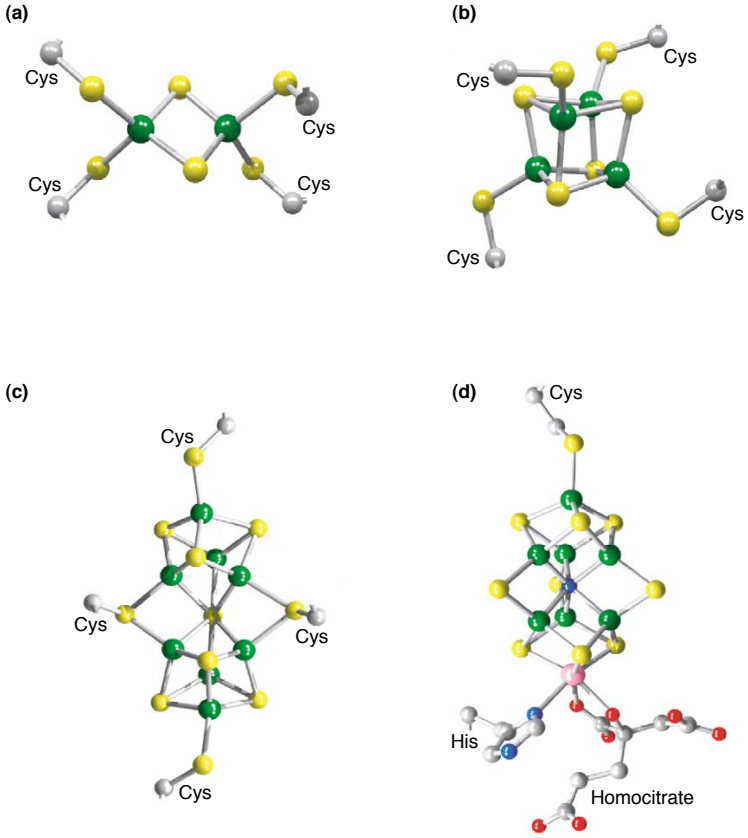

Figure 1.1 Various [Fe-S] clusters found in iron–sulfur proteins. The most common **(a)** [2Fe–2S] and **(b)** [4Fe–4S] clusters are coordinated to their protein partners by cysteine ligands. Iron–sulfur clusters of higher nuclearity such as **(c)** the [8Fe–7S] cluster and **(d)** the [Mo–7Fe–9S] FeMo-cofactor from nitrogenase represent just some of the intricate possibilities of more complex biological iron–sulfur clusters. (Iron is represented in green, sulfur in yellow and molybdenum in magenta) (Frazzon and Dean 2003).

Because of their structural and chemical versatility, Fe-S clusters present an extreme functional flexibility. The electronic structures of Fe-S clusters have been studied by a variety of spectroscopic techniques (Glaser, Hedman et al. 2000) showing that they are ideal agents for electron storage and transfer, signaling and regulation, via their tunable sensitivity to various oxidants or reductants. Fe-S

clusters are well suited to supply single electrons, as required in homolytic reactions (Beinert and Kiley 1999), but they can also act as sensors of molecules in their immediate environment (Jervis, Crack et al. 2009). Fe-S clusters are sensitive to cellular oxidants and *in vitro* they may also respond to strong reducing agents or ligands for iron that are stronger than their sulfur ligands. Oxidation of Fe-S clusters may cause cluster rearrangement or total disassembly (Crack, Green et al. 2012).

A first example is fumarate and nitrate reductase FNR, an *E. coli* regulator controlling the synthesis of proteins required for anaerobic respiration with nitrate, fumarate, trimethylamine oxide and similar electron acceptors replacing oxygen. FNR is functional only in its dimeric form, stabilized by [4Fe-4S] cluster. Binding DNA with high affinity, it controls gene expression. The [4Fe-4S] cluster is very sensitive to oxygen, which rapidly converts it to the more air-stable [2Fe-2S] form making FNR inactive and monomeric (Johnson 1998, Beinert and Kiley 1999, Zhang, Crack et al. 2012).

Another example is SoxR that contains [2Fe-2S] cluster and is activated on exposure of cells specifically to superoxide O_2^- and NO, but not to H_2O_2 or HO•. In enteric bacteria active SoxR activates transcription of only a single gene, *soxs*, leading to the formation of the SoxS protein which regulates expression of a number of genes whose products function in the defense against O_2^- and NO (Beinert and Kiley 1999).

Fe-S clusters can serve also as active sites of enzymes as, for instance, in mitochondrial aconitase involved in the tricarboxylic acid cycle and able to convert citrate to isocitrate (Beinert, Kennedy et al. 1996). A [4Fe-4S] cluster is bound to the enzyme through cysteine groups. Three iron are involved in the binding and the fourth serves as a Lewis acid in catalyzing the transformation of the substrate (Beinert 2000). The cluster destruction, due for example to deleterious free radicals, or (re)synthesis will determine the activity of aconitase and hence control the citric acid cycle (Beinert and Kiley 1999). Cytosolic aconitase, a close relative of the mithochondrial enzyme, can switch to the IRP1 form by loosing the Fe-S cluster

binding. In iron-deficient cells, the Fe-S devoid form (IRP1) regulates the expression of iron metabolism genes by the binding to iron-responsive elements (IRE), specific mRNA targets found in the mRNAs of ferritin, the transferritin receptor and other iron metabolism transcripts. (Rouault 2006).

1.2 Systems of Fe-S cluster biosynthesis

Fe-S clusters can be spontaneously assembled *in vitro* from the required components and under the proper conditions: the presence of iron and a source of sulfur such as lithium sulfide (Bonomi, Iametti et al. 2005). However, in both prokaryotes and in eukaryotes, enzymes have been identified that use pyridoxal phosphate for desulfurase activity, transforming cysteine into alanine and elemental sulfur. Similarly, specific carrier-proteins for Fe are likely to be used. Thus, the formation of clusters is driven by the availability of iron and four cysteines: one to provide sulfur for the synthesis and three others to stabilize the Fe-S cluster created. When only two cysteines are available per peptide, the peptide will dimerize to make a [4Fe-4S] cluster (Beinert 2000).

Investigation on Fe-S cluster maturation in bacteria has led to the identification of two operons termed *nif* (nitrogen fixation) and *isc* (iron–sulfur cluster assembly). The *nif* operon encodes proteins that execute specific functions in the assembly of nitrogenase, a complex metalloenzyme that catalyses the fixation of nitrogen. The *isc* operon encodes proteins necessary for the maturation of bacterial Fe-S proteins. Many of the gene products encoded by the *nif* and *isc* operons have sequence similarity to the eukaryotic components of Fe-S protein maturation (Lill and Kispal 2000).

In addition to the Isc, in *E. coli* it was identified another system responsible for the Fe-S cluster biosynthesis: Suf. Although Isc and Suf are systems that rely on to the same activities (i.e a cysteine desulfurase, a scaffold protein, an ATPase and a Fe-S acceptor protein), genetic and biochemical characterizations revealed differences in their ability to function under stress conditions (Tokumoto, Kitamura et al. 2004).

In fact they are considered the house-keeping and stress-dedicated systems, respectively. Both operons are co-regulated by the same transcriptor factor, IscR, able to bind the cluster. Apo-IscR activates the expression of the *suf* genes whereas the holo-form represses the expression of the *isc* operon. It was also pointed out that the Isc system is inactivated by reactive oxygen species (ROS) since a solvent-exposed Fe-S cluster, built on the scaffold IscU, can be easily oxidized by ROS. On the other hand, Suf might have evolved to be efficient when Fe and S are present in limited amount. As a result of that, Isc is the primary system used in exponentially growing cells, whereas Suf is used under oxidative stress and iron starvation conditions (Outten, Djaman et al. 2004, Py, Moreau et al. 2011).

In eukaryotes an Isu system has been discovered in mitochondria and it is able to mediate the Fe-S cluster assembly and to transfer it to apo-acceptors. Isu and Isc proteins are very similar in sequence and function (Cowan 2009). A parallel cytoplasmic Fe-S cluster machinery, CIA, is responsible for the maturation of Fe-S proteins autside mitochondria (Stehling and Lill 2013).

1.3 Isc system

Understanding the functions of Isc proteins in prokaryotes is important to provide insights into Fe-S cluster assembly in mitochondria, with potential relevance in iron-storage diseases and the control of cellular iron uptake.

The *isc* operon in the bacterium *E. coli* encodes eight proteins: IscR, IscS, IscU, IscA, HscB, HscA, Fdx and YfhJ (Tokumoto and Takahashi 2001).

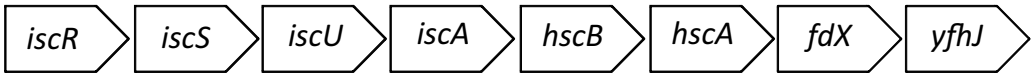

Figure 1.2 The *isc* operon. In *E. coli* the *Isc* operon encodes the proteins involved in the Fe-S cluster biogenesis.

To elucidate their function, a systematic mutational analysis of the genes has been

undertaken by Tokumoto et al. Mutants with inactivated *iscR* or *orf3* showed no differences from wild-type cells while inactivation of the *iscS* gene elicited the most drastic alteration. Strains with mutations in the *iscU*, *hscB*, *hscA*, and *fdx* genes exhibited conspicuous phenotypical consequences almost identical to one another. The effect of the inactivation of *iscA* was small but appreciable on Fe-S enzymes (Tokumoto and Takahashi 2001). Tokumoto et al. also demonstrated a network of protein-protein interactions among Isc proteins. They speculated that the Fe-S cluster assembly works with a sequential association and dissociation among them. Combinations of IscS and IscU, IscU and HscB, IscU and HscA and HscB and HscA were observed as well as interaction between IscS and FdX, IscS and IscR, IscA and HscA and HscA and FdX (Tokumoto, Nomura et al. 2002). IscS accommodates the binding of at least two more proteins involved in the Fe-S cluster biosynthesis: the Isc-belonging YfhJ (Pastore, Adinolfi et al. 2006) and frataxin CyaY (Adinolfi, Iannuzzi et al. 2009). Figure 1.3 shows all the interactions currently evidenced between the Isc components.

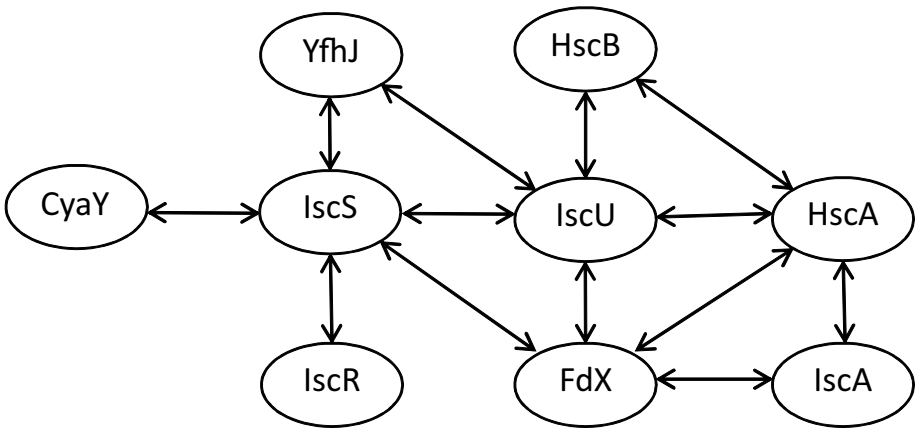

Figure 1.3 Isc Interactome. Isc proteins map a complex network of interactions. Each arrow evidences a proved direct molecular binding between two proteins.

1.3.1 IscR

IscR contains a [2Fe-2S] cluster and has a function as a regulator. Schwartz et al. discovered that *iscR* is co-transcribed with *iscSUA* and transcription of *iscRSUA*

originates from a single promoter upstream of *iscR* that is repressed by IscR itself (Schwartz, Giel et al. 2001). When Fe-S cluster assembly becomes rate limiting, levels of [2Fe-2S]-IscR decrease as a result of a diminution in its rate of synthesis, and repression of *iscRSUA* is relieved. The resulting increase in the Isc assembly proteins subsequently leads to an increase in the rate of Fe-S cluster formation, causing levels of [2Fe-2S]-IscR to rise, thus resetting repression of the *isc* operon (Schwartz, Giel et al. 2001).

The Isc proteins are able to distinguish between IscR and other apo-protein targets and IscR acquires a Fe-S cluster once the cellular demand for Fe-S cluster biogenesis is satisfied. IscR could be differentiated from other apo-proteins because the cluster is bound with an atypical ligation scheme of three cysteines and one histidine $(Cys)_3(His)_1$. The atypical amino acid ligand could make IscR a poor substrate for the Isc proteins and thus able to sense the cellular demand for Fe-S cluster biogenesis (Fleischhacker, Stubna et al. 2012). Giel et al. reported that the *isc* operon was more repressed under anaerobic conditions rather than under aerobic conditions (Giel, Nesbit et al. 2013). Fe-S clusters are sensitive to O_2 (Imlay 2006) so it is likely that Fe-S clusters are continuously damaged or destroyed during aerobic growth. As a result, levels of substrate proteins that need Fe-S biogenesis or repair increase. The higher rate of cluster turnover in aerobic condition leads to decrease *isc* repression. It suggests that there may be more competition between IscR and substrate proteins for the Isc machinery when O_2 is present. In contrast, under anaerobic conditions, the Isc machinery appears to satisfy the Fe-S demand more efficiently, thus less competition among substrate proteins is observed and an increased repression of *isc* is due to increased of [2Fe–2S]-IscR (Giel, Nesbit et al. 2013).

These mechanisms would provide a global regulation to ensure that Fe-S clusters are synthesized when there is an increased demand.

1.3.2 IscS

IscS is an extremely conserved protein that forms an obligatory dimer composed of two identical 45 kDa subunits. It is a pyridoxal phosphate (PLP) binding enzyme and it catalyzes the desulfurization of L-cysteine to yield L-alanine and generates a sulfur atom that is subsequently transferred to IscU (Urbina, Silberg et al. 2001) or other protein, for example ThiS, which plays an essential role with ThiI in the synthesis of thiamine (Kambampati and Lauhon 2000, Lauhon and Kambampati 2000). In addition to the covalently bound PLP group, the active site of IscS contains a catalytic cysteine (Cys328) hosted in a flexible and conserved loop (residues 323-335) and a conserved lysine (Lys206). During catalytic activity, the loop is thought to move from the active site to the scaffold protein to deliver the persulfide (di Maio, Chandramouli et al. 2017). Similarly to what was suggested for NIFS (the *A. vinelandii* homologue) mechanism, IscS catalyzes the formation of an external aldimine Shiff base between the amino group of the substrate and PLP. The cysteinyl thiolate anion of Cys328 generated in the active site makes a nucleophilic attack on the sulfur of the cysteine-PLP adduct and finally the cysteine persulfide and an enamine derivative of alanine are formed (Zheng, White et al. 1994, Fujii, Maeda et al. 2000).

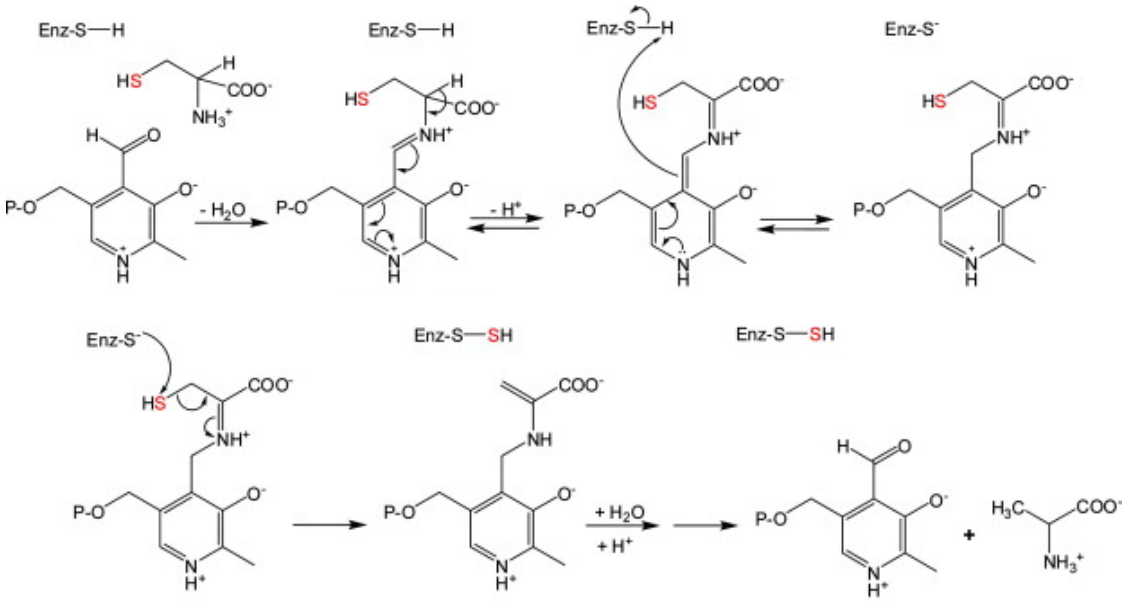

Figure 1.4 Proposed mechanism of desulfuration reaction.

Increasing evidences revealed an important role of IscS in several biological pathways such as the biosyntheses of Fe-S clusters, thiamine, thionucleosides in tRNA, biotin, lipoic acid, molybdopterin, and NAD. The enzyme is also proposed to be involved in cellular iron homeostasis and in the biosynthesis of selenoproteins (Mihara and Esaki 2002).

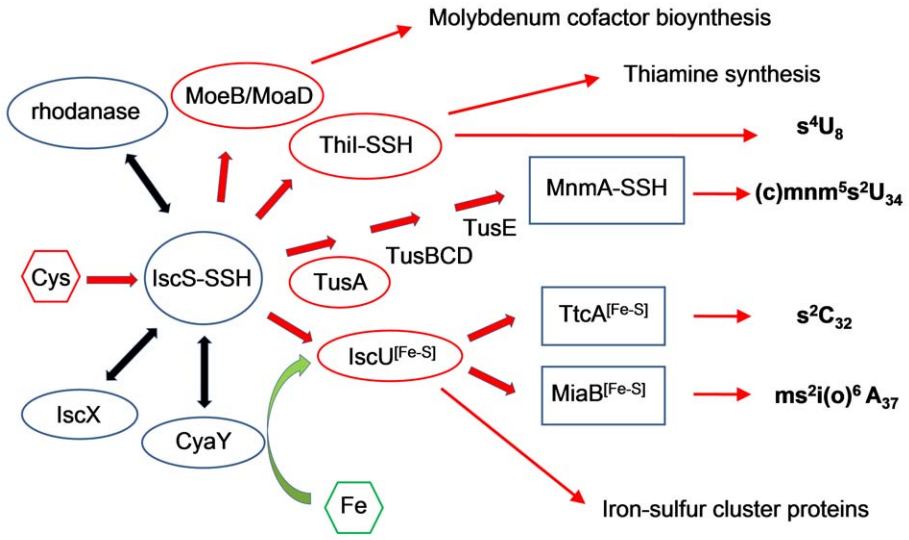

Figure 1.5 Network of protein-protein interactions involving IscS. IscS initiates intracellular sulfur trafficking, delivering the sulfur to several sulfur-accepting proteins such as IscU, ThiI, TusA, and MoaD/MoeB that commit the sulfur to different metabolic pathways. IscU is the primary scaffold for assembly of Fe-S clusters. Frataxin/CyaY has been postulated as a Fe chaperone, a Fe donor for Fe-S cluster assembly, or a regulator of Fe-S cluster formation (Shi, Proteau et al. 2010).

1.3.3 IscU

IscU has been widely conserved throughout evolution and is considered to be one of the most conserved protein sequences in nature (Hwang, Dempsey et al. 1996). It contains three conserved cysteine residues (Cys37, Cys63, and Cys106) (Zheng, Cash et al. 1998), a conserved histidine residue (His205) and a conserved 'LPPVK' motif (Johnson, Dean et al. 2005, Shimomura, Kamikubo et al. 2007) and it has the ability to accommodate both [2Fe-2S] and [4Fe-4S] clusters (Agar, Krebs et al. 2000).

IscU is the scaffold protein on which Fe-S cluster are assembled and sustained until

the transfer to targed apo-proteins. To accept a sulfur atom IscU interacts with IscS, but the iron donor is still unknown, even if frataxin CyaY was suggested for this role. *In vitro* studies on *A. vinelandii* IscU showed that [2Fe-2S] clusters are assembled first and that reductive coupling between two of them produces one [4Fe-4S] cluster that can be then transferred (Agar, Krebs et al. 2000).

Whereas IscU homologues generally have been described as dimers (as, for example, the IscU from *Thermatoga maritima,* an evolutionarily ancient hyperthermophilic bacterium) (Bertini, Cowan et al. 2003, Gerber, Muhlenhoff et al. 2003) monomeric forms were identified for the human protein (Gerber, Muhlenhoff et al. 2003) and for *Haemophilus influenzae* and *E. coli* IscUs (Adinolfi, Rizzo et al. 2004). Adinolfi et al. showed that *E. coli* IscU is well folded with a high melting temperature and reversibility of the thermal unfolding curve (Adinolfi, Rizzo et al. 2004).

IscU exists as two slowly interconverting species: a conformation (S-state) largely structured and the other (D-state) partially dynamically disordered (Kim, Fuzery et al. 2009). In both crystal and NMR structures of IscU, a zinc metal ion is found in the site which hosts the cluster coordinated by three conserved cysteine residues and one conserved aspartate. (Ramelot, Cort et al. 2004, Liu, Oganesyan et al. 2005, Kornhaber, Snyder et al. 2006, Bonomi, Iametti et al. 2011). This cation is thought to stabilize the folded form (Markley, Kim et al. 2013). For this reason, Zn^{2+} is often introduced in the culture medium to facilitate IscU expression in the stably folded form (Prischi, Pastore et al. 2010). The presence of zinc does not alter the interaction with the enzyme IscS, that is probably the most important of the natural partners of cluster-free IscU, and it increases the Fe-S cluster formation by preventing oxidation of the cysteines until the cluster is in place and this ion can readily be expelled (Iannuzzi, Adrover et al. 2014).

1.3.4 IscA

Although IscA orthologues maintain a high degree of evolutionary conservation, its

role is yet unknown. Bilder et al. solved and refined the 2.3 Å resolution crystal structure of *E. coli* IscA, a polipeptide of 107 residues with a novel fold in which mixed β-sheets form a compact α-β sandwich domain (Bilder, Ding et al. 2004). Three cysteine residues (Cys35, Cys99, Cys101) in IscA are implicated in Fe-S cluster binding (Bilder, Ding et al. 2004) and it has been proposed to function as an alternative scaffold protein for assembling and transfer of Fe-S clusters (Krebs, Agar et al. 2001, Bonomi, Iametti et al. 2005). Holo-IscA and eukaryotic homologues of IscA have been shown to complex and transfer [2Fe-2S] clusters to the apo-form of *E. coli* ferredoxin, another protein synthesized from the *isc* operon (Jensen and Culotta 2000, Ollagnier-de-Choudens, Mattioli et al. 2001). IscA also has high affinity for iron and it may serve as an iron-delivery protein (Ding and Clark 2004, Ding, Clark et al. 2004).

1.3.5 HscA and HscB

The *hscA* and *hscB* genes of *Escherichia coli* encode novel chaperone and co-chaperone proteins, designated HscA and HscB, respectively. They represent a molecular system similar to the prokaryotic DnaK/DndJ and the eukaryotic hsp70/hsp40 systems (Vickery, Silberg et al. 1997) where chaperone DnaK is an enzyme with a weak ATPase activity stimulated by its interaction with another co-chaperone, DnaJ (Vickery, Silberg et al. 1997).

HscB structure consists in 8 helices and is divided in two domains: the C-terminal domain (95 residues) is involved in binding the substrate, IscU, whereas the N-terminal J-domain (76 residues) is responsible for the interaction with HscA (Walsh, Bursac et al. 2004).

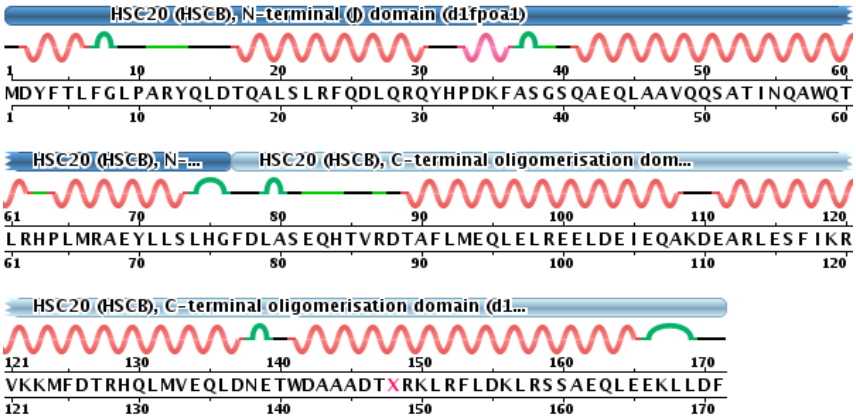

Figure 1.6 Sequence chain view of HscB as reported in PDB (ID entry 1FPO)**.** Red curve indicates an alpha helix, pink curves a 3/10-helix, green curve indicates a turn and light green line a bend.

Purified HscA exhibits a low intrinsic ATPase activity (~0.6 min^{-1} at 37°C and pH 7.5), and HscB was found to stimulate this activity up to 3.8-fold**.** To better understand the mechanism and regulation of HscA, Silberg and Vickery investigated the kinetics of ATP hydrolysis and proposed a model for the ATPase reaction cycle. HscA binds ATP in a two-step process in which HscA is converted from a high peptide affinity (R-state) to a low peptide affinity (T-state). The ATP hydrolysis is the rate limiting step and it seems likely to be subject to co-chaperone regulation (Silberg and Vickery 2000).

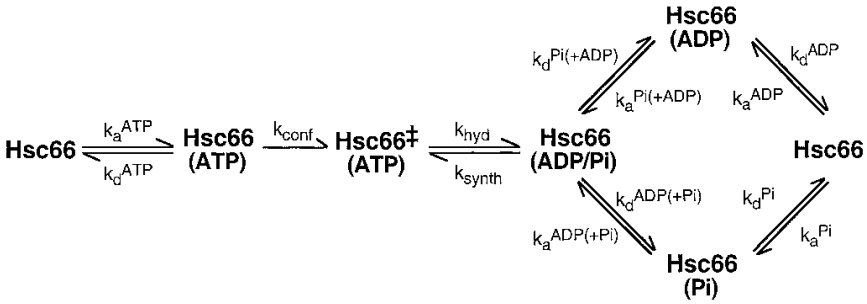

Figure 1.7 Kinetic scheme of the HscA ATPase reaction cycle. In the scheme HscA is indicated as Hsc66 and Hsc66‡ represents the T-state (Silberg and Vickery 2000).

HscA interacts with the scaffold protein IscU. The binding was shown to stimulate its ATPase activity (Hoff, Silberg et al. 2000) and ATP destabilizes HscA-IscU

complexes (Silberg, Hoff et al. 2001). HscA may assist in Fe-S cluster formation by maintaining IscU in a conformation suitable for cluster assembly; alternatively, HscA may facilitate the transfer of the cluster from holo-IscU to an acceptor apo-protein (Hoff, Silberg et al. 2000). IscU also directly interacts with HscB, and HscB may serve to control the association of IscU with HscA because in its presence, the affinity of IscU for HscA is increased >18-fold. HscB also has a synergistic effect on the IscU stimulation of the ATPase activity of HscA, increasing the rate >50-fold over that found at saturating levels of IscU alone (Hoff, Silberg et al. 2000). To better understand the mechanism by which HscB and IscU regulate HscA, Silberg et al. examined their binding to the different conformational states of HscA and their effects on the kinetics of the individual steps of the ATPase reaction cycle (Silberg, Tapley et al. 2004). Whereas IscU binds both ADP (R-state) and ATP (T-state) HscA complexes, HscB interacts only with an ATP-bound state. Both IscU and HscB modestly accelerate the rate-determining steps in the HscA reaction cycle, the hydrolysis of ATP. Furthermore, when present together an enhancement of HscA(ADP)-IscU complex formation is observed. Following the ADP/ATP exchange, IscU seems also to stimulate the HscA transition from the R to the T-state and thereby accelerates the rate at which the HscA-ATP is regenerated (Silberg, Tapley et al. 2004).

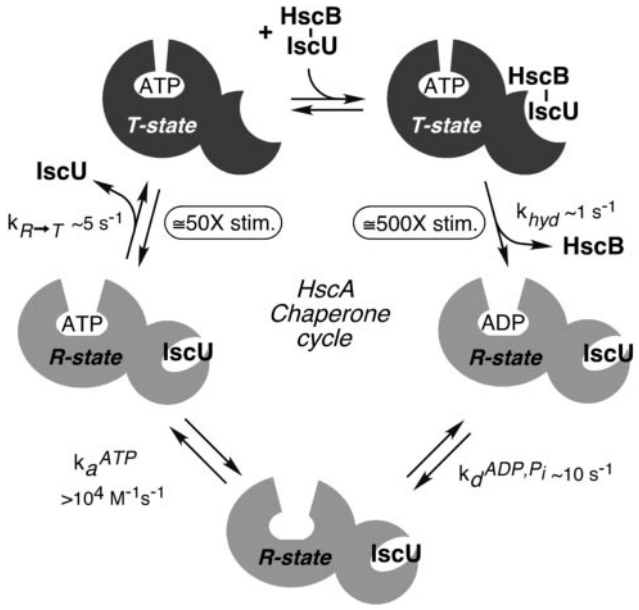

Figure 1.8 A model for the IscU binding cycle of HscA. Kinetic constants shown correspond to rates in the presence of IscU and HscB (Silberg, Tapley et al. 2004).

Kinetic studies of Fe-S cluster transfer from holo-IscU to apo-Fdx in the presence of *T. maritima* chaperone DnaK demonstrated an inhibitory effect on the rate of Fe-S cluster transfer from IscU (Wu, Mansy et al. 2005). In contrast with this result, Chandramouli et al. showed that HscA/HscB facilitate [2Fe-2S] cluster transfer *in vitro* from the holo-IscU scaffold protein to apo-Fdx and that cluster transfer involving IscU is an ATP-dependent process (Chandramouli and Johnson 2006). However, in the presence of the only HscB, the cluster assembled on IscU is transferred to apo-FdX at slower rate than those formed in the absence of HscB unless ATP and HscA are also present. (Bonomi, Iametti et al. 2008, Iametti, Barbiroli et al. 2015).

1.3.6 Ferredoxin (FdX)

E. coli isc ferredoxin contains a [2Fe-2S] centre and it is demonstrated that the cluster transfer from IscU to the apo-Fdx is a key step for its activation (Wu, Mansy et al. 2005). IscS binds Fdx with a mainly electrostatic mechanism that involves complementary surfaces of opposite charge. Fdx leaves the interaction of IscS with IscU unchanged, but it competes for the same binding site that accommodates

bacterial frataxin CyaY (Yan, Konarev et al. 2013) and at least two other proteins, YfhJ, which belongs to the Isc system, and TusA, a protein responsible of delivering sulfur for tRNA modification (Shi, Proteau et al. 2010). *In vivo* Fdx may carry out the role of the reducing agent required for accelerating reduction of S^0 to S^{2-} in the transfer step from the persulfide of IscS to the [2Fe-2S] cluster on IscU and regenerating the reaction (Yan, Adinolfi et al. 2015). As prove of that it was shown that the presence of Fdx is sufficient for the IscS enzymatic reaction to occur without the need of other reducing agents (Kim, Frederick et al. 2013).

1.3.7 YfhJ

The last *isc* operon gene encodes YfhJ (also called ORF3 or IscX) (Tokumoto and Takahashi 2001), a small, acidic protein of 66 residues. Very little is known about this protein and its role is still not clear. It is supposed to be not essential because it is exclusively present in prokaryotes. In solution YfhJ is stably folded in a compact globular domain (Pastore, Adinolfi et al. 2006) and crystal structure of YfhJ exhibits five α-helices organized in a helix-turn-helix motif typical of DNA-binding proteins, suggesting a function as a transcription regulator of the *isc* operon. However it is unlikely that YfhJ binds to DNA because the surface of YfhJ presents a negatively charged patch (Shimomura, Takahashi et al. 2005). *In vitro* experiments have shown an interaction between YfhJ and IscS (Tokumoto, Nomura et al. 2002) indicating that YfhJ is involved in the Isc function modulating this protein (Pastore, Adinolfi et al. 2006). YfhJ seems to be able to bind both Fe^{2+} and Fe^{3+} but with modest affinity since equimolar ratios of frataxin CyaY are able to compete partially with the binding. Furthermore the surface involved in binding IscS is the same as that implicated in iron binding and the binding affinity to IscS is modulated by the presence of iron cations. In addition, YfhJ and frataxin CyaY compete for the same site on IscS (Prischi, Konarev et al. 2010, Shi, Proteau et al. 2010, Kim, Bothe et al. 2014). This strongly suggests that YfhJ could be a molecular adaptor that mediates the interaction of IscS with a yet unidentified partner through an iron-mediated

mechanism (Pastore, Adinolfi et al. 2006).

1.4 Mechanism of Fe-S cluster assembly mediated by the Isc system

The Fe-S cluster biosynthesis is a complicated process that still needs to be elucidated. However it could be simplified in two steps: first the Fe-S cluster is assembled on IscU that acts as a scaffold protein, then the Fe-S cluster is transferred to a target apo-protein (Ayala-Castro, Saini et al. 2008).

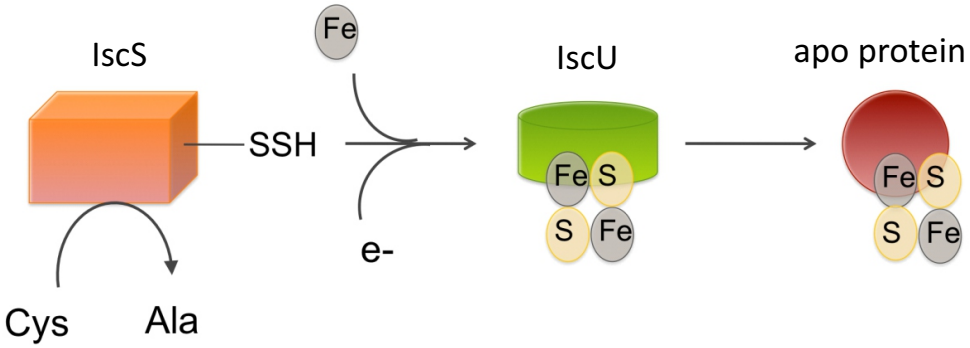

Figure 1.9 Fe-S cluster biosynthesis could be simplified in two steps: sulfur is liberated by the cysteine desulfurase IscS and donated to the scaffold protein IscU for nascent Fe-S cluster assembly. The Fe-S cluster is then transferred to a target apoprotein.

After IscS has catalyzed the desulfurization of L-cysteine to produce L-alanine and sulfur, the sulfur atom is transferred directly from IscS to IscU via the formation of an IscS-IscU covalent complex: a disulfide bond was found between Cys328 of IscS and Cys63 of IscU. The covalent bond between these two proteins is produced only in the presence of L-cysteine, the substrate for IscS. Since it is indispensable for IscS activation it was supposed that the target of IscU is IscS with sulfane sulfur derived from L-cysteine attached at Cys328 (Kato, Mihara et al. 2002). Once iron is bound, the release of persulfide sulfur (S^0) to the metal cluster as sulfide (S^{2-}) requires reduction. (Urbina, Silberg et al. 2001).

This process *in vitro* is facilitated by the non-physiological reducing agent DTT but it is known that FdX could be the molecule responsible for electron transfer in Fe-S

cluster biogenesis (Yan, Adinolfi et al. 2015). Curiously Markley et al. proposed that IscS binds preferentially to the disordered D-state of IscU. By selecting the D-state, IscS ensures that the cysteine residues of IscU are unligated by metals and available to react with the sulfur generated by the catalytic conversion. With cluster formation, IscU converts to the S-state, which has a lower affinity for IscS (Markley, Kim et al. 2013) but is selectively recognised by HscB (Kim, Fuzery et al. 2009).

Then the holo-IscU-HscB complex represents a target for HscA in its ATP-bound form. After the formation of HscA(ADP), the equilibrium between IscU conformations is shifted to the D-state ensuring release of the cluster and HscB (Kim, Tonelli et al. 2012). Chandramouli et al. studied the cluster transfer from IscU to target apo-ferredoxin mediated by HscA and HscB chaperones. Since ATP hydrolysis and the presence of HscB accelerate this process, they suggest that conformational changes accompanying the ATP (T-state) to ADP (R-state) transition in the HscA chaperone are required for catalysis. ATP binding to HscA leads to a tense (T) state with decreased substrate-binding affinity. HscB binds and escorts IscU to HscA and enhances HscA binding of IscU in the ATP-bound T-state, leading to a transient HscA-ATP-HscB-IscU complex which undergoes ATP hydrolysis and loss of HscB to yield an ADP-bound relaxed (R) state with increased affinity for IscU. The IscU substrate is subsequently released after ADP/ATP exchange and the R to T transition that occurs following ATP binding to HscA. They proposed two mechanistic schemes for chaperone-catalyzed Fe-S cluster transfer from [2Fe-2S]-IscU to apo-acceptor proteins. The first involves direct coupling between ATP hydrolisis and cluster transfer and requires interaction between apo-FdX and the T-state HscA-ATP-HscB-IscU complex. The second involves ATP hydrolysis preceding cluster transfer and involves interaction between apo-FdX and the R-state HscA-ADP-IscU complex (Chandramouli and Johnson 2006). The chaperones could act by causing changes in IscU conformation that facilitate cluster release or capture by the acceptor protein (Bonomi, Iametti et al. 2008). HscA binds IscU via a conserved ^{99}LPPVK^{103} sequence (Hoff, Ta et al. 2002, Hoff, Cupp-Vickery et al.

2003, Cupp-Vickery, Peterson et al. 2004) positioned close to the conserved Cys106 that may be involved in the cluster coordination. Conformational changes coupled to the HscA T-state to R-state transition during ATP hydrolysis may act to make the cluster more available (Bonomi, Iametti et al. 2008).

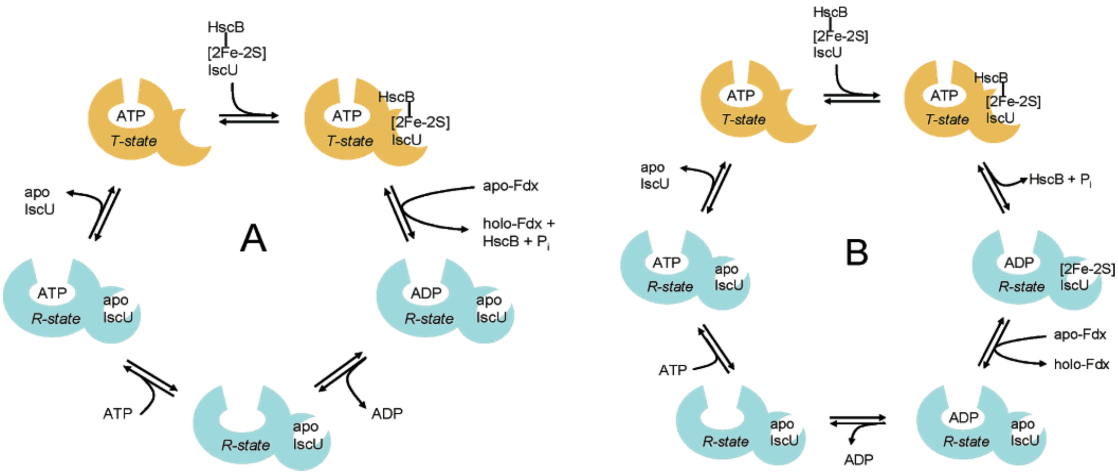

Figure 1.10 Possible mechanistic schemes for chaperone-catalyzed Fe-S cluster transfer from [2Fe2S]-IscU to apo-FdX (Chandramouli and Johnson 2006).

Although several attempts have been performed to clarify the molecular bases of the Fe-S cluster formation, they still appear to be not completely understood.

2. FRIEDREICH'S ATAXIA AND FRATAXIN

Dysfunctions in Fe-S protein biogenesis and in mitochondrial iron homeostasis in heart and neurones cause pathological conditions, such as the neurodegenerative diseases Friedreich's ataxia.

2.1 Friedreich's ataxia: symptoms and causes

Nerves and cells of the heart muscle respire exclusively aerobically, so that they are totally dependent on mitochondrial oxidative phosphorylation. Mitochondrial dysfunction usually causes both myopathy and neuropathy and very often, the two occur together. Often mitochondrial myopathies are caused by mutations in the mitochondrial genome and more rarely these are found in nuclear-encoded enzymes of mitochondrial intermediary metabolism (Gibson, Koonin et al. 1996). Ataxia, meaning impaired movement due to loss of motor coordination, is associated with many of the mitochondrial myopathies, and in these cases is usually due to progressive neural degeneration (Gibson, Koonin et al. 1996).

Friedreich's ataxia (FRDA) is the most frequent hereditary ataxia occurring with a frequency of about 1:30000 to 50000 people within Caucasian populations and it presents a onset typically before age of 25 years and a mortality between 40 and 50 years (Ashley, Hoang et al. 2012). It is characterized by a variety of symptoms, as progressive gait and limb ataxia, dysarthria, lower limb areflexia, decreased vibration sense, muscular weakness of the legs, positive extensor plantar response, hypertrophic cardiomyopathy and, often, diabetes mellitus or carbohydrate intolerance. Most neurological symptoms are a consequence of degeneration of the large sensory neurons of dorsal root ganglia and spinocerebellar tracts. The disease primarily affects neurones with very long axons, which appear to die back from the periphery (Gibson, Koonin et al. 1996, Schmucker and Puccio 2010).

FRDA is an autosomal recessive disease and it is associated with the mutation of a gene mapped to chromosome 9q13–q21 which encodes a small mitochondrial

protein called frataxin (Gibson, Koonin et al. 1996). The most common mutation is a GAA triplet-repeat expansion within the first intron of the frataxin gene. In healthy patients, the number of repeats ranges from 6 to 36 repeats, whereas in FRDA patients, the number of repeats ranges from 70 to 1700 repeats, most commonly 600 to 900 GAA. The severity of the disease correlates with the number of repeats. While most patients (96%) carry two expanded GAA alleles, which lead to strongly reduced frataxin expression in all tissues, 4% of FRDA patients present a $(GAA)_n$ mutation on one allele and a micromutation on the other. These mutations are small deletions or point mutations that can disturb the normal function of frataxin, either by affecting protein folding or by affecting functional residues (Schmucker and Puccio 2010). An exemple is point mutation G137V that does not impair the structure or the activity of frataxin but reduces the folding stability (Faggianelli, Puglisi et al. 2015).

Frataxin-defective organisms exhibit iron metabolism and other metabolic disturbances and damage caused by oxidative stress. The first evidence is the iron accumulation in the mitochondria of heart cells and neurones correlated with deficit of iron-sulfur clusters synthesis, a process in which frataxin is directly involved. This causes dysfunction of Fe-S cluster enzymes (Pandolfo and Pastore 2009).

In addition, an increase of H_2O_2 levels is observed. Impairment of the respiratory complexes I, II, and III containing Fe-S clusters lead to a decrease of the respiratory chain activity. Direct addition to oxygen of electrons from the leakage of the defective respiratory chain generates O_2^-. In mitochondria superoxide dismutase2 (SOD2) catalyses dismutation of superoxide (O_2^-) with formation of H_2O_2. Cells from FRDA patients show highly sensitivity to hydrogen peroxide: H_2O_2 generates the highly toxic hydroxyl radical (OH•) by reacting with Fe^{2+} (Fenton reaction) and OH• damages proteins, lipids, and nucleic acids. H_2O_2 is eliminated by mitochondrial glutathione peroxidase, at the expense of the small-molecule anti-oxidant glutathione, which appears to be decreased, possibly because of an excess of consumption (Tozzi, Nuccetelli et al. 2002).

For reasons that are unclear, frataxin-deficient cells also seem to have a reduced

ability to activate antioxidant defenses (Pandolfo and Pastore 2009) and FRDA patients exhibit increases in nuclear and mitochondrial DNA damage (Schmucker and Puccio 2010). Additional abnormalities in multiple metabolic pathways have been revealed. In particular, defects in heme synthesis, sulfur amino acid metabolism, energy metabolism, stress response, and mitochondrial function (Pandolfo and Pastore 2009).

2.2 Frataxin: structure and function

Frataxin is a ubiquitous mitochondrial protein that is highly concentrated in the cells of heart, spinal and dorsal root ganglia (Koutnikova, Campuzano et al. 1997). It is present in living organisms ranging from bacteria to humans and it seems to be essential for survival (Gibson, Koonin et al. 1996). Frataxin is highly conserved and orthologues of frataxin as bacterial frataxin (named CyaY) and yeast frataxin (named Yfh1) are currently in use as model systems for understanding the properties of the frataxin family (Adinolfi, Trifuoggi et al. 2002).

Frataxin is composed, in humans, of 210 amino acids and the protein, after the mitochondrial import sequence cleavage, forms two structurally distinct regions. Among these only the evolutionary conserved C-terminus is folded and forms a compact globular domain with a stable β-sheet consisting of seven strands packed against a pair of parallel helices (Musco, Stier et al. 2000).

The bacterial frataxin, CyaY, is a highly acidic protein consisting of 106 residues. NMR and crystallographic structural studies on human frataxin and crystallographic studies on bacterial frataxin revealed a similar fold for both proteins, even if no similarity to known protein folds in the protein databases were found (Nair, Adinolfi et al. 2003). Comparing the C-terminus length of CyaY with that of human frataxin, it was shown that in bacteria it is nine residues shorter than in human. The length of this tail has been demonstrated to be an important factor influencing the intrinsic thermal stability *in vitro* (Adinolfi, Nair et al. 2004, Sanfelice, Puglisi et al. 2014).

By testing the effects of individual residue mutations that cause the disease, it was

discovered that all missense mutations observed map in the evolutionary conserved frataxin C-terminus, supporting the hypothesis that the C-terminus is the functionally most relevant region of the protein (Musco, Stier et al. 2000). The most common frataxin mutants associated to Friedreich's ataxia retain the native fold under physiological conditions, but have a reduced thermodynamic stability, a higher tendency towards proteolytic digestion (Correia, Adinolfi et al. 2006) and an enhanced tendency to aggregate (Correia, Pastore et al. 2008).

The structure is compact with no grooves or cavities. However, an exposed surface of negatively charged and conserved residues responsible for iron binding can be identified (Musco, Stier et al. 2000). Frataxin has poor sequence homology with other known proteins involved in iron or heme metabolism and the iron binding surface involves a region that contains mainly carboxylate residues, but not residues traditionally observed in other non-heme iron binding proteins, such as histidine, cysteine, or tyrosine (Nair, Adinolfi et al. 2004). Investigating iron donor proteins, Yoon and Cowan demonstrated that human frataxin is able to bind from six to seven iron ions (Yoon and Cowan 2003). The bacterial hortologue CyaY is able to bind iron as well, but with low selectivity (Pastore, Franzese et al. 2007). Low affinity in the iron binding and formation of a transient complex are clues of a role as iron carrier in the cell: it was supposed that frataxin could pass iron on to other proteins with an iron storage mechanism in order to keep iron in a bio-available and non-toxic form (Gakh, Adamec et al. 2002). Some reports have shown that frataxin is able to donate iron to IscU (Yoon and Cowan 2003), ferrochelatase (Yoon and Cowan 2004), and aconitase (Bulteau, O'Neill et al. 2004). Layer et al. demonstrated that the bacterial frataxin orthologue, CyaY, *in vitro* is able to provide iron to the bacterial scaffold IscU in the presence of the cysteine desulfurase IscS and cysteine to generate Fe-S cluster (Layer, Ollagnier-de Choudens et al. 2006). IscS binds monomers of CyaY with a 1:1 stoichiometry and, contrary to what was observed for human frataxin with the scaffold protein ISU (Yoon and Cowan 2003), contacts with IscU are possible only in the context of the ternary complex with IscS

(Prischi, Konarev et al. 2010). The surface of interaction with the desulfurase involves a direct recognition of the negatively charged region of CyaY, that corresponds to the iron binding surface, by a positively charged patch on IscS, thus rendering an active role of iron in complex formation unlikely (Foury, Pastore et al. 2007).

It was reasoned that if frataxins were iron providers, the presence of CyaY should either enhance the enzymatic rates of the Fe-S cluster formation or otherwise have no effect. On the contrary, the presence of CyaY inhibits the reaction. In particular CyaY seems not to alter the IscS desulfurase activity but it is an inhibitor of cluster formation and its effect does not depend on the specific acceptor. Since conversion of cysteine into alanine is unperturbed by the presence of CyaY (Adinolfi, Iannuzzi et al. 2009), it could interfere with the sulfur transfer from IscS to IscU, impairing the motions of the flexible catalytic loop containing Cys328 or increasing the affinities between IscU and IscS through the stabile ternary complex, thus decreasing the dissociation rate constant (Prischi, Konarev et al. 2010).

In contrast of CyaY, human frataxin activates both the cysteine desulfurase and Fe-S formation reactions (Tsai and Barondeau 2010). To solve this discrepancy, enzyme kinetic experiments were performed by Bridwell-Rabb et al. interchanging analogous cysteine desulfurase, Fe-S assembly scaffold, and frataxin components for the human and *E. coli* systems (Bridwell-Rabb, Iannuzzi et al. 2012). They observed that activation or inhibition by the frataxin homologue is not controlled by the frataxin itself but rather dictated by the cysteine desulfurase: addition of bacterial or human frataxin inhibits Fe-S assembly by complexes of bacterial desulfurase and activates Fe-S assembly by complexes containing human desulfurase, albeit inhibition of the *E. coli* complex by CyaY was more efficient than by human frataxin and activation of the human complex by human frataxin was more efficient than by CyaY. They suggest that binding of the effector molecule switches the activity, either from “off” to “on” or from “on” to “off”. It was supposed that CyaY modulates the Fe-S cluster formation by inducing an “off” conformation of bacterial system, on the

other hand the human frataxin is able to trap an “on” conformation of human complex (Bridwell-Rabb, Iannuzzi et al. 2012).

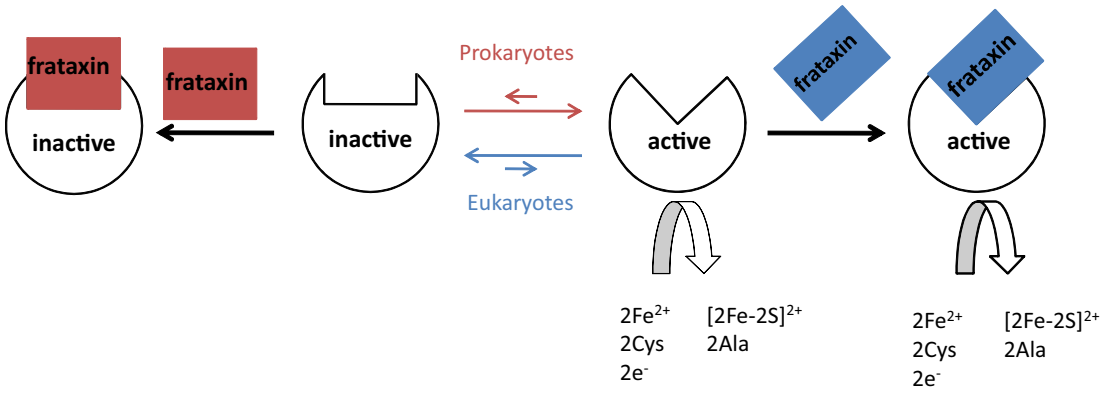

Figure 2.1 Working model for frataxin regulation of Fe-S cluster biosynthesis. Fe-S cluster assembly complex exists as a mixture of functional and nonfunctional states, which are stabilized by binding of frataxin homologues. In eukaryotes, a pre-equilibrium model is proposed in which the Fe-S cluster assembly deficient form is favored over the functional form. Frataxin binding stabilizes the functional form. In contrast, the prokaryotic complex that lacks frataxin exhibits activities of cysteine desulfurase and Fe-S cluster assembly. Frataxin binding abolishes Fe-S cluster synthesis (Bridwell-Rabb, Iannuzzi et al. 2012).

The effect of CyaY on Fe-S cluster formation is iron-dependent, so that Adinolfi et al proposed that frataxin function as iron sensor tuning the quantity of Fe-S clusters formed to match the concentration of the apo-acceptors (Adinolfi, Iannuzzi et al. 2009). Frataxin would have low affinity for the IscS-IscU system at normal iron levels, but at any even small iron imbalance, the affinity of the protein for IscS would increase (Adinolfi, Iannuzzi et al. 2009). Several studies support the role of frataxin as regulator of Fe-S cluster biogenesis and disfavour its involvement as an iron storage protein (Iannuzzi, Adinolfi et al. 2011, Garcia-Serres 2012).

3. PRELIMINARY PREPARATION

The *isc* operon encodes a complex system and its mechanism involves several proteins with different characteristics of structure and stability. Before starting its investigation, the preliminary preparation of all the constituents (desulfurase IscS, the scaffold protein IscU, the chaperone system of HscA and HscB and ferredoxin) was required, meaning their expression, purification and eventual characterization. Fortunately they had already been studied in depth in the Pastore lab and all the protocols of purification were already available and well optimized.

3.1 Protein purification

All the genes encoding the Isc proteins had been inserted in pET24 vectors and plasmids were already available in the group. They were introduced in BL21(DE3) *E. coli* competent cells by transformation. These cells contain the T7 RNA polymerase gene and are under the control of the *lac*UV5 promoter, so IPTG was used to induce the expression. Proteins were expressed with a His-tagged glutathione S-transferase (GST) that was separated from the Isc protein by a cleavage site for Tobacco Etch Virus (TEV) protease, corresponding to the amino acid sequence ENLYFQG where the cleavege is made specifically between the glutammine and the glycine.

Figure 3.1 Example of a Isc protein sequence expressed with GST,His-tag and the specific TEV cleavege site ENLYFQG.

Proteins were purified by affinity chromatography using Ni-nitrilotriacetic (Ni-NTA) columns, which interact with the His-tag, washed with two buffers at different salt concentration and then eluted with an imidazole solution. The tag of the collected

proteins was cleaved by TEV protease. The reaction mixture was passed again through a Ni-column to separate the protein from the His-tagged GST. Further purification was carried out by size exclusion chromatography on a Superdex column. After each step an SDS PAGE was run to check the purity of the recombinant protein. The same protocol has been followed for the purification of IscS, IscU, HscA, HscB and FdX. In figure 3.2 is reported the SDS PAGE gel run during HscB purification as representative.

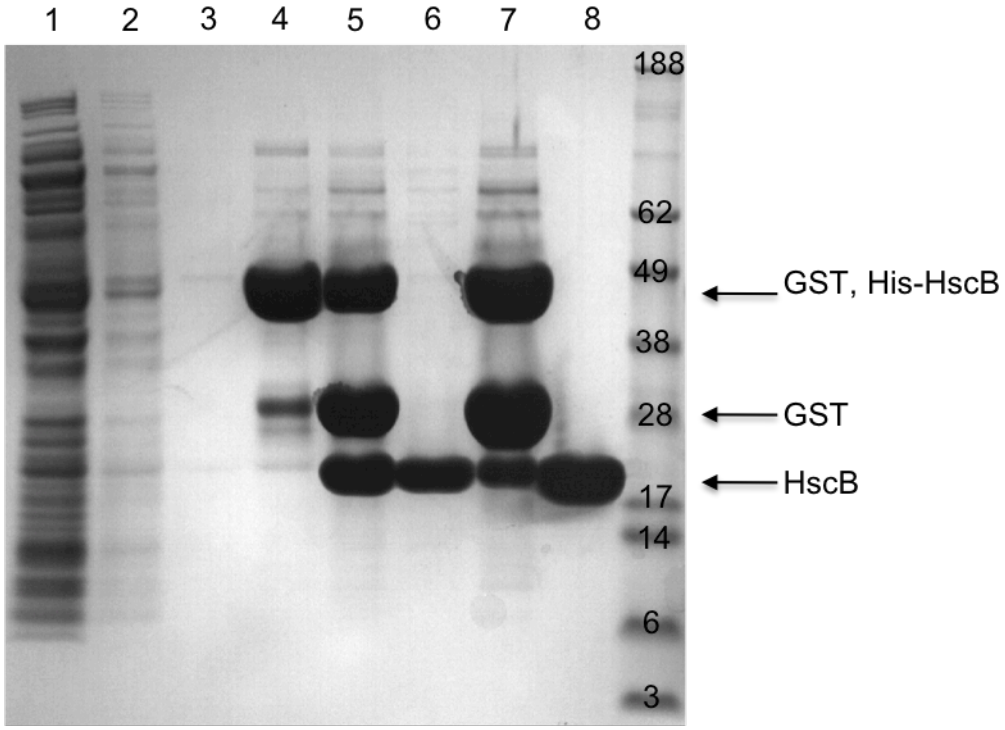

Figure 3.2 SDS PAGE run during HscB purification. Each column shows the sample purity after a specific step of the purification process. Components are separated by molecular weight. Initially proteins were purified on a Ni-NTA column (1. Throughflow the column. 2. First step of wash 3. Second step of wash. 4. Step of elution of the fusion protein between HscB (21 kDa) and GST (26 kDa) with a 300mM imidazole solution). After the overnight cleavage step by TEV protease dialysing in 20 mM Tris-HCl pH 8, 150 mM NaCl, spots corresponding to GST and HscB appeared (5) and the sample was loaded again on the Ni-NTA column (6. Throughflow the column). The liquid eluted after the cleavage still presented His-tagged proteins (7). The process was terminated with a step of FPLC purification on a 16/60 Superdex G75 column with 20 mM Tris-HCl pH 8, 150 mM NaCl and 2 mM DTT buffer (8).

Figure 3.3 shows the sample purity obtained at the end of IscS (45kDa), IscU

(14kDa), HscA (66kDa) and FdX (12kDa) purification.

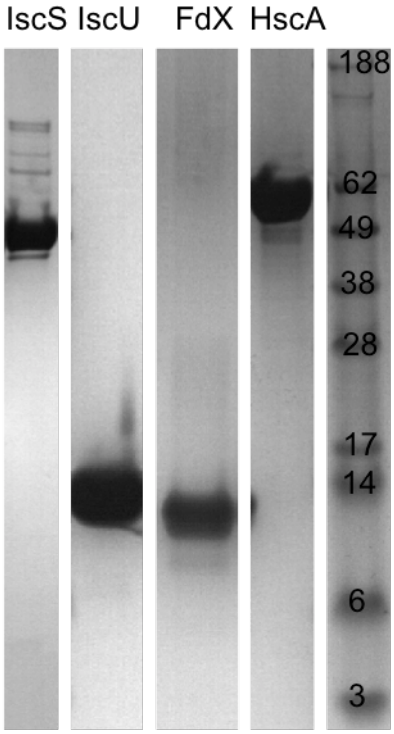

Figure 3.3 SDS PAGE run after the purification of IscS, IscU, HscA and FdX.

3.2 HscB and HscA characterization

In my work, I focused the attention on the involvement of the two chaperones HscA and HscB in the Fe-S cluster enzymatic formation and transfer. Before starting, their fold and activity were tested.

3.2.1 CD study of HscB

Circular dichroism (CD) is usefull in the study of proteins for structural and conformational purpose because each type of secondary structur presents a characteristic shape in the spectrum. The folding of HscB was thus controlled recording its CD spectrum in the range between 195 and 260 nm.

BOX 1 ***Principle of Circular Dichroism of proteins***

Circular Dichroism is the difference in absorption of left and right circularly polarised light due to the chirality of molecules.

$$CD = A_l - A_r$$

The main uses of CD in the study of proteins are for structural or stability purposes, since CD contains information about the asymmetric features. Proteins are formed by L-amino acid that arrange in chiral secondary structures. CD gives thus information about the backbone and CD signal arises from the backbone amide transitions in the range of ~190 to 260 nm. Distinctive CD spectra have been described for pure conformations such as α-helix, β-sheets, β-turns and also the random coil. CD of a native protein is then the sum of the appropriate percentages of each component spectrum.

The CD spectra of α-helices are characterized by a negative band with two separate minima of similar magnitude at 222nm and 208 nm. The α-helix CD is larger in magnitude than the one due to other motifs.

The general characteristics of β-sheet CD may be taken to be a negative band at about 216 nm and a positive band of a comparable magnitude near 195 nm.

The label β-turns is usually used to include all possible turns that occur to enable a single strand to become an anti-parallel β-sheet. A typical β-turn CD spectrum has been identified with a weak negative band near 225 nm, a strong positive transition between 200 and 205 nm and a strong negative band between 180 and 190 nm.

When we refer to random coils, we are generally grouping the parts of the folded protein that do not fit into any one of the previously discussed categories which means that there may be ordered structures included in this residual. The CD of these parts of the protein has a strong negative CD signal just below 200 nm, a positive band at about 218 nm in many systems and perhaps a very weak negative band at 235 nm.

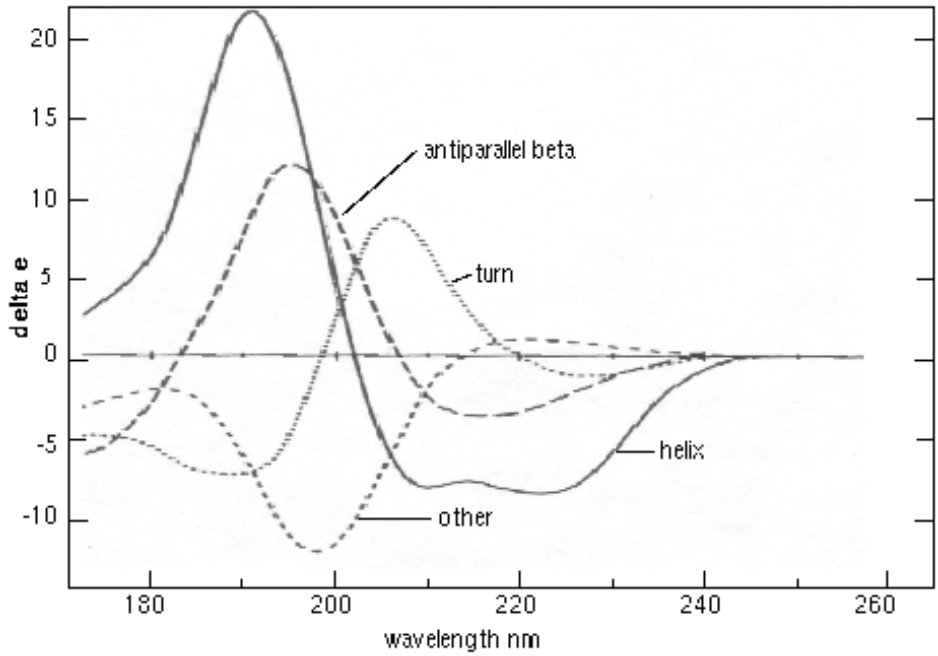

Figure 3.4 CD spectra of pure secondary structures (Brahms and Brahms 1980).

Protein CD spectra are empirically analyzed by expressing them as a combination of standard spectra corresponding to a limited number of well-defined backbone geometries. There is a range of different computer programs available for determining the percentage of different structural motifs from CD spectrum. All use standard reference spectra (S_{b1}; S_{b2}…S_{bn}) with respect to which a measured spectrum is decomposed so that the difference between the appropriately weighted sum of the reference spectra and the experimental spectrum is minimum (Rodger 1997).

$$\sum \left| S^{\exp} - \sum_i a_i S_{bi} \right| = \min$$

As it is shown in figure 3.5, HscB CD spectrum presents two bands at around 222 and 208 nm confirming that it is predominantly a α-helical protein and has an ordered and well folded secondary structure (90.5 % α-helix, 0.8% β-strand, estimated with K2D3 web server).

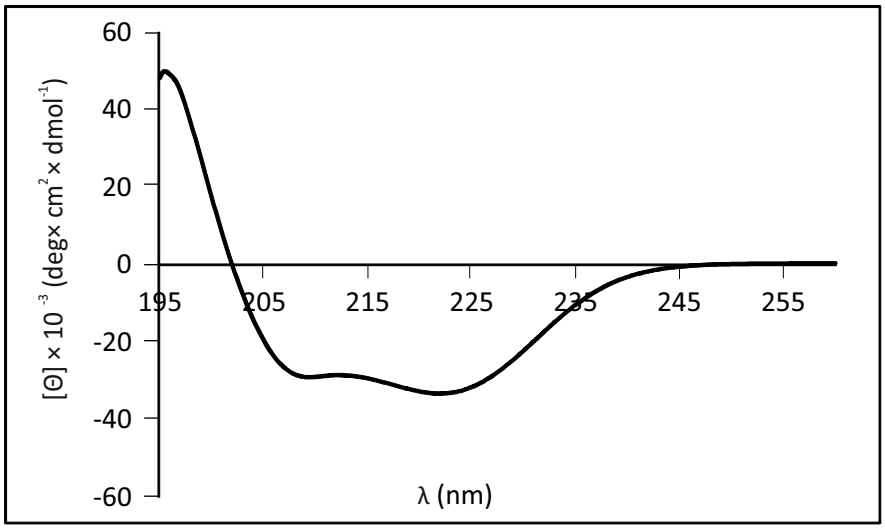

Figure 3.5 CD spectrum of HscB with a protein concentration of 10 µM in 20 mM Tris-HCl pH 8, 150 mM NaCl and 2 mM DTT, at room temperature, in cuvettes of 1 cm path length with 0.1 nm of resolution, a band width of 2 nm and a scan speed of 200 nm/min and accumulated 30 times. The baseline correction was obtained by subtraction of the buffer spectrum.

3.2.2 HscA ATPase activity

HscA is a constitutively expressed chaperone, belonging to the Hsp70 class. Its activity is coupled to ATP binding and hydrolysis with conformational changes that control the peptide substrate affinity (Silberg and Vickery 2000). HscA is regulated by the scaffold protein IscU and the co-chaperone HscB. IscU behaves as a substrate for HscA and HscB enhances the binding of IscU to HscA. Individually, HscB and IscU weakly stimulate HscA ATPase activity, but together the stimulation is synergistic (Silberg, Tapley et al. 2004).

I thus checked the ability of freshly purified HscA to hydrolise ATP in the presence and absence of HscB and both HscB and IscU. I used an enzyme assay based on a procedure originally described by Webb that provides a spectrophotometric method for the quantification of inorganic phosphate (P_i) (Webb 1992). In the presence of Pi, the substrate 2-amino-6-mercapto-7-methylpurine riboside (MESG) is converted enzymatically by purine nucleoside phosphorylase (PNP) to ribose 1-phosphate and 2-amino-6-mercapto-7-methylpurine that shows a maximum in absorbance at 360 nm.

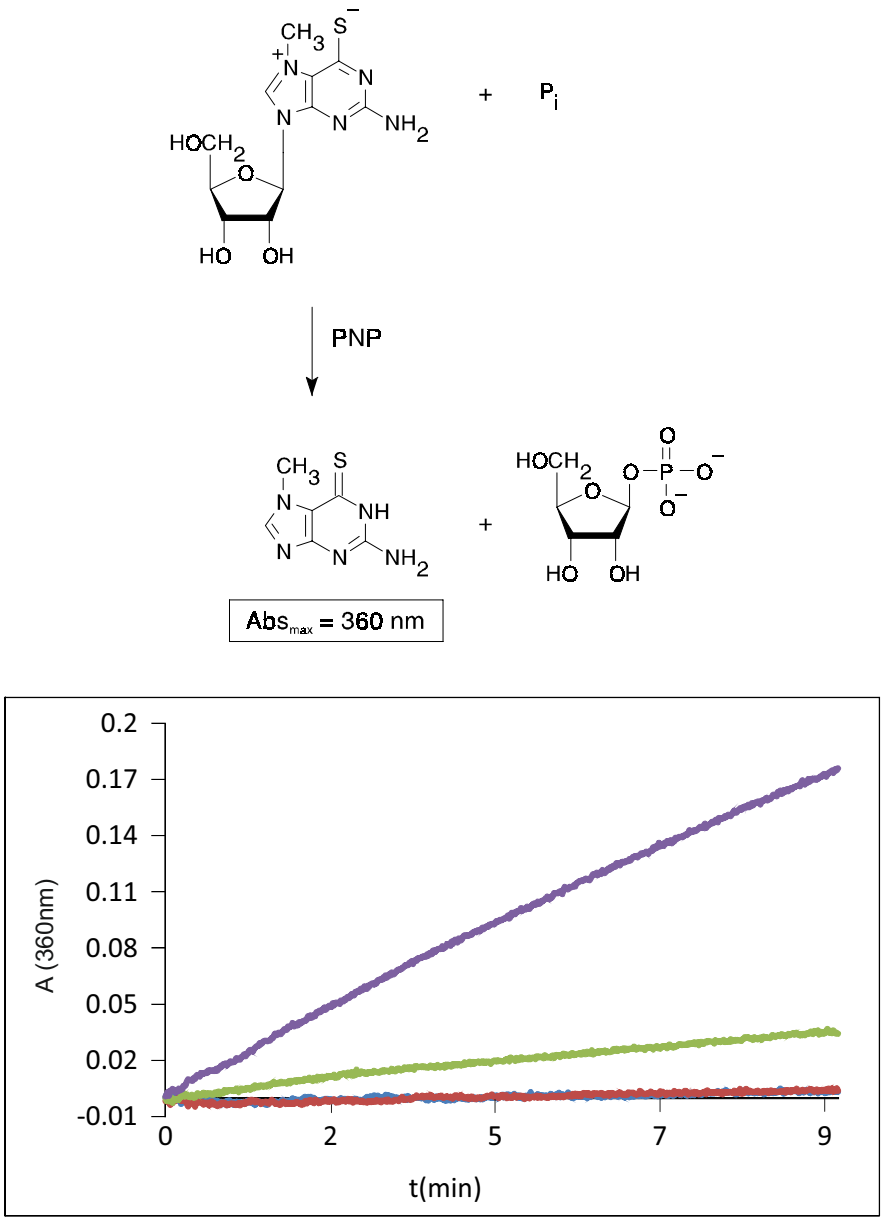

Figure 3.6 ATPase activity of HscA. The enzymatic conversion of MESG to ribose 1-phosphate and 2-amino-6-mercapto-7-methylpurine is accompanied by a change in absorption at 360 nm that allows the quantification of inorganic phosphate consumed in the reaction (top). On the bottom it is shown the measurement of the ATPase activity. The following reagents were combined: 200 μM of MESG, PNP and 150 μM ATP (blue), 150 μM ATP and 1 μM HscA (red), 150 μM ATP, 1 μM HscA and 50 μM HscB (green), 150 μM ATP, 1 μM HscA, 50 μM HscB and 50 μM IscU (purple). The substrate ATP was added after incubation at 22 °C for 30 minutes and the absorbance at 360 nm was measured.

Curves in figure 3.6 confirm what was already shown by Chandramouli et al. (Chandramouli and Johnson 2006): HscA exhibits a low basal level of ATPase

activity that is enhanced in the presence of HscB and even more with both HscB and IscU.

3.3 Methods

List of reagents

Reagents and consumables used in the experiment presented in my work were ordered from the following companies:

BL21(DE3) competent cells (Novagen); LB Broth (Fisher Scientific); LB-Agar (Sigma); kanamycin (Sigma); IPTG (generon); Igepal (Sigma-Aldrich); Lysozyme (Sigma); DNase I (Roche); Complete EDTA-free (Roche); DTT (Sigma-Aldrich); TCEP (Sigma); Tris-HCl (Thermo Scientific); NaCl (Fisher Scientific); Imidazole (Sigma-Aldrich).

Ni-NTA affinity resin (Generon); glutathione sepharose 4B (Pharmacie Biotech), Dialysis Membrane (Spectrum Laboratories).

$Fe(NH_4)_2(SO_4)_2$ (Sigma); L-cysteine (Sigma); ATP (Sigma); $MgCl_2$ (Sigma).

12% Tris-Glycine gel (Novex life technologies); Nu-MES Buffer (Novex life technologies); Instant Blue (expedeon).

Acetic acid (Fisher Chemical); acetonitrile (ROMIL).

DMA (Thermoscientific); BS^3 (Thermoscientific); PBS buffer[1] (common buffer preparation service at the National Institute for Medical Research); NAP-5 Sephadex columns (Healthcare).

M9 salts[2] (common buffer preparation service at the National Institute for Medical Research); D-(+)-Glucose (Fisher Chemical); $(NH_4)_2SO_4$ (^{15}N, 99%) (Cambridge Isotope Laboratories Inc.); D_2O (D, 99.96%) (Cambridge Isotope Laboratories Inc.).

Agarose (Sigma).

---

[1] PBS composition: 1.37 M NaCl, 27 mM KCL, 100 mM Na_2HPO_4, 18 mM KH_2PO_4, pH 7.4

[2] M9 salts composition: Na_2HPO_4 6 g/l, KH_2PO_4 3 g/L, NaCl 0.5 g/L, $MgSO_4$ 2 mM, $CaCl_2$ 0.1 mM D-biotin 1 mg/L, thiamine 10 µM, trace elements.

Protein Purification

Proteins were individually expressed from pET-derived plasmid vectors as fusion proteins with His-tagged glutathione S-transferase (GST) and a cleavage site for Tobacco Etch Virus (TEV) protease. They were expressed and purified from *E. coli* strain BL21(DE3) as previously described (Adinolfi, Trifuoggi et al. 2002, Adinolfi, Rizzo et al. 2004, Prischi, Pastore et al. 2010). Cells were inoculated at 37 °C in LB medium with kanamycin (30 µg/mL) and induced overnight at 18 °C by the addition 500 µL of 0.5 mM isopropyl β-D-thiogalactopyranoside (IPTG) when the culture reached an optical density (OD) at 600 nm of 0.6 - 0.8. Cell pellets were centrifuged at 3500 rpm for 25 minutes at 4 °C with a JA-10 rotor. They were resuspended in a lysis buffer (20 mM Tris-HCl pH 8, 150 mM NaCl, 10 mM imidazole, 20% v/v Igepal, DNAse I, lysozyme, antiprotease, 1 mM TCEP) and frozen. Cell pellets were then thawed and sonicated and centrifuged at 18000 rpm for 40 minutes at 4 °C with a JA-20 rotor. Proteins were purified by affinity chromatography (using Ni-nitrilotriacetic agarose), eluted with wash1 (20 mM Tris-HCl pH 8, 150 mM NaCl, 10 mM Imidazole, 1 mM TCEP), wash2 (20 mM Tris-HCl, pH 8, 1 M NaCl, 10 mM Imidazole, 1 mM TCEP) and finally with elution buffer (300 mM Imidazole, 1 mM TCEP). They were cleaved overnight from His, GST-tag by TEV protease dialysing in 20 mM Tris-HCl pH 8, 150 mM NaCl, 1 mM DTT. Further purification was carried out by gel filtration chromatography on a 16/60 Superdex G75 column. Samples were eluted in 20 mM Tris-HCl pH 8, 150 mM NaCl and 2 mM DTT and monitoring absorbance at 280 nm. Protein concentration was determined by UV spectroscopy using the following extinction coefficients derived computationally whit Expasy from the sequences (http://web.expasy.org/protparam/): ε_{280} (IscS)= 41370 $M^{-1}cm^{-1}$; ε_{280} (HscA)= 20400 $M^{-1}cm^{-1}$; ε_{280} (HscB)= 16960 $M^{-1}cm^{-1}$ and ε_{280} (FdX)= 6990 $M^{-1}cm^{-1}$. Protein purity was checked by SDS PAGE after each step of the purification.

CD spectra

Far-UV CD spectra were recorded on a Jasco J-815 CD Spectrometer. Measurements were repeated at least twice on independent protein preparations to ensure reproducibility of the results. Samples were prepared using a HscB concentration of 0.15 mg/mL in 20 mM Tris-HCl pH 8, 150 mM NaCl and 2 mM DTT. Measurements were carried out at room temperature in fused silica cuvettes of 1 cm path length (Hellma). Tipically CD spectra were recorded between 190 and 260 nm, accumulated 30 times, with 0.1 nm of resolution, a band width of 2 nm and a scan speed of 200 nm/min. A nitrogen flow assured anaerobic conditions and a baseline correction was obtained by subtraction of the appropriate buffer spectrum. The web server K2D3 (http://cbdm-01.zdv.uni-mainz.de/~andrade/k2d3/) was used to estimate the α-helix and β-strand content of the protein from its CD spectrum.

ATPase activity assay

The ATPase activity of HscA in the presence and absence of HscB or both HscB and apo-IscU was assessed at room temperature by measuring the phosphate released via a coupled enzyme assay with the EnzChek phosphate assay kit (Invitrogen). The reaction mixture was set up with 10 μM HscA; 10 μM HscB and 10 μM IscU were added when necessary. The substrate, ATP 150 μM, was added after 10 minutes of incubation and the absorbance at 360 nm was read as a function of time.

4. BIOCHEMICAL APPROACH

To understand the mechanism of Fe-S cluster biosynthesis and the role that each component of the machinery has in it, I designed an experiment that allowed the following of cluster formation *in vitro* using the *E. coli* Isc system. The aim was to find a way to detect the Fe-S cluster formed through an assay selective and at the same time easy to perform and reproducible.

4.1 The kinetic assay

It was already well described that Fe-S cluster can be formed *in vitro* in the presence of IscS, that behaves as a source of sulfur converting cysteine into alanine, the scaffold protein IscU, Fe^{2+} and a reducing agent. It was essential to completely remove the oxygen from the system to avoid the oxidation of iron and thus to perform the assay under an inert atmosphere of nitrogen (Adinolfi, Iannuzzi et al. 2009). The Fe-S cluster was then transferred from the scaffold to an apo-protein and detected by a spectrophotometric technique. Enzymatic rates were determined by detecting the absorbance of the reporter acceptor as a function of time. All proteins able to accept the Fe-S cluster present a specific wavelength of absorbance in the UV-Vis range when they are bound to the cluster and they can thus be used as reporter for this assay. Among them are ferredoxin, aconitase2 and IscU.

Ferredoxin is known to be able to bind Fe-S cluster and its holo-form shows a characteristic absorbance at 458 nm (Yan, Adinolfi et al. 2013). It means that when it receives a Fe-S cluster, an increase in the absorbance at this wavelegth could be observed (figure 4.1).

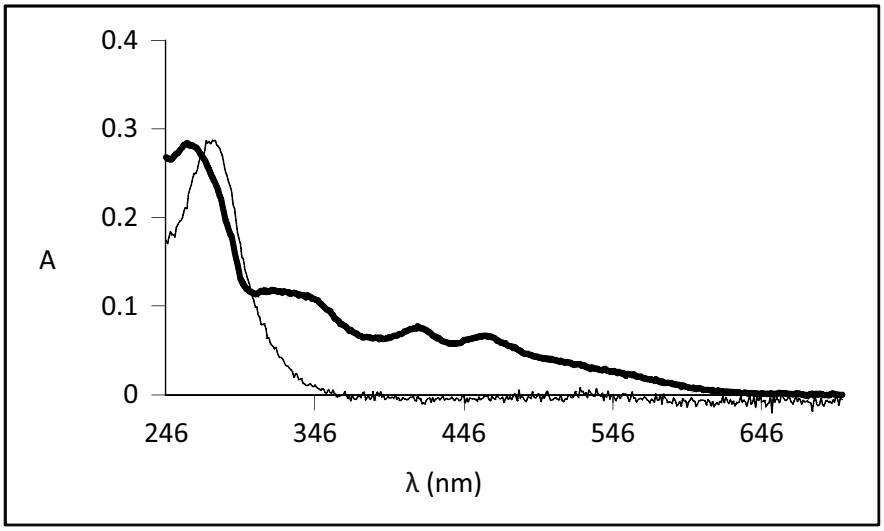

Figure 4.1 UV-Vis spectrum of apo-ferredoxin (dashed line) and [2Fe-2S]-ferredoxin (solid line) with a protein concentration of 10 µM in 20mM Tris-HCl pH 8, 150 mM NaCl and 2 mM DTT. A baseline correction was obtained by subtraction of the buffer spectrum.

Aconitase2 is one of the most common Fe-S proteins. I proved its ability to accept Fe-S clusters synthetised and released in the presence of the desulfurase IscS and of the scaffold IscU. I mixed under strictly anaerobic conditions the desulfurase IscS, the scaffold IscU, the substrates Fe^{2+} and cysteine with aconitase2 and the variation in absorbance between 240 and 800 nm was monitored every 2 minutes. A characteristic spectrum was recorded with specific absorbance peaks at 490, 450, 406 and 315 nm (figure 4.2). A major change in the intensity was observed for the peak at 406 nm. Plotting the absorbance value at this wavelength against the time, the kinetic curve of the Fe-S cluster synthesis and transfer to the aconitase2 was obtained (figure 4.3). The reaction reached a plateau very quickly and the variation in absorbance appeared pronounced. Aconitase2 seems to be a good acceptor of Fe-S cluster formed on IscU in the presence of desulfurase IscS.

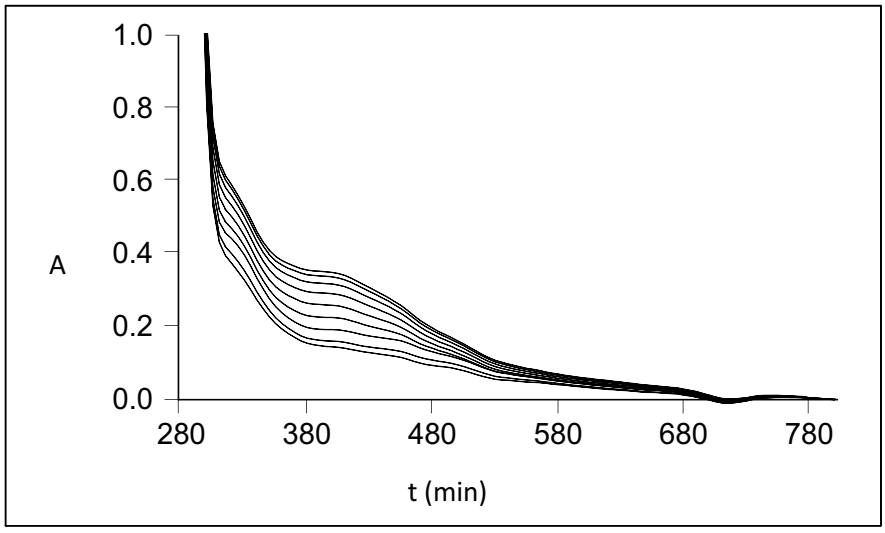

Figure 4.2 UV-Vis spactra of aconitase2 reconstitution (30 μM) measured in presence of 1 μM IscS, 5 μM IscU, 3 mM DTT after 0, 4, 10, 20, 30 and 40 minutes from the addition of substrates 250 μM Cys and 75 μM Fe^{2+} in 20 mM Tris-HCl pH 8, 150 mM NaCl.

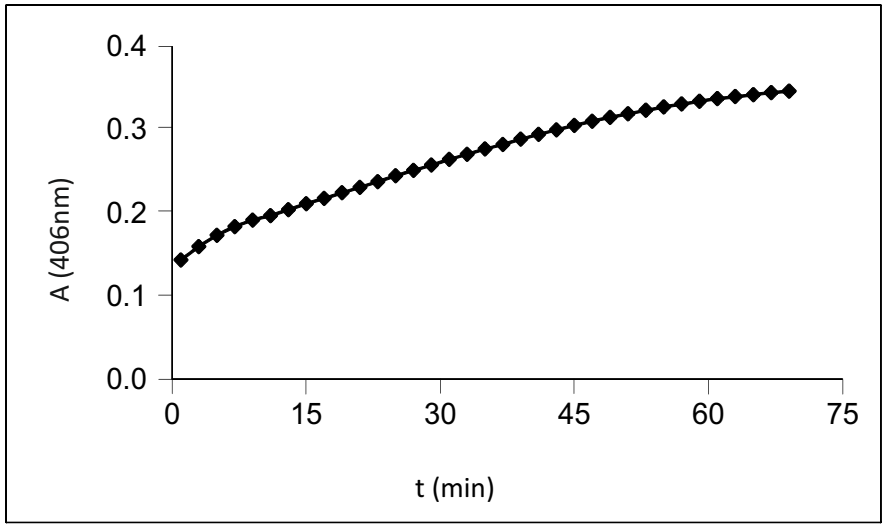

Figure 4.3 Kinetic of aconitase2 reconstitution. Absorbance at 406 nm against the time in the reconstitution of 30 μM Aco2 in the presence of 1 μM IscS, 5 μM IscU, 3 mM DTT, 250 μM Cys and 75 μM Fe^{2+} in 20 mM Tris-HCl pH 8, 150 mM NaCl.

The use of IscU is a special case because IscU is itself the scaffold protein and in this case the step of transfer is absent. When the cluster is formed on it, the absorbance at 456 nm increases (figure 4.4).

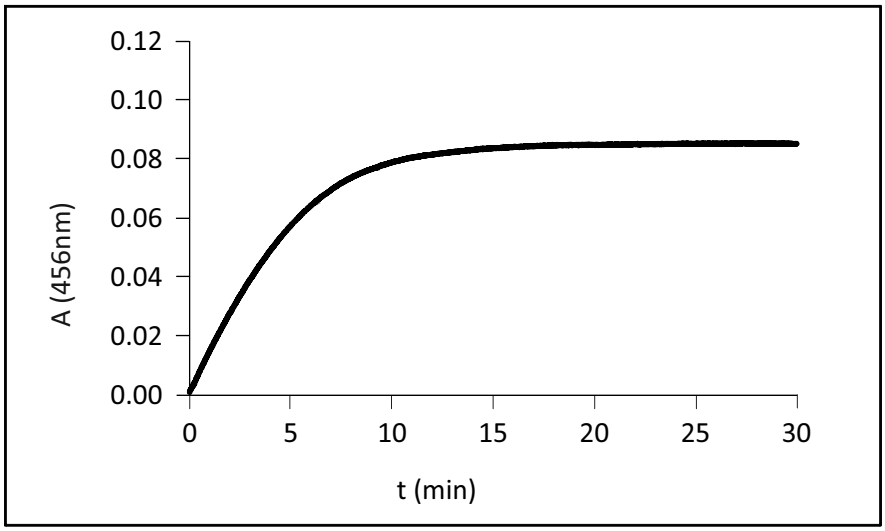

Figure 4.4 Kinetic curves of formation of Fe-S cluster on IscU. Absorbance at 456 nm against the time in the reconstitution of 30 μM IscU in presence of 1 μM IscS and 3 mM DTT with 250 μM Cys and 25 μM Fe^{2+} in 20 mM Tris-HCl pH 8, 150 mM NaCl.

In practice the assay consisted in adding Fe^{2+} and DTT in a cuvette containing the Isc proteins under inert atmosphere of nitrogen to avoid oxidation. The cluster was formed enzymatically by IscS and IscU and in the eventual presence of other proteins as chaperones HscA and HscB. Chaperones are thought to assist the step of transfer and, if this was the rate limiting step, in their presence I would expect an increase in the activity of Fe-S cluster constitution. Since HscA shows and ATPase activity fundamental for the system, ATP was added as well. After 30 minutes, when the system was equilibrated, cysteine and ATP were added to start the reaction. Fe-S cluster formation and its transfer to an acceptor were then easily followed by measuring the change in absorbance at the specific wavelength.

4.2 Optimization of IscU, HscA, HscB and ATP concentrations

Because I worked with a complex multi-component system, I first optimized the relative concentrations of the components. The concentration of apo-ferredoxin, which I chose as final cluster acceptor in the assay, was set to 50 μM to easily measure the signal of the cluster. IscS was set to catalytic concentrations (1 μM) to avoid even minimal contributions of unspecific iron-thiolate polysulphides bound to IscS (Bonomi, Pagani et al. 1985). The presence of reductant DTT was necessary to provide reducing equivalent required for cluster generation and to regenerate the prosthetic group pyridoxal phospate (Urbina, Silberg et al. 2001). I started using 1 μM IscU, 1 μM HscA, 1 μM HscB and 3 mM DTT with 250 μM Cys, 150 μM ATP and 25 μM Fe^{2+} as basic condition. For each experiment, the variation of the absorbance at 458 nm against time was reported.

Although some curves showed a delay, which probably reflects diffusion of the components, the slope of the kinetic curves (absorbance versus time) was measured after the detention time to quantitatively compare the reaction rate. The plot of these values against the protein concentration allowed me to determine the change on the activity of the Fe-S cluster formation.

Increasing IscU concentrations (1, 5, 10, and 20 μM) enhanced the reconstitution rate and shortened the lag phase, reaching a plateau above 5 - 10 μM (figure 4.5). To ensure the higher activity and, at the same time, avoid the contribution to the absorbance due to Fe-S cluster binded to IscU, I thus adopted 8μM concentrations of IscU in the following experiments.

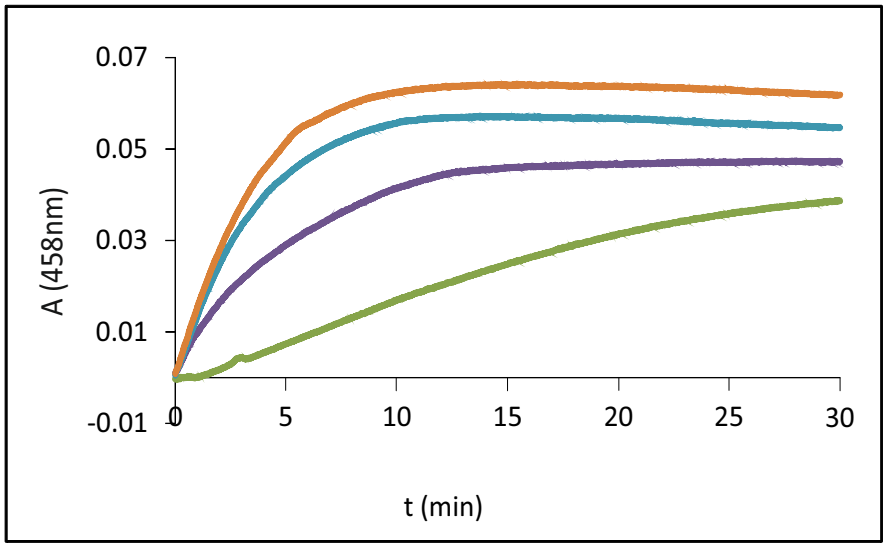

Figure 4.5 (A) Scan of the IscU concentration. Absorbance at 458 nm against the time in the cluster formation on 50 μM Fdx in the presence of 1 μM IscS, 1 μM HscA, 1 μM HscB, 3 mM DTT, 250 μM Cys, 150 μM ATP, 25 μM Fe^{2+} and 10 mM Mg^{2+} in 20 mM Tris-HCl pH 8, 150 mM NaCl. IscU was varied from 1 μM (green) to 5 μM (violet), 10 μM (cyan), 20 μM (orange).

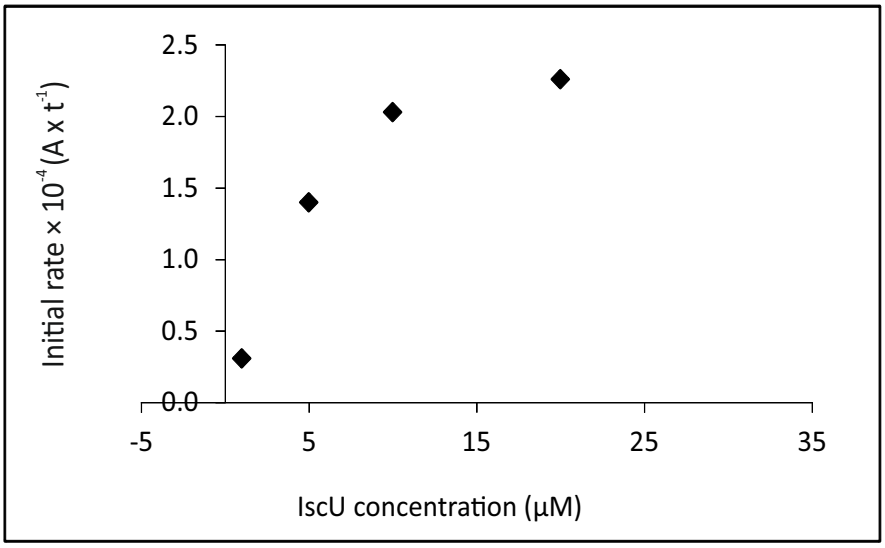

Figure 4.5 (B) Scan of the IscU concentration. Corresponding rates estimated from the slope of the initial part of the curves after the lag time.

A progressive increase of the HscB concentration caused a clear reduction in the reaction rate and in addition the delay was extended (figure 4.6). A 3 μM HscB concentration was adopted in the following experiments to ensure a small excess of protein with respect to IscS in a range of concentrations where inhibition is not dominant.

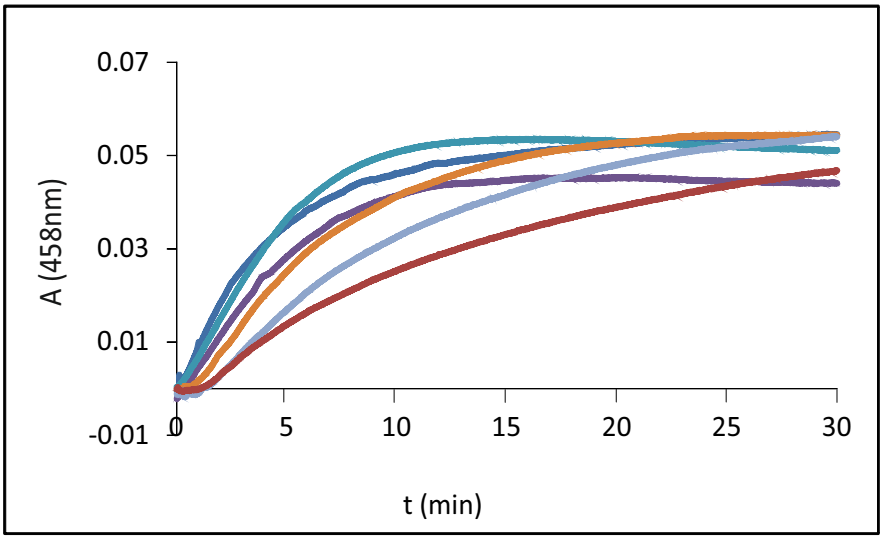

Figure 4.6 (A) Scan of the HscB concentration. Absorbance at 458 nm against the time in the cluster formation on 50 µM Fdx. The concentrations of IscU and HscA were fixed to 8 µM and 1 µM. The other components were as above. HscB was varied from 0 µM (blue) to 5 µM (violet), 10 µM (cyan), 15 µM (orange), 20 µM (pale blue) and 30 µM (red).

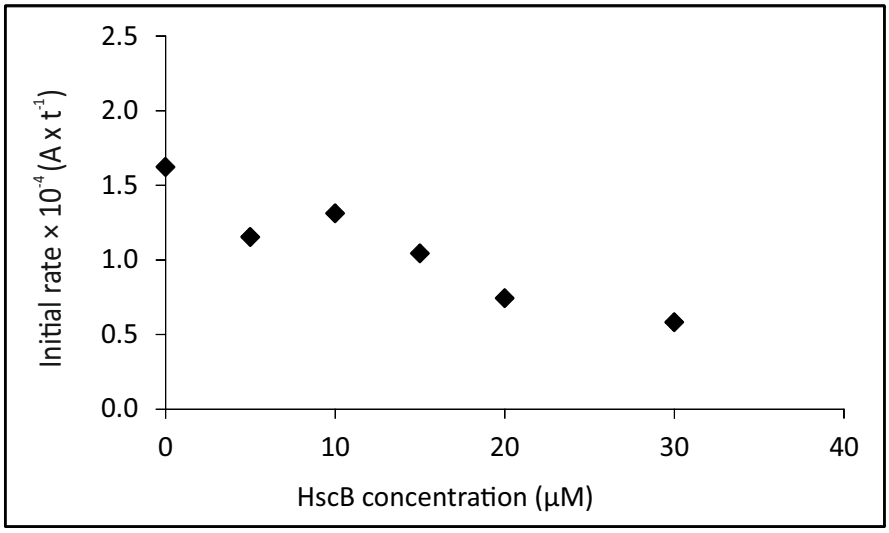

Figure 4.6 (B) Scan of the HscB concentration. Corresponding rates estimated from the slope of the initial part of the curves after the lag time.

Variation of the HscA concentration in the range 1 - 5 µM led to no change of the cluster formation rates. Above ~5 µM, I observed a deep decrease of the rates (figure 4.7). A 2 µM concentration was thus adopted in the following measurement to ensure a small excess of protein with respect to IscS.

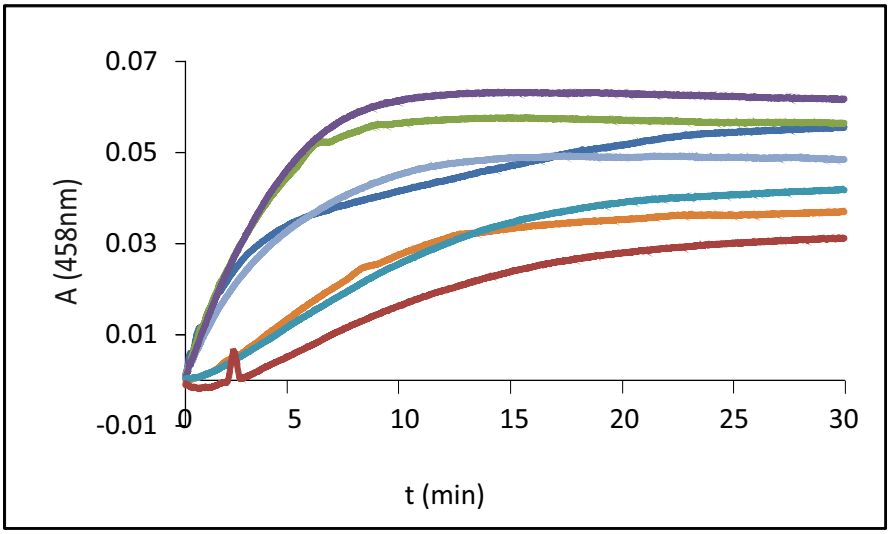

Figure 4.7 (A) Scan of the HscA concentration. Absorbance at 458 nm against the time in the cluster formation on 50 μM Fdx. The concentrations of IscU and HscB were fixed at 8 μM and 3 μM. HscA was varied from 0 μM (violet) to 1 μM (pale blue), 5 μM (green), 10 μM (violet), 15 μM (orange), 20 μM (cyan) and 30 μM (red). The other components were as in the previous experiment.

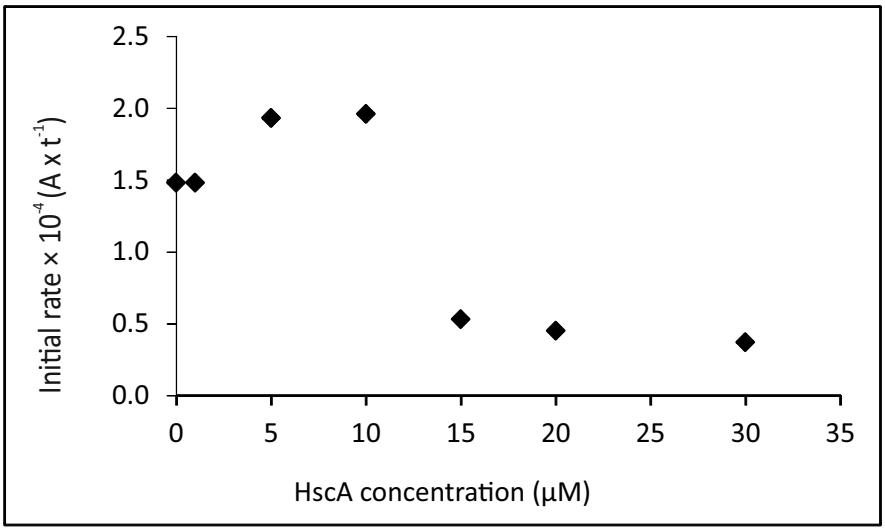

Figure 4.7 (B) Scan of the HscA concentration. Corresponding rates estimated from the slope of the initial part of the curves after the lag time.

Finally, I screened the effect of ATP varying it from 0 to 1 mM in the absence and in the presence of 10 mM Mg^{2+}. When no Mg^{2+} was added I observed a dramatic reduction of the rates up to almost complete inhibition of the reaction (figure 4.8 (A)). The effect was drastically reduced and practically abolished at 10 mM Mg^{2+} which are the concentrations typically used for this assay because close to the cellular conditions (figure 4.8 (B)).

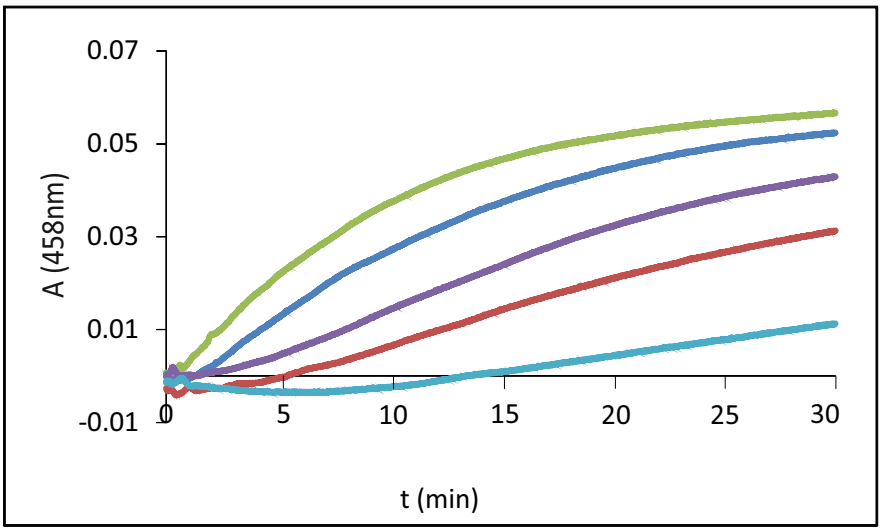

Figure 4.8 (A) Scan of the ATP concentration in the absence of Mg^{2+}. Absorbance at 458 nm was plotted against the time in the cluster formation on 50 µM Fdx. IscS, IscU, HscA and HscB were fixed at 1 µM, 8 µM, 2 µM and 3 µM respectively in 20 mM Tris-HCl pH 8, 150 mM NaCl, 3 mM DTT, 250 µM Cys and 25 µM Fe^{2+}. ATP was varied from 0 µM (green) to 150 µM (blue), 250 µM (violet), 500 µM (red) and 1 mM (cyan).

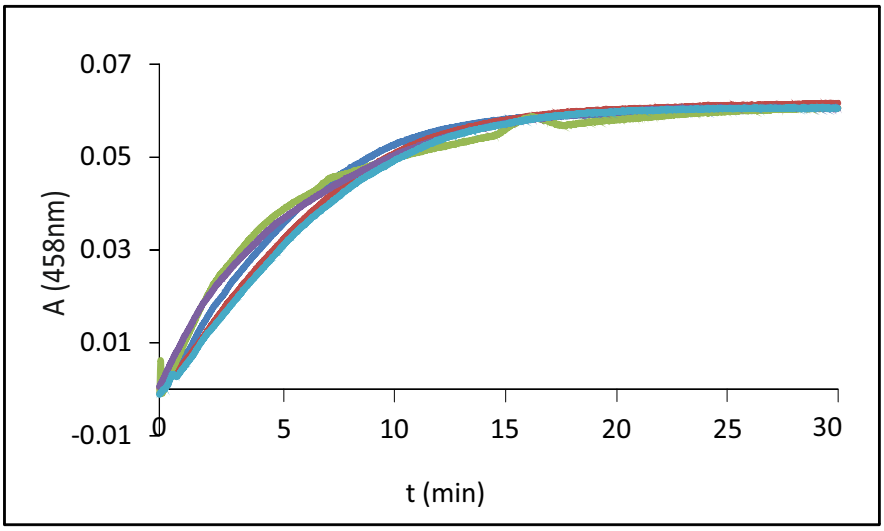

Figure 4.8 (B) Scan of the ATP concentration in the presence of 10 mM Mg^{2+}. Absorbance at 458 nm was plotted against the time in the cluster formation on 50 µM Fdx. IscS, IscU, HscA and HscB were fixed at 1 µM, 8 µM, 2 µM and 3 µM respectively in 20 mM Tris-HCl pH 8, 150 mM NaCl, 3 mM DTT, 250 µM Cys and 25 µM Fe^{2+}. ATP was varied from 0 µM (green) to 150 µM (blue), 250 µM (violet), 500 µM (red) and 1 mM (cyan).

These results showed the effects of the most important Isc components in the kinetics of Fe-S cluster biosynthesis: the increase of IscU concentrations facilitates the constitution of the initial IscS-IscU complex and accelerates the reaction. On the

contrary, the increase of HscA and HscB amounts slows down the process. These results reproduced a previous study that was however carried out mainly in the absence of IscS (Iametti, Barbiroli et al. 2015). ATP content in the presence of Mg^{2+} does not influence the reaction rate, however it has a strong decreasing effect in its absence. A plausible way to explain this is that ATP is well known to chelate iron (Mansour, Thompson et al. 1985, Patchornik, Goldshleger et al. 2000). It would then result in depletion of Fe^{2+} from solution. Mg^{2+}, the counter ion always used with chaperones with ATPase activity, is thus particularly important to compete with Fe^{2+} binding.

4.3 Dissecting the effects on enzymatic activity

I repeated the kinetic experiments of Fe-S cluster formation, exploring the effects of each component to understand the factors for which HscA and HscB behave as inhibitors. I introduced them individually and in pair in the absence and in the presence of 150 μM ATP. I used again Fdx as the reporter, 1 μM of IscS and 8 μM of IscU, in the presence of 250 μM Cys, 25 μM Fe^{2+} and 10 mM Mg^{2+}.

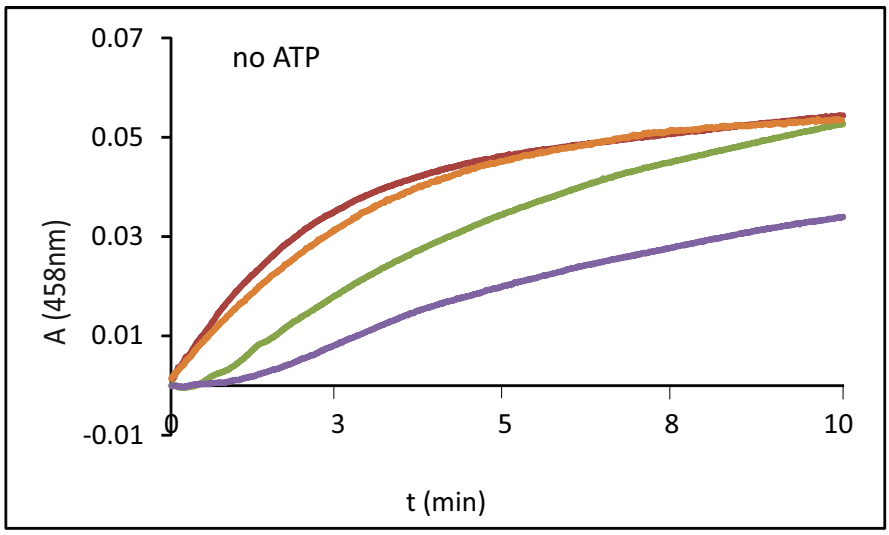

Figure 4.9 Effect of the individual components in the absence of ATP. Absorbance at 458 nm was plotted against the time in the cluster formation on 50 μM Fdx in the presence of 1 μM IscS and 8 μM IscU (control, orange), 10 μM HscA (red), 10 μM HscB (green), 10 μM HscA/HscB (violet) in 20 mM Tris-HCl pH 8, 150 mM NaCl, 3 mM DTT, 250 μM Cys and 25 μM Fe^{2+}.

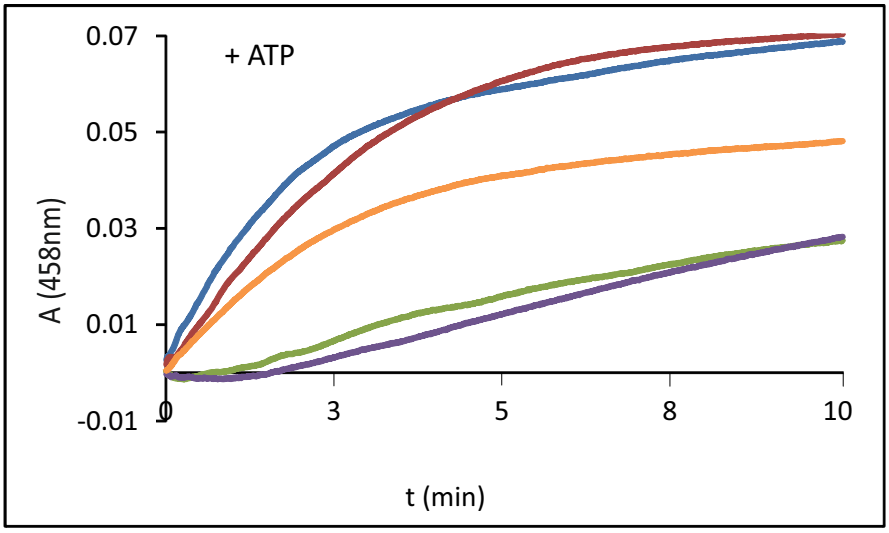

Figure 4.10 Effect of the individual components in the presence of ATP. Absorbance at 458 nm was plotted against the time in the cluster formation on 50 µM Fdx in the presence of 1 µM IscS and 8 µM IscU (control, orange), 150 µM ATP (blue) and with 10 µM HscA (red), 10 µM HscB (green), 10 µM HscA/HscB (violet) in 20 mM Tris-HCl pH 8, 150 mM NaCl, 3 mM DTT, 250 µM Cys, 25 µM Fe^{2+} 150 µM ATP and 10 mM Mg^{2+}.

In the absence of ATP, introduction of HscA (10 µM) does not produce appreciable effects on the enzymatic rates. Addition of HscB (10 µM) remarkably inhibits the rates, while co-addition of HscA and HscB produces a further drop (figure 4.9). In the presence of ATP, addition of HscA increases the rates in a comparable way than when adding only ATP. Addition of HscB, alone or together with HscA and ATP appreciably reduces the rates (figure 4.10). This tells that the effect is mainly due to HscB, either in the presence or absence of HscA.

The effect of HscA appears to be complex and is further complicated by the presence of ATP. I decided to focus on the investigation of the causes of the inhibition effect of HscB. I first repeated the screening of HscB concentrations, but this time in the absence of ATP and HscA.

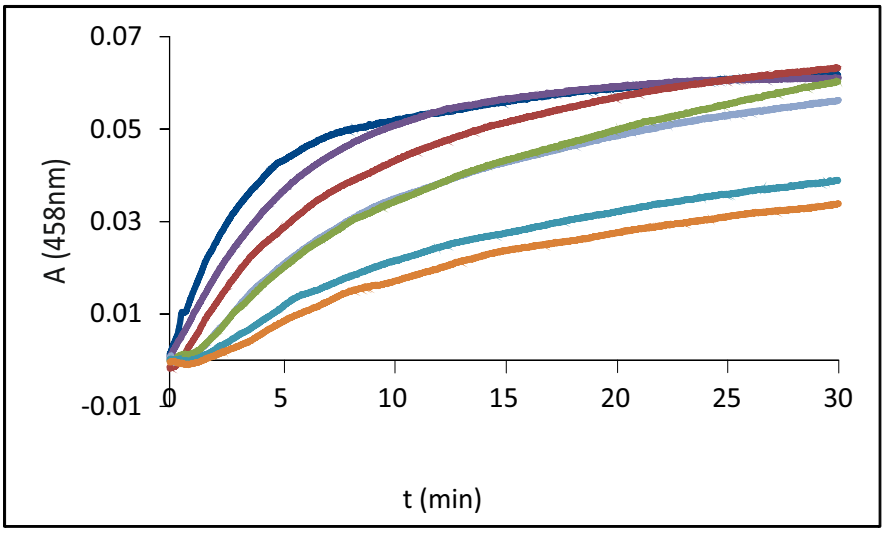

Figure 4.11 (A) Time course of cluster formation on Fdx (50 μM) in the presence of 1 μM IscS, 8 μM IscU, 3mM DTT with 250 μM Cys and 25 μM Fe^{2+} and increasing concentrations of HscB. The curves correspond to no HscB (blue), 3 μM (violet), 5 μM (red), 8 μM (pale blue), 10 μM (green), 20 μM (cyan) and 40 μM (orange) in 20 mM Tris-HCl pH 8, 150 mM NaCl.

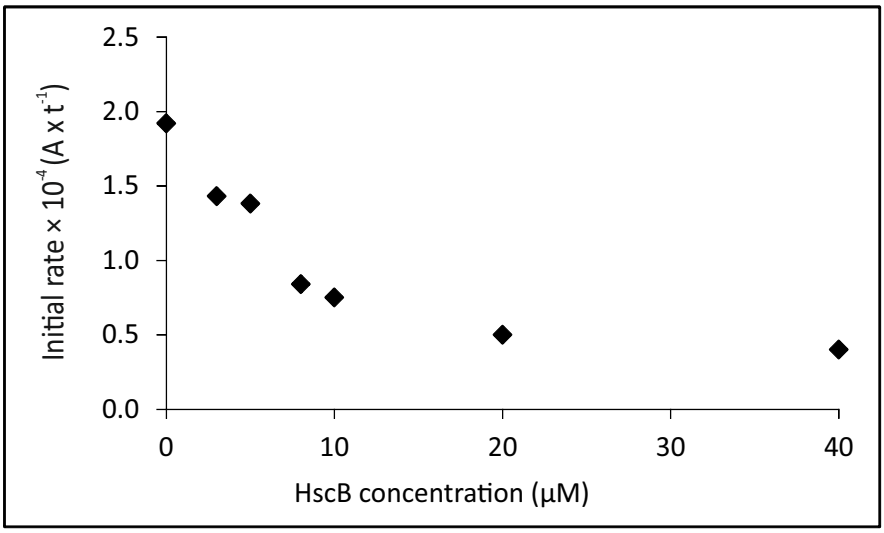

Figure 4.11 (B) Time course of cluster formation on Fdx. Corresponding rates estimated from the slope of the initial part of the curves after the lag time.

I observed a clear progressive drop of the rates. Plotting the slope of the curves versus the concentration I obtained a rate decrease, which reaches a plateau between 20 - 40 μM (figure 4.11). I wondered if the effect could be consequence of the protein reporter used given that Fdx is somewhat a special case because itself belongs to the Isc system and it interacts specifically with IscS (Yan, Konarev et al.

2013). I thus repeated the measurements using aconitase2 (figure 4.12) (Beinert, Kennedy et al. 1996) or IscU (figure 4.13) as reporter (35 µM).

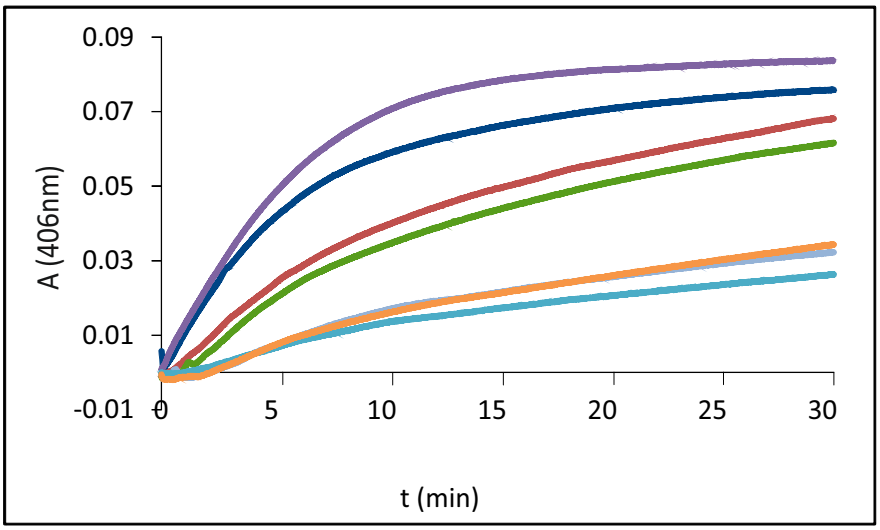

Figure 4.12 (A) Kinetics of cluster formation on aconitase2 (35 µM) in the presence of 1 µM IscS, 8 µM IscU, 3mM DTT with 250 µM Cys, 25 µM Fe^{2+} and increasing concentrations of HscB. The curves correspond to no HscB (blue) and HscB 1 µM (violet), 5µM (red), 10 µM (green), 15 µM (pale blue), 20 µM (cyan) and 40 µM (orange) in 20 mM Tris-HCl pH 8, 150 mM NaCl.

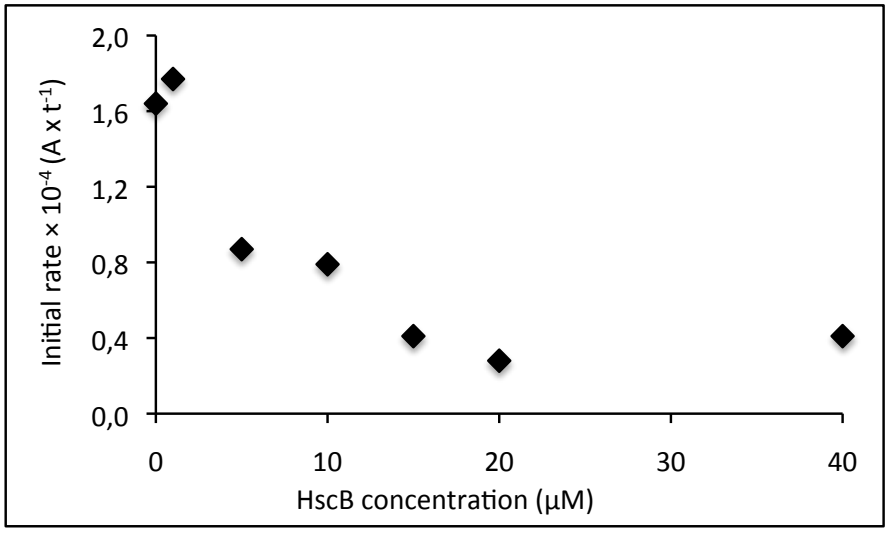

Figure 4.12 (B) Kinetics of cluster formation on aconitase2. Corresponding rates estimated from the slope of the initial part of the curves after the lag time.

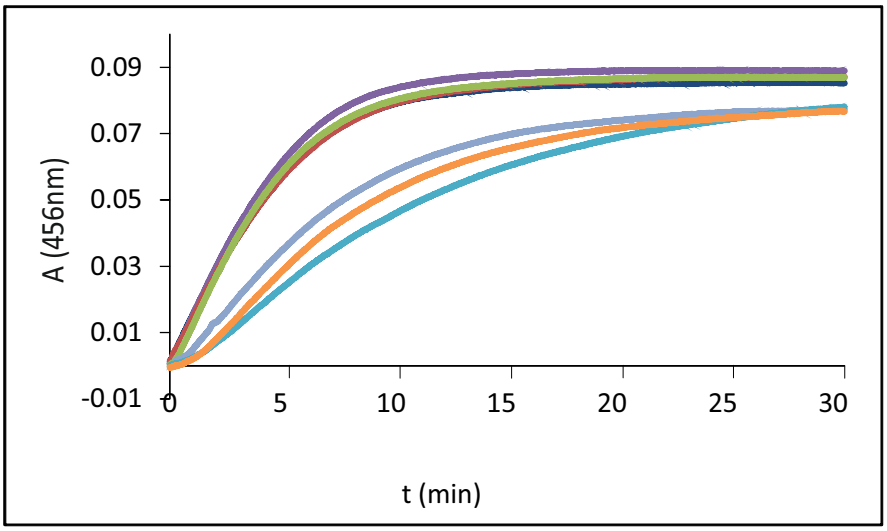

Figure 4.13 (A) Kinetics of cluster formation on IscU (35 µM) in the presence of 1 µM IscS, 3mM DTT with 250 µM Cys, and 25 µM Fe^{2+} and increasing concentrations of HscB. The curves correspond to no HscB (blue), HscB 5 µM (violet), 10 µM (red), 20 µM (green), 25 µM (pale blue), 30 µM (cyan) and 40 µM (orange) in 20 mM Tris-HCl pH 8, 150 mM NaCl.

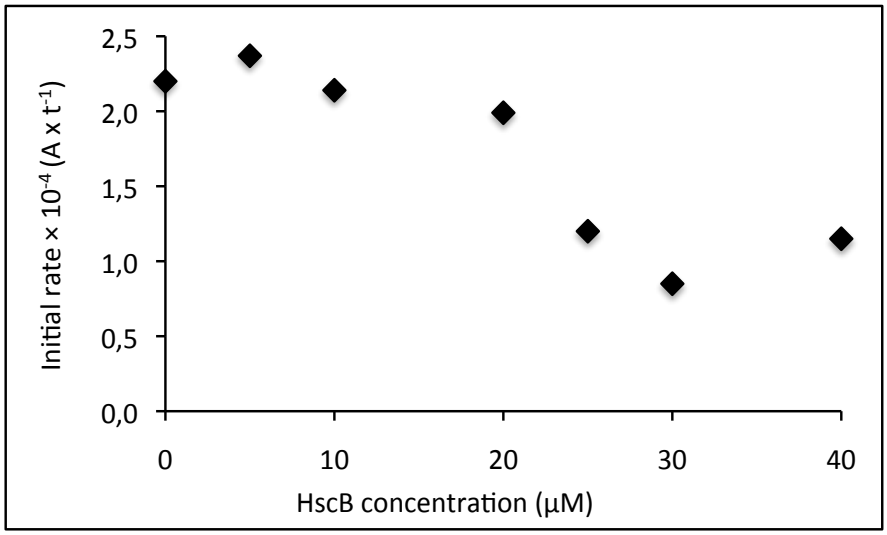

Figure 4.13 (B) Kinetics of cluster formation on IscU. Corresponding rates estimated from the slope of the initial part of the curves after the lag time.

Addition of HscB decreases both rates as in the previous case. The effect is thus due to HscB specifically and it is independent from the reporter.

4.4 Discussion

In the last fifteen years, increasing efforts have been dedicated to understand the mechanism of iron-sulfur cluster biogenesis. *In vitro* studies are essential to clarify

the role of each of the players and understand the chemistry which drives cluster synthesis. A main difficulty in analysing the machine *in vitro* is, however, the complexity of the multi-component system in which each protein can further be in several possible states (oxidized/reduced, cluster-loaded/cluster-free, etc.). The additional presence of iron cations, nucleotides (as ATP) and cysteine further complicate the picture. This increases the number of possible interactions combinatorially.

Probably for this reason, there are still relatively few studies that address the role of HscB and HscA in the Isc machine. Chandramouli and Johnson showed that HscA and HscB from *A. vinelandii* stimulate [2Fe-2S] cluster transfer from IscU to apo-Fdx in an ATP-dependent reaction (Chandramouli and Johnson 2006). These researchers, however, probed only the second step of the reaction recording formation of the cluster on Fdx in the absence of the desulfurase. More recently, a study of the role of HscB and HscA from *E. coli* was carried out by Iametti who showed that HscA/HscB/ATP system has an inhibitory effect when the cluster is formed on IscU and independently from the source of sulfur (chemical or enzymatic) (Iametti, Barbiroli et al. 2015). They also used Fdx as the reporter for chemical cluster formation and observed an enhancement. The effect was explained by the well described interaction between IscU and the chaperones (Hoff, Silberg et al. 2000, Fuzery, Tonelli et al. 2008).

I started my study with the purpose of investigating the effect further. I first explored the multidimensional space of the Isc interactome keeping the minimal number of components (IscA and IscR are thought to enter in the picture as independent players) and optimising the relative concentrations within ranges of concentration biologically reasonable. Comparing the initial reaction rates, it was observed that in the presence of HscA and HscB the activity decreases.

To put more efforts to better understand the role of the chaperones in the Fe-S cluster, I introduced the components individually to identify their contributions. I

observed that HscB, alone and in the co-presence of HscA, could have detrimental effects on the rate of cluster formation depending on their range of concentrations. This is at strong variance with what could have been expected for chaperones intended as “helper of folding” (Silberg and Vickery 2000, Silberg, Tapley et al. 2004).

I then focused on the investigation of the effect of the co-chaperone HscB only. It can be noted that ferredoxin, the protein used as reporter, could be involved itself in the Fe-S cluster biosynthesis since it is encoded by the *isc* operon (Yan, Adinolfi et al. 2013, Yan, Konarev et al. 2013). For these reasons, I looked at HscB influence when Fe-S cluster is formed directly on the scaffold protein IscU or after it is transferred to Aco2. The inhibitor effect of HscB was thus confirmed to be independent from the reporter used.

4.5 Methods

Ferredoxin UV-Vis spectrum

UV-Vis spectra of 10 µM apo and holo-FdX in 20mM Tris-HCl pH 8, 150 mM NaCl and 2 mM DTT were recorded using a Cary 50 Bio Spectrophotometer (Varian) in the range between 240 and 750 nm. A baseline correction was obtained by subtraction of the appropriate buffer spectrum.

Aconitase2 reconstitution experiments

Cluster reconstitution was performed under strict anaerobic conditions in a Belle chamber kept under nitrogen atmosphere. The reaction was followed by absorbance spectroscopy using a Cary 50 Bio Spectrophotometer (Varian). Absorbance between 240 and 800 nm were recorded every 2 minutes. A solution of 30 µM of Aconitase2 was incubated in sealed cuvettes typically using 3 mM DTT, 5 µM IscU, 1 µM IscS and 75 µM $Fe(NH_4)_2(SO_4)_2$ for 30 minutes in 20 mM Tris-HCl pH 8 and

150 mM NaCl. The reaction was initiated by adding 250 µM of the substrate L-cysteine.

Reconstitution experiments

Enzymatic cluster formation was achieved under strict anaerobic conditions in a Belle chamber kept under nitrogen atmosphere. The reaction was followed by absorbance spectroscopy using a Cary 50 Bio Spectrophotometer (Varian). Absorbance variations at 458 nm or 406 nm or 456 nm were measured as a function of time. A solution of 50 µM of apo-Fdx (or 35 µM aconitase2 or 35 µM IscU, depending on the reporter used) was incubated in sealed cuvettes typically using 3 mM DTT, IscU, HscA, HscB, 1 µM IscS and 25 µM $Fe(NH_4)_2(SO_4)_2$ for 30 minutes in 20 mM Tris-HCl pH 8, 150 mM NaCl and 10 mM $MgCl_2$. The reaction was initiated by adding 250 µM of the substrate L-cysteine and when specified 150 µM ATP. Each experiment was repeated at least 3 times on different batches of proteins. To simplify the analysis, I took the initial slopes of the curves (absorbance versus time) to qualitatively compare the time courses.

5. BIOPHYSICAL APPROACH

Investigation of Fe-S cluster enzymatic constitution made by desulfurase IscS and the scaffold protein IscU, showed that the presence of the chaperones HscA and HscB, and in particular the co-chaperone HscB, unexpectedly decreases the initial reaction rate. This is at variance with the hypothesis that they assist the step of cluster transfer causing an increase of the system activity (Chandramouli and Johnson 2006). A reasonable working hypothesis to explain this observation was that one of them could bind the desulfurase IscS interfering with the first step of the cluster biogenesis.

5.1 Effect of HscB on the desulfurase activity

In the reconstitution assay it was not possible to distinguish between the two steps of Fe-S cluster formation and cluster transfer to the acceptor. Several studies have been performed by Bonomi and collaborators to explore the transfer of the Fe-S cluster from holo-IscU to an acceptor in the presence of chaperones (Chandramouli and Johnson 2006, Bonomi, Iametti et al. 2008) and cluster formation on IscU (Iametti, Barbiroli et al. 2015), but the cysteine desulfuration has never been investigated.

To establish if HscB has also an inhibitory effect at the desulfuration step, I turned to Mass Spectrometry. This technique allows the determination of the amount of molecules of a specific molecular weight in the sample. I measured the amount of cysteine and alanine, respectively the substrate and product of the IscS activity. It allowed me to follow the rates of desulfuration.

BOX 2 ***Principle of Mass Spectrometry***

Electrically charged particles are affected by a magnetic field while electrically neutral ones aren't. In Electronspray Mass Spectrometry, proteins and peptides are positively ionised by adding protons. Ions are accelerated so that they all have the same kinetic energy (and speed, v). Their formation and manipulation must be conducted in a vacuum because ions are very reactive and short-lived. They are then deflected by a magnetic field (B) according to their masses (m). The lighter they are, the more they are deflected. The amount of deflection (r) also depends on the number of positive charges (z) on the ion. The more the ion is charged, the more it gets deflected. These two factors are combined into the mass/charge ratio (m/z).

$$r = \frac{m}{z} \cdot \frac{v}{B}$$

The beam of ions passing through the machine is detected electrically: when an ion hits the metal box, its charge is neutralised by an electron jumping from the metal on to the ion. That causes a flow of electrons which is detected as an electric current. The more ions arriving, the greater is the current. By varying the strength of the magnetic field B, ions of different mass can be focused progressively on the detector. The machine can be calibrated to record current against m/z directly.

I designed an experiment with the purpose of measuring the desulfurase activity of IscS by detecting the progressive disappearance of cysteine and concomitant appearance of alanine. The assay was carried out in the absence of IscU. I prepared samples containing 1 µM IscS and 3 mM DTT in 20 mM Tris-HCl pH8 and 150 mM NaCl. Once the reaction was initiated by adding 250 µM of cysteine, a mixture of acetic acid/acetonitrile was used to stop it at different time points (0, 10, 20, 40, 60 min). This agent precipitates and denatures proteins. The experiment

was then repeated in the presence of 3 μM of HscB. The samples were then given to the Mass Spectrometry facility at King's College London for the determiation of the amino acid amounts.

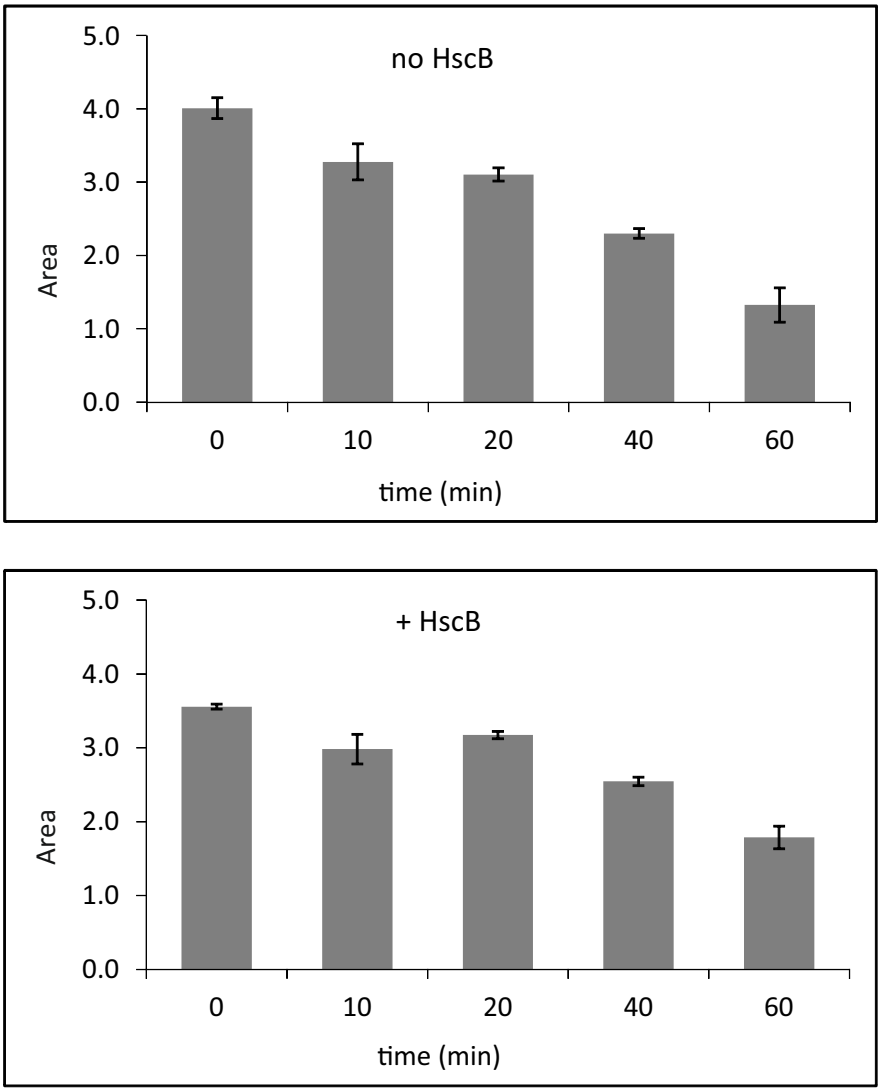

Figure 5.1 Quantification by MS of Cysteine consumption by IscS (1 μM) in 20 mM Tris-HCl at pH 8, 150 mM NaCl and 3mM DTT (top) and in the presence of 3 μM HscB (bottom).

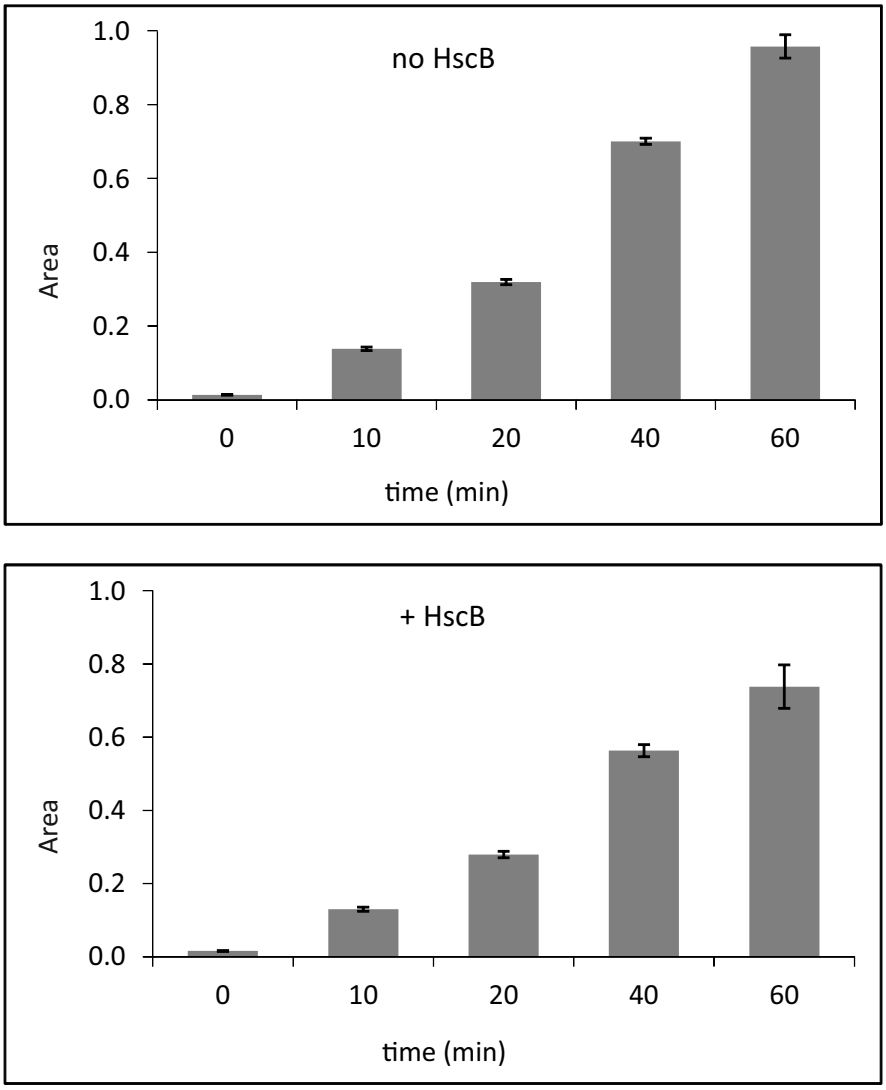

Figure 5.2 Quantification by MS of Alanine production by IscS (1 µM) in 20 mM Tris-HCl at pH 8, 150 mM NaCl and 3mM DTT (top) and in the presence of 3 µM HscB (bottom).

Comparison showed a lower consumption of cysteine in the presence of co-chaperone HscB (figure 5.1) that results in a lower formation of alanine (figure 5.2). I concluded that the reaction is slowed down.

Altogether, this result with the previous biochemical investigation (see chapter 4) tell that the inhibitory effect is mainly linked to HscB but it is not only due to the interaction between IscU and HscB as previously suggested by Iametti (Hoff, Silberg et al. 2000, Iametti, Barbiroli et al. 2015): HscB has also effects on the desulfurase step and thus on IscS.

5.2 HscB interacts with IscS

A reason why HscB could affect the enzymatic activity of IscS is the formation of a complex between the two proteins. This hypothesis is reasonable not only if a binding is proved but also if HscB binds on a surface important for the progress of IscS activity.

I thus carried out several assays to test the binding and find the surface involved.

5.2.1 Pull-down assays

The pull-down assay represents a simple method to determine interactions between proteins.

BOX 3 ***Principle of pull-down assay***

A pull-down assay is a small-scale affinity purification technique. A bait protein is tagged and immobilized on a surface by affinity ligand specific for the tag. It generates a secondary affinity support for the purification of other proteins (prey proteins) that bind with the bait protein. Proteins are then together eluted depending on the affinity of primary ligand and revealed by SDS-Page.

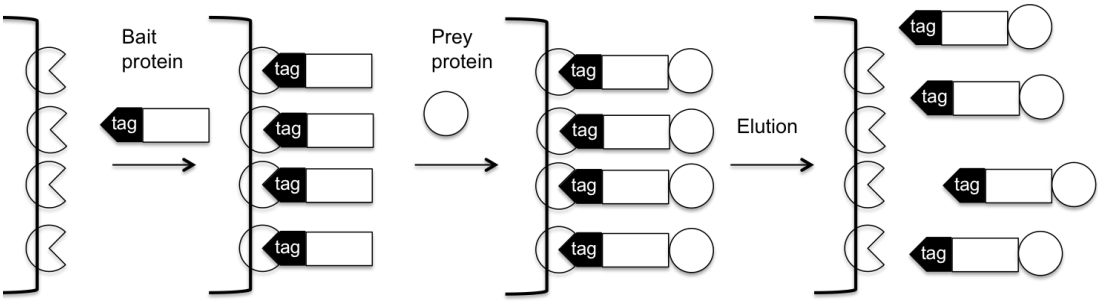

Figure 5.3 Schematic representation of a pull-down assay.

His-tag and GST-tag are suitable tags for this kind of assay because the His-tag allows proteins to bind specifically the Ni-NTA resin and the GST-tag allows the binding to glutathione sepharose resin.

First IscS was chosen as the bait protein: it was expressed and purified in a His-tagged form. It was incubated for 30 minutes with the partner HscB in a ratio of 1:10 and then passed on Ni-NTA resin equilibrated with 20 mM Tris-HCl pH 8, 150 mM NaCl and 2 mM DTT. The same assay was carried out with the reverse combination of bait/prey protein. HscB was expressed and purified with a His,GST-tag, incubated half an hour with untagged IscS in a ratio of 1:10 and loaded on a glutathione sepharose resin. After extensive washing with the same buffer, supernatant and resins were loaded on a SDS PAGE gel to reveal proteins present in the final mixtures.

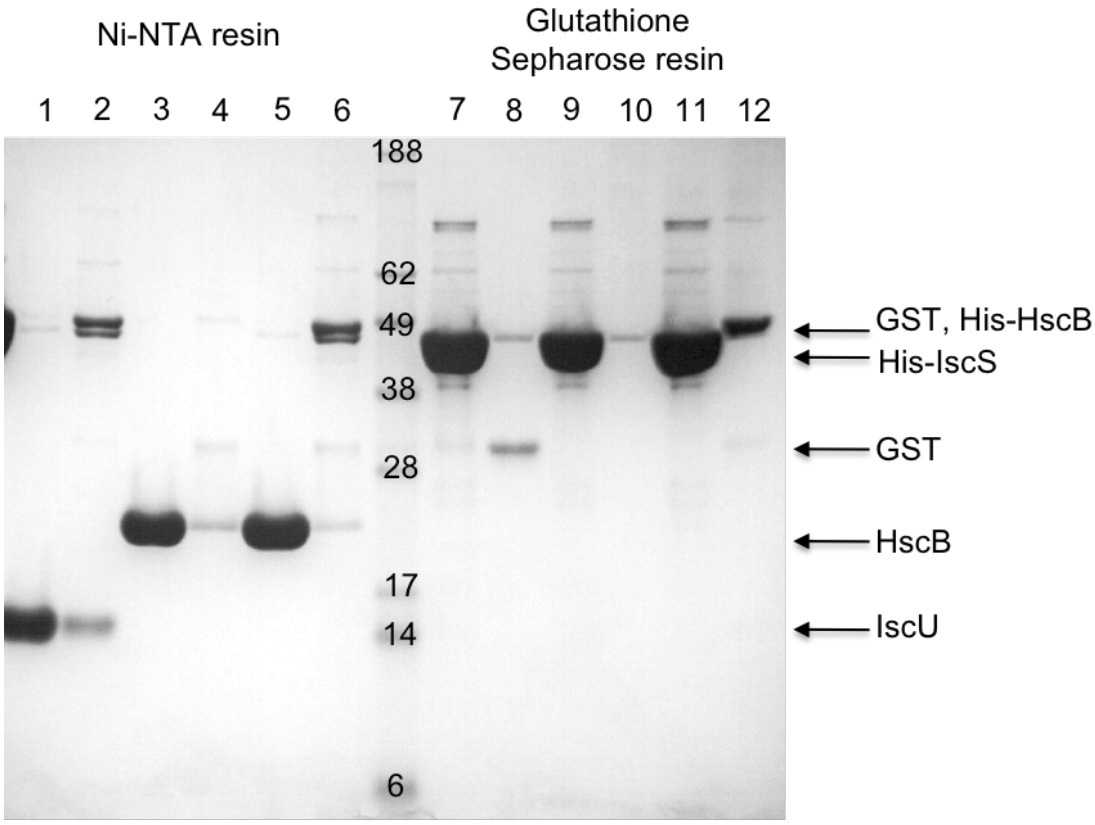

Figure 5.4 SDS PAGE after pull-down assays. Each column shows the sample purity components separated by molecular weight. 1. His-IscS+IscU (1:10) supernatant. 2. His-IscS+IscU (1:10) Ni-NTA resin. 3. HscB supernatant. 4. HscB Ni-NTA resin. 5. His-IscS+HscB (1:10) supernatant. 6. His-IscS+HscB (1:10) Ni-NTA resin. 7. GST+IscS supernatant. 8. GST+IscS Glutathione Sepharose resin. 9. IscS supernatant. 10. IscS Glutathione Sepharose resin. 11. His,GST-HscB+IscS (1:10) supernatant. 12. His,GST-HscB+IscS (1:10) Glutathione Sepharose resin.

The PAGE gel in figure 5.4 distinguishes protein in accordance with their molecular weight. On the left side of the marker were loaded the samples flowed (odd numbers) or captured on Ni-NTA resin (even numbers), on the right side samples flowed (odd numbers) or captured on Glutathione Sepharose resin (even numbers). To test the effectiveness of the procedure, the assay was carried out with a mixture of His-IscS and IscU, whose interaction is already well characterized in the literature (Urbina, Silberg et al. 2001, Kato, Mihara et al. 2002). IscU was captured by His-IscS on the Ni-NTA resin (sample 2) and the excess was discarded in the supernatant (sample 1). Samples 3 and 4 were run as a control to ensure that HscB does not bind the Ni-NTA column in the absence of the tag. A weak affinity was observed (sample 4). Then the binding between His-IscS and HscB was tested. The prey protein HscB was found in the supernatant (sample 5) without binding the bait protein significantly (sample 6). Analogous results were obtained with His,GST-HscB and IscS on Glutathione Sepharose resin (samples 11 and 12). Samples 7 and 8 showed a small affinity of IscS for GST protein. Samples 9 and 10 showed that the prey protein IscS has a small affinity also for the Glutathione Sepharose resin.

The pull-down assay results to be ineffective to determine binding with low affinity as it could be supposed for IscS and HscB.

5.2.2 Size Exclusion Chromatography

Size Exclusion Chromatography (SEC) is applied to separate a wide range of molecules according to size. It is helpful to determine the molecular weight and analyse aggregates and complex formation. A mixture made by HscB and IscS was passed on a SEC column to determine the formation of their complex.

BOX 4 *Principle of Size Exclusion Chromatography*

Size Exclusion Chromatography is a chromatographic method in which molecules are separated by their size. The column used is filled with material containing many pores. When molecules of various sizes flow into the column, smaller molecules flow more slowly through the column because they penetrate deep into pores, whereas large molecules flow quickly because they do not enter the pores. Consequently larger molecules elute from the column sooner and smaller later. Proteins are usually separated by gel filtration chromatography, which uses a hydrophilic packing material and an aqueous mobile phase.

A Superdex 200 HR 10/30 column was chosen because it gives an excellent resolution of proteins and peptides in the molecular weight range of 10 and 600 kDa. In principle, it is able to discriminate between IscS (dimer of 90 kDa), HscB (21 kDa) and their complex of around 130 kDa.

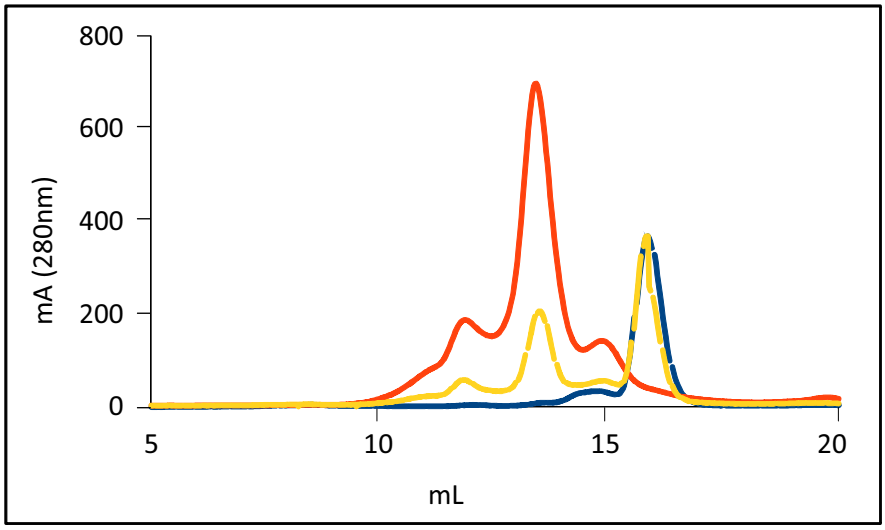

Figure 5.5 SEC chromatogram. Absorbance at 280nm of the 120 μM HscB sample during SEC course (blue), 140 μM IscS (red) and the mixture 1:2 of IscS:HscB (yellow) in 20 mM Tris-HCl pH 8, 150 mM NaCl, 2 mM DTT.

The desulfurase IscS (140 μM), the co-chaperone HscB (120 μM) and then a mixture of them (IscS:HscB 1:2), were loaded on the column and eluted with a 20 mM Tris-HCl pH8, 150 mM NaCl and 2 mM DTT buffer. A SDS PAGE gel confirmed the purity of proteins in the fractions. While IscS seemed to be present mostly as a dimer but also as a bigger aggregate (maybe as tetramer) and as monomer, HscB appeared as a single peak. The mixture of the two proteins showed a curve that corresponds exactly to the superimposition of the two single contributes and no other peak corresponding at higher molecular weight appeared (figure 5.5). This result suggests that the complex is not enough stable and is disassembled through the resin.

5.2.3 Crosslinking

After the above experiments, I became convinced that if there was an interaction between IscS and HscB, it was too weak because the complex could survive and be detected with methods of protein separation. I attempted thus the chemical crosslinking which is a technique able to capture weak or transient protein-protein interactions (Watson, Mahajan et al. 2012).

BOX 5 ***Principle of crosslinking***

Crosslinking is the process of chemically joining two or more molecules by a covalent bond. Crosslinkers are used for the identification of near-neighbor protein relationships as well as ligand-receptor interactions.

Crosslinking reagents could have spacer arm of different length and they contain ends reactive to specific functional groups, such as primary amines and sulfhydryls. Homobifunctional, amine-reactive NHS esters or imidates, and heterobifunctional, amine-reactive photoactivable phenyl azides are the most commonly used crosslinkers for these applications. Sometimes can be used reversibles crosslinkers

with a disulfide bond in the spacer arm that can be easily reduced with DTT.

The availability of several chemical groups in proteins and peptides make them favourable targets for conjugation using crosslinking methods.

To identify the interaction, I tested two homobifunctional amine-to-amine crosslinkers that use imidoester and N-hydroxysuccinimide ester (NHS-ester) reactive groups for selective conjugation of primary amines: Dimethyl adipimidate (DMA) and Bis[sulfosuccinimidyl]suberate (BS^3).

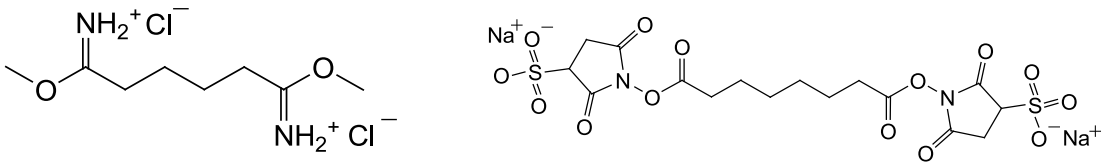

Figure 5.6 Crosslinkers structure of DMA and BS^3.

DMA is a water soluble homobifunctional imidoester crosslinker. The imidoester functional group is one of the most specific acylating group available for the modification of primary amines and has minimal cross reactivity toward other nucleophilic groups in proteins. It obviously means that in the assay, buffers amine-containing (such as Tris-HCl) must be avoided. Proteins have primary amines in the side chain of lysine residues and in the N-terminus of each polypeptide that are available as targets. DMA reacts with amines at pH 7 - 10 and its reaction is reversible at high pH values. It has a spacer arm length of 8.6 Å.

BS^3 is a water-soluble and non-cleavable crosslinker. It has an 8-carbon spacer arm of 11.4 Å that contains an N-hydroxysuccinimide ester at each end. NHS esters react efficiently with primary amino groups (-NH_2) in pH 7 to 9 buffers to form a

stable amide bond. Buffers must not contain primary amines. Thus phosphate, borate, carbonate and HEPES are useful. The reaction results in the release of N-hydroxysuccinimide.

Before starting with the crosslinking assay, the buffer had to be exchanged from 20 mM Tris-HCl pH 8, 150 mM NaCl, 2 mM DTT to PBS with NAP-5 Sephadex columns. I then added the crosslinking agent in excess (1.3 mM) to a mixture containing HscB (30 μM) and IscS (5 μM). After 30 minutes the reaction was quenched with 20 mM Tris-HCl.

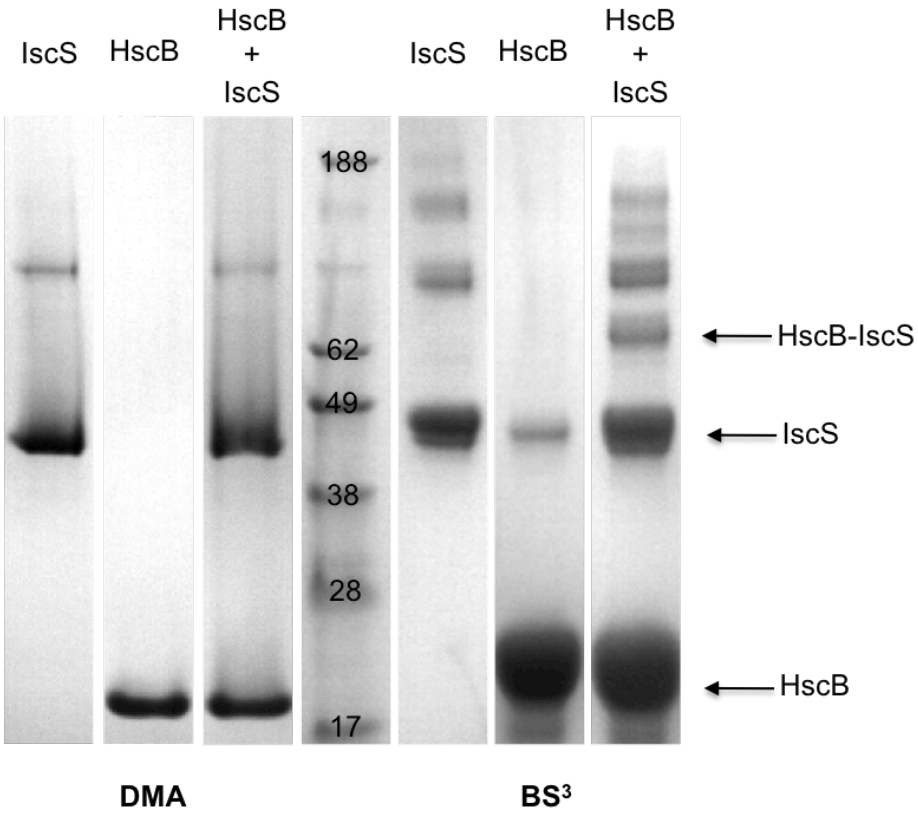

Figure 5.7 SDS PAGE after crosslinking assay. Each column shows the sample purity components separated by molecular weight. IscS (5 μM), HscB (5 μM) and IscS:HscB (1:6) mixture in the presence of crosslinker DMA 1.3 mM (left) or BS^3 1.3 mM (right) in PBS buffer.

SDS PAGE on figure 5.7 revealed the species present in the samples by separating them as a function of their molecular weight. In the mixture containing HscB and IscS with DMA no other band in addition to the free proteins appeared. On the

contrary, the presence of a new species at around 65 kDa, which corresponds to HscB-IscS covalently bound, was revealed in the sample with BS^3. Other bands can be observed at higher molecular weight that correspond to IscS dimer (and possibly trimer and tetramer, as observed in the control containing IscS alone) and the IscS-HscB dimer. While DMA has not a spacer arm sufficiently long, BS^3 is able to join together HscB and IscS. This proved that the two proteins could weakly bind each other.

5.2.4 NMR-T1 relaxation measurement

The observation of a crosslinked band at the expected mass for the HscB-IscS complex is a good evidence, but the interaction had to be confirmed with an independent and complementary method. I used the nuclear magnetic resonance (NMR) technique as time of relaxation changes if a species of higher dimension is formed.

BOX 6 ***Principle of NMR and time of relaxation***

Nuclear Magnetic Resonance uses the difference of energy of nuclear spin $\Delta E = \gamma \hbar B_0$ that arises in the presence of a magnetic field B_0. This corresponds to the frequency, called Larmor frequency, $\nu = \frac{\gamma B_0}{2\pi}$, where γ is the gyromagnetic ratio, an intrinsic and specific property of the nucleus. Spins align along B_0 and the resultant magnetisation M_0 starts a precessional orbit around it. When a radio frequency (RF) pulse is applied, it causes another simultaneous precessional movement of the magnetization along the direction of this second magnetic field, B. The signal is recorded as energy emitted after the RF pulse as function of time (free induction decay, FID) and then it is Fourier transformed to give a plot as function of frequency.

In NMR the relaxation is the phenomenon by which the system returns to

equilibrium after the impulse and the magnetisation comes back along the direction of B_0. There are several phenomena of relaxation. The most important are the spin-lattice relaxation (T1) and the spin-spin relaxation (T2). The relaxation is induced by field fluctuation due to molecular motion and local field experienced when the molecule reorients.

The spin-lattice relaxation is the process that returns the magnetization to the B_0 direction (Z-axis). This process can be measured with inversion recovery experiment.

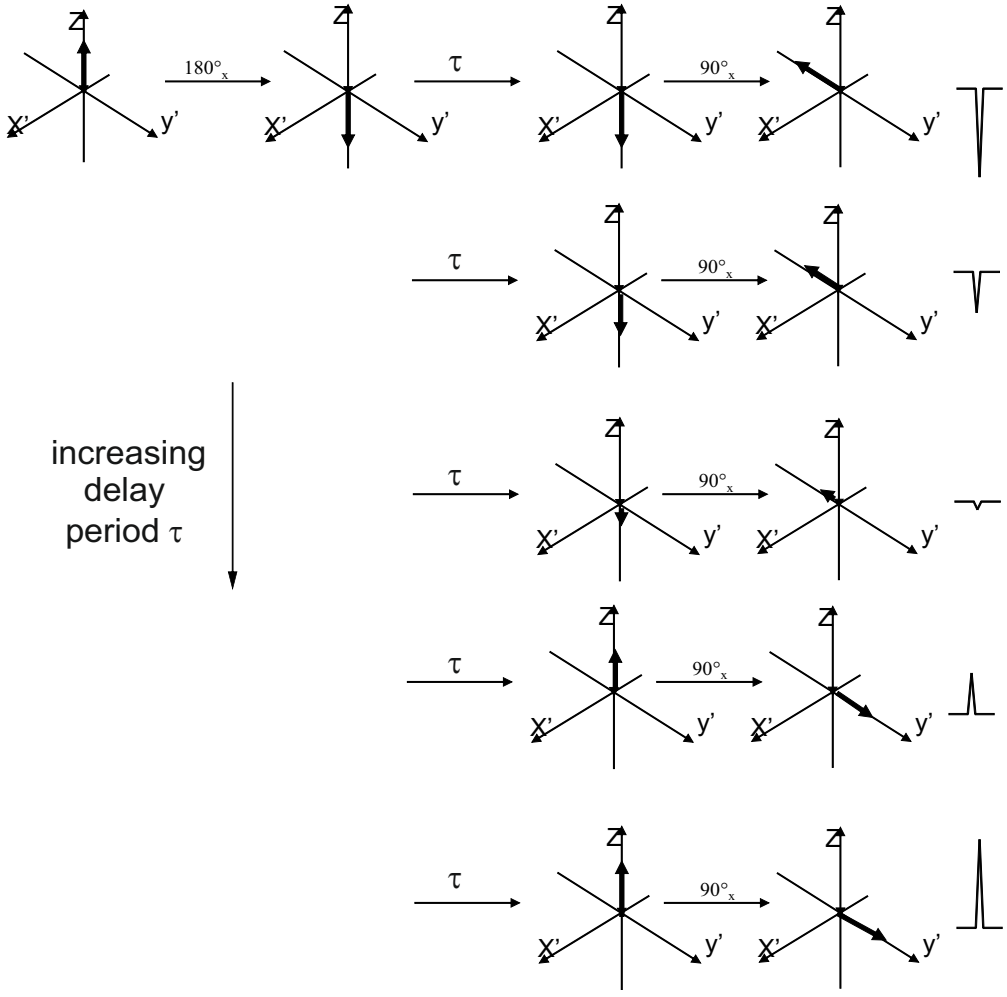

Figure 5.8 Inversion recovery schematization. The magnetization is first inverted before the acquisition. After a delay a second pulse is applied and the signal is rcorded.

In the inversion recovery pulse sequence, a $180°_x$ pulse is first applied. This rotates the net magnetization down to the –Z axis. The magnetization undergoes

spin-lattice relaxation and returns towards its equilibrium position along the +Z axis. Before it reaches equilibrium, a $90°_x$ pulse is applied which rotates the longitudinal magnetization into the XY plane. Once the magnetization is present in the XY plane, it rotates about the Z axis and dephases giving a FID. The equation that describes this phenomenon is

$$M_z = M_0(1 - e^{-t/T1})$$

T1 relaxation is caused by transient magnetic fields (usually due to molecular motions) at the Larmour precession frequency, so relaxation is optimal if the average rate of molecular reorientation in space is at this frequency. For small molecules at room temperature the average rates of molecular rotation are several orders of magnitude higher leading to very inefficient relaxation (long T1). For bigger molecules motions become slower and more efficient relaxation results (short T1). However, at some point the average molecular motions become so slower than Larmour precession frequency that T1 becomes longer again.

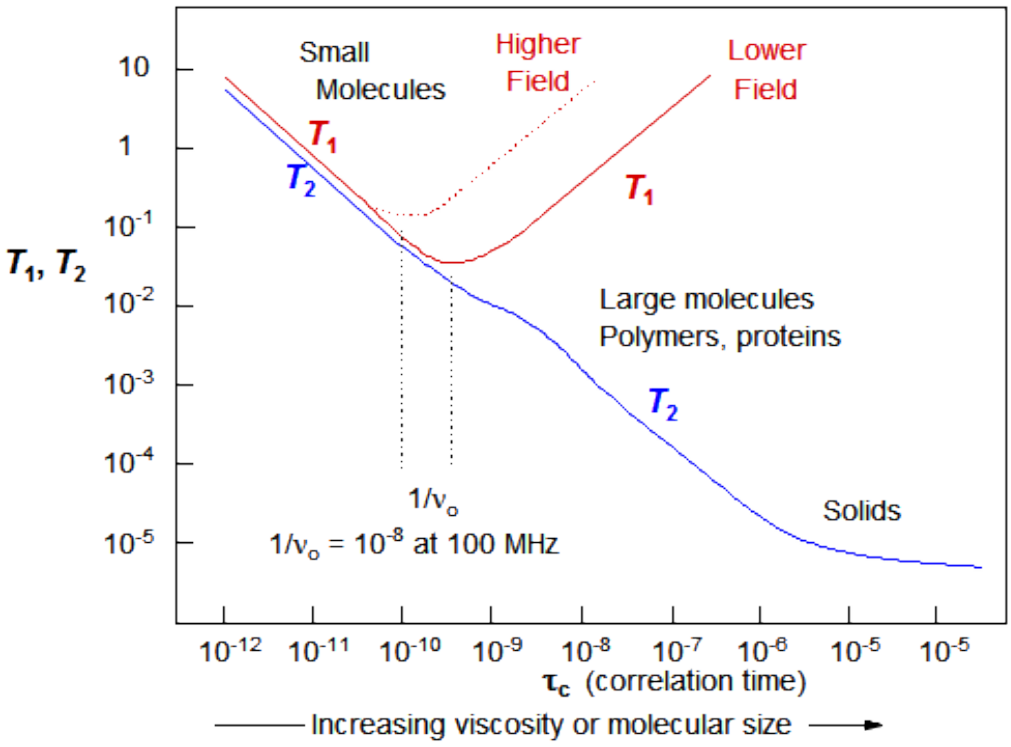

Figure 5.9 Behaviour of T1 and T2 as a function of the correlation time, τ_C, the time it takes the average molecule to rotate one radian (Purcell 1948).

After a pulse, the magnetization becomes coherent in phase in the XY plane. However, each spin undergoes to a different magnetic field and rotates with its own Larmor frequency. This causes a loose of phase coherence of the magnetization. With time the difference of phase increase. This relaxation phenomenon is called Spin-Spin relaxation. This process can be measured with the Spin-Echo experiment. The spin-spin relaxation is described by the equation

$$M_{xy} = M_0 e^{-t/T2}$$

While the longitudinal magnetization increase along the Z axes to reach the M_0 value, the resultant magnetization in the XY plane decrease to zero. T2 relaxation is caused by transient magnetic fields at any frequency. It is determined by the combination of two contributions: molecular interactions and magnetic field disomogenity. T2 keeps getting shorter as molecular reorientation rates slow down.

Molecular motions induce a magnetic field fluctuation and affect the relaxation times. These are affected also by system dimensions because larger proteins show overall slower molecular motions.

NMR experiments were carried out to determine T1 relaxation time of free HscB ^{15}N labelled (160 μM). The spectrum was recorded with an inversion recovery sequence and using delays (τ) of 10, 100, 200, 400, 700, 1000, 1500, 2000 and 2500 ms. The same was repeated for the complex formed by ^{15}N-HscB:IscS (1:0.6). For every residue the T1 relaxation time was calculated by fitting the intensity of the peak against the time (τ). Only residues with a weighted root mean square (wrms) between 0.75 and 1.25 were considered.

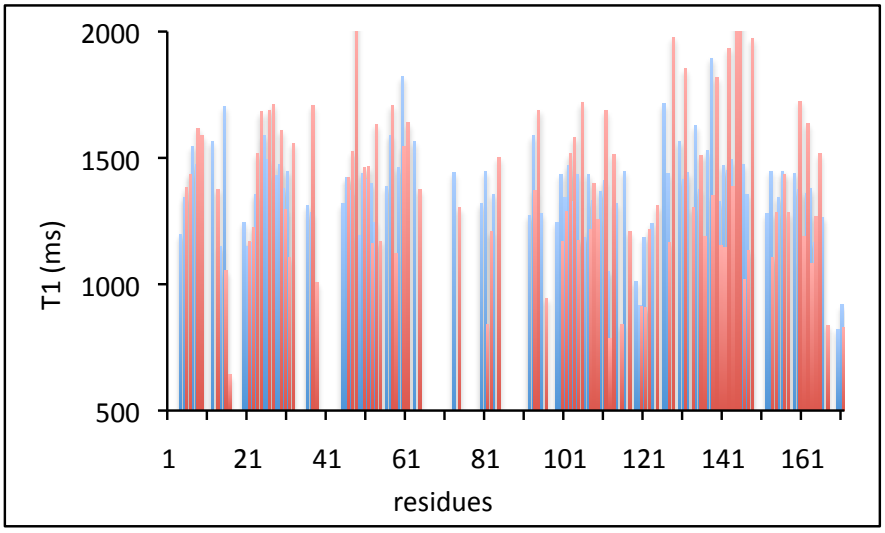

Figure 5.10 (A) Relaxation T1 comparison between residues of free HscB (blue) and HscB:IscS mixture (1:0.6) (red) at 298 K.

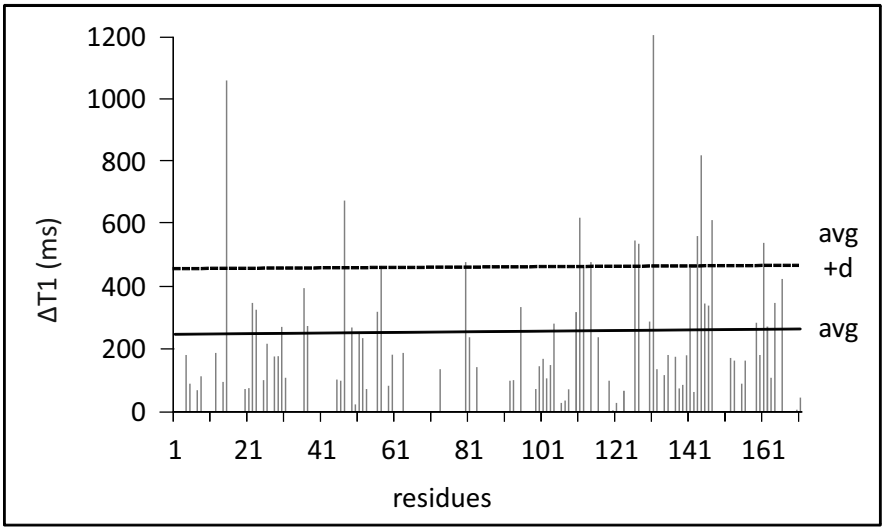

Figure 5.10 (B) Relaxation T1 comparison. Difference between T1 values for the expected complex HscB:IscS and for the free protein HscB at 298 K.

The estimated T1 resulted to be 1385±81 ms for the HscB:IscS mixture and 1356±342 ms for free ^{15}N-HscB. This would not support an overall change of the average value. However, when I calculated the difference between the T1 values for the expected complex and for the free protein, I could observe that for a relevant number of residues in a specific region of the protein (C-teminus), the T1 value variation overseeded the average of the differences (249 ms) plus one standard deviation (figure 5.10 (B)). This suggests that the protein is locally affected by the presence of IscS and it is consistent with a local weak interaction.

The change in relaxation time, together with the crosslinking assay, confirmed that HscB could bind the desulfurase IscS.

5.3 HscB binds IscS with micromolar affinity

To complete the characterization of the interaction between IscS and HscB, this was quantified by determining the affinity constant of binding (K_D). Several techniques allow the determination of the binding constant by measuring a biophysical property of the system. Among those I attempted was the most common, Isothermal Titration Calorimetry, which measures the heat exchanged, and Microscale thermophoresis which measures changes in the mobility of molecules in microscopic temperature gradients.

5.3.1 Isothermal Titration Calorimetry

When binding occurs, heat is either absorbed or released. This is measured by a sensitive calorimeter during gradual titration of the ligand into the sample cell containing the protein. The quantity of the heat measured is in direct proportion with the amount of the binding and provides the binding constants (K_D), the reaction stoichiometry (n), the enthalpy (ΔH) and the entropy (ΔS), without the need for labels.

BOX 7 ***Principle of Isothermal Titration Calorimetry***

Isothermal Titration Calorimetry (ITC) measures heat evolved or absorbed in solutions as a result of mixing precise amounts of reactants. A pair of identical cells is enclosed within two shields; the inner shield is referred to the jacket. Both cells are completely filled with liquid during operation to avoid differences in volume. Temperature differences between the reference cell and the sample cell are measured. The output signal is the differential power (DP) between the reference

cell and the sample cell. It represents the power used to maintain temperature equilibrium.

In a typical experiment, a syringe containing a ligand is used to inject into the cell containing the protein to be titrated. If the reaction is exothermic, the injection results in the evolution of heat within the sample cell and causes a negative change in the DP. The opposite is true for endothermic reactions.

The time integral of the peak yields a measurement of the thermal energy. This heat is released or absorbed in direct proportion to the amount of binding that occurs.

When the protein in the cell becomes saturated with added ligand, the heat signal diminishes until only background heat of dilution is observed. A fitting model can be used to analyze ITC data and calculate reaction stoichiometry (n), binding constant (K_D), enthalpy (ΔH) and entropy (ΔS) using the equations of thermodynamic.

$$\Delta G = \Delta H - T\Delta S = RT \ln K_D$$

Titrating a solution of 40 μM IscS with a series of small aliquots of 320 μM HscB, I obtained a noisy curve perfectly superimposable with the curve of dilution of HscB in the buffer (20 mM Tris-HCl pH 8, 150 mM NaCl, 2 mM DTT) (figure 5.11). Furthermore a precipitate appeared in the cell suggesting that IscS is not stable in these conditions.

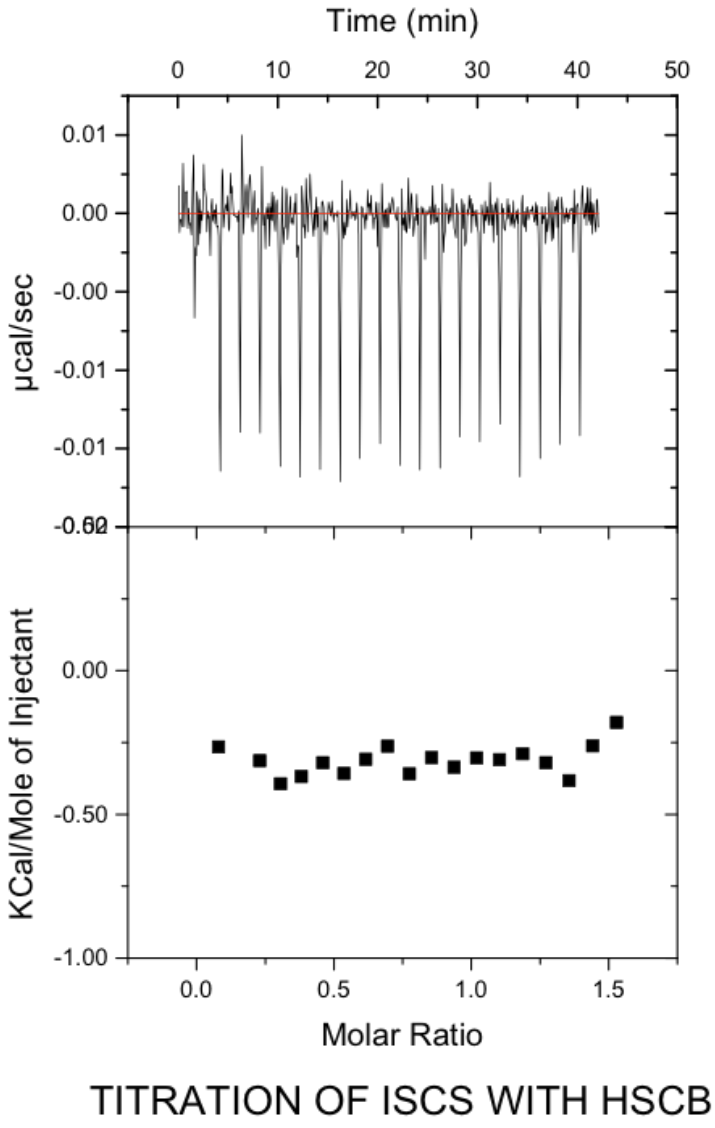

Figure 5.11 (A) ITC measurements. Peaks indicate the heat released after each addition of binding protein HscB 320 µM into the cell containing IscS 40 µM in 20 mM Tris-HCl pH 8, 150mM NaCl, 2 mM DTT. In the lower panel data were converted in heat released per mole of HscB added.

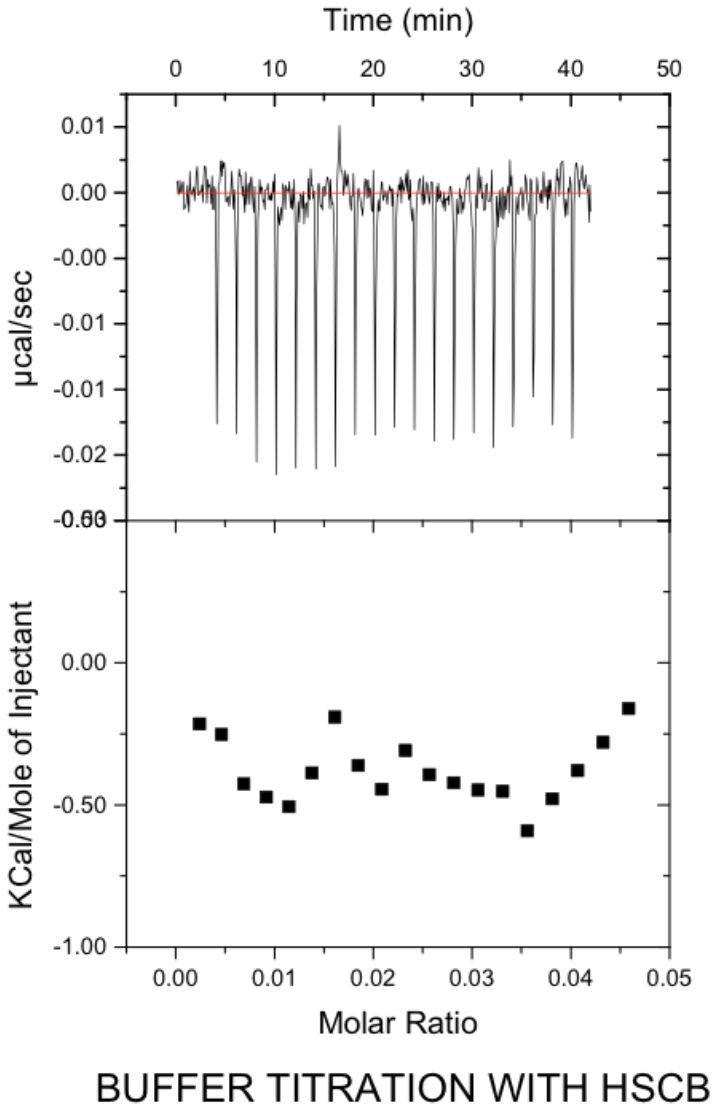

Figure 5.11 (B) ITC asurements. Buffer (20 mM Tris-HCl pH 8, 150mM NaCl, 2 mM DTT) was titrated with 320 µM HscB to obtain a reference curve.

ITC assays proved inconclusive to obtain a binding constant, as it can be expected for weak complexes. The quantitative determination of the binding between IscS and HscB needed an approach where a sensitive technique was used, able to reveal also weak interaction, and without particular conditions of temperature or pH that could result unfavourable for the protein folding.

5.3.2 Microscale Thermophoresis

Changes in the hydration shell, charge or size, of molecules cause changes of the mobility of molecules in a temperature gradient. This phenomenon is called thermophoresis. As the interaction of a molecule with another changes at least one of these properties, Microscale Thermophoresis (MST) turns out to be a sensitive means to measure also weak interactions (Jerabek-Willemsen, Andre et al. 2014) with a K_D in the range of 1 nM - 500 mM. In MST molecular movements inside a capillary of a protein labelled with a fluorescent-dye are monitored by measuring the fluorescence distribution.

BOX 8 ***Principle of MicroScale Thermophoresis***

MicroScale Thermophoresis (MST) can quatify a binding of two molecules by measuring the change in their mobility in a microscopic temperature gradient (thermophoresis). The target protein is labelled with a fluorescent dye and the movement is measured by monitoring the fluorescence distribution inside a capillary. The microscopic temperature gradient is generated by an IR-Laser, which is focused into the capillary and is strongly absorbed by water.

Before heating, the initial constant value of fluorescence is recorded. When the IR-Laser is switched on, an abrupt change in its intensity is observed. Fluorescence of the dye changes because of its intrinsic temperature dependence and also because molecules move from the locally heated region to the outer cold region. It reaches a plateau representing the steady state in which thermodiffusion is counterbalanced by mass diffusion. Immediately after the heating laser is turned off, fluorescence recovers and finally reaches a constant value (Seidel, Dijkman et al. 2013). Relative fluorescence is used to quantify binding via MST:

$$F_{norm} = \frac{F_{hot}}{F_{initial}}$$

Where $F_{initial}$ is the fluorescence measured before and F_{hot} after a defined time of IR-

laser heating (Jerabek-Willemsen, Wienken et al. 2011).

A typical MST experiment for quantification of an interaction is set up as a titration experiment. The concentration of a fluorescently labelled molecule is kept constant, whereas the concentration of an unlabeled binding partner is varied starting with a value at least 10 times above the expected dissociation constant down to sub-stoichiometric concentration. Within the titration experiment F_{norm} changes as

$$F_{norm} = (1 - x)F_{norm}(A) + xF_{norm}(AT)$$

Where $F_{norm}(A)$ is the contibution of the unbound fluorescent molecule A and $F_{norm}(AT)$ the contribution of the complex of the fluorescent molecule A with the interacting titrant T, *x* the fraction of the fluorescent molecules that formed the complex.

By increasing the concentration of the non-labeled titrant, the fraction of complex increases until all fluorescent molecules formes complex with the titrant.

$$x = \frac{[AT]}{[A]_0}$$

The fraction of bound molecules *x* can be derived from the measured change in fluorescence. Considering that the concentration of free fluorescent molecule is $[A] = [A]_0 - [AT]$, where $[A]_0$ is kept constant during the experiments, and that for the free tritant it is $[T] = [T]_0 - [AT]$, where $[T]_0$ is the known concentration of added titrant, the dissociation constant K_D can be derived.

$$K_D = \frac{[A][T]}{[AT]}$$

In the results the relative fluorescence F_{norm} is plotted in $‰_0$ (Jerabek-Willemsen, Wienken et al. 2011).

NHS-ester is a suitable dye because it reacts efficiently with primary amines of proteins. Primary amine groups are found in lysine residues which are usually

solvent accessible and therefore convenient for labelling reactions. NT-647-NHS labelled proteins show fluorescence excitation and emission maxima of approximately 650 and 670 nm respectively.

NHS was used to form highly stable dye-IscS conjugates as desulfurase IscS contains 15 lysines per monomer (30 per dimer) solvent exposed and suitable for the labelling.

Obviously, the purified protein should be in a buffer that does not contain primary amines (e.g. Tris-HCl, glycine, glutathione) or imidazole and reducing agent, as DTT or β-mercaptoethanol, should also be avoided. I thus previoulsly exchanged the buffer from 20 mM Tris-HCl pH 8, 150 mM NaCl, 2 mM DTT to 100 mM carbonate/bicarbonate at pH 8.3 - 8.5 buffer with a PD-10 column.

The reactive mixture containing IscS 20 μM and dye 60 μM was incubated overnight at 4 °C. Other conditions were avoided because IscS is not stable for long time at room temperature and it tends to aggregate. A clean-up step eliminated the unreacted free dye and exchanged again the buffer to 20 mM Tris-HCl pH 8, 150 mM NaCl, 2 mM DTT passing the mixture through a NAP-5 column. The yield of the reaction was assessed spectroscopically by measuring the ratio of dye concentration with respect to total protein concentration.

$$\%[NHS - IscS] = \frac{[NHS]}{[IscS]} \cdot 100$$

Measuring the absorption at 280 nm for IscS and at 650 nm for the dye I determined that 1.3 μM of IscS contained NHS up to 4 μM of total protein. It means that only a third (32.5%) of molecules of IscS contained the dye. The detergent Tween-20 was added to the sample to avoid the presence of potential aggregates that influence the fluorescence signal.

To avoid experimental artifacts, which can be caused by protein adsorbance to the glass capillary or by protein aggregations, different capillary types were tested. The fluorescence of three capillaries for each available type (standard, hydrophobic and

hydrophilic) was measured. With standard and hydrophobic capillaries I observed shoulders in the fluorescence peaks. On the contrary non-sticking behaviour with symmetric shape was showed with hydrophilic capillaries (figure 5.12).

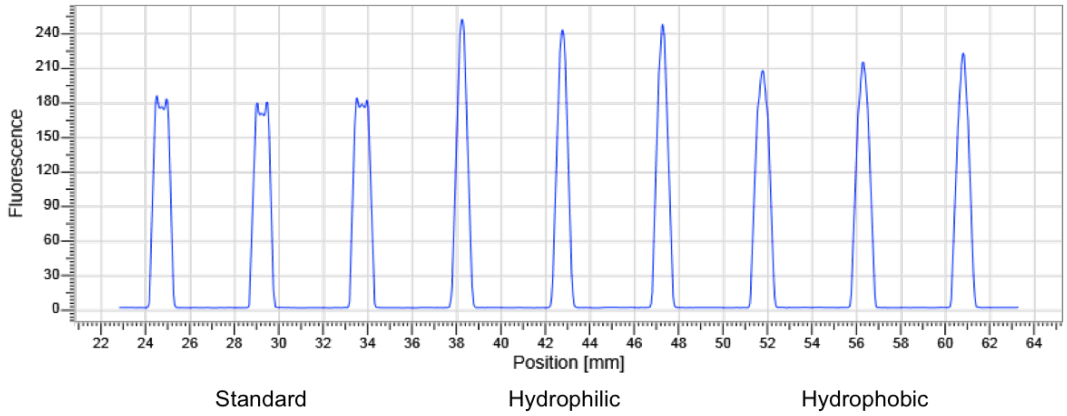

Figure 5.12 Test of MST standard (left), hydrophobic (center) and hydrophilic (right) capillaries containing IscS 50nM.

HscB was dissolved to a final concentration of 473 µM in a buffer containing 20 mM Tris-HCl pH 8, 150 mM NaCl, 0.5 mM TCEP, 0.05% Tween-20 and with labelled IscS at a concentration of 50 nM. This stock solution was then serially diluted 1:1 using the same buffer to give 12 working solutions with different HscB concentration but the same fluorophore concentration (from 473 µM to 115 nM). The thermophoretic movements of labelled IscS in the sample solutions were assessed by measuring fluorescence distribution inside the capillary. Measurements were performed using different light-emitting diode power and 17% of infrared-laser power.

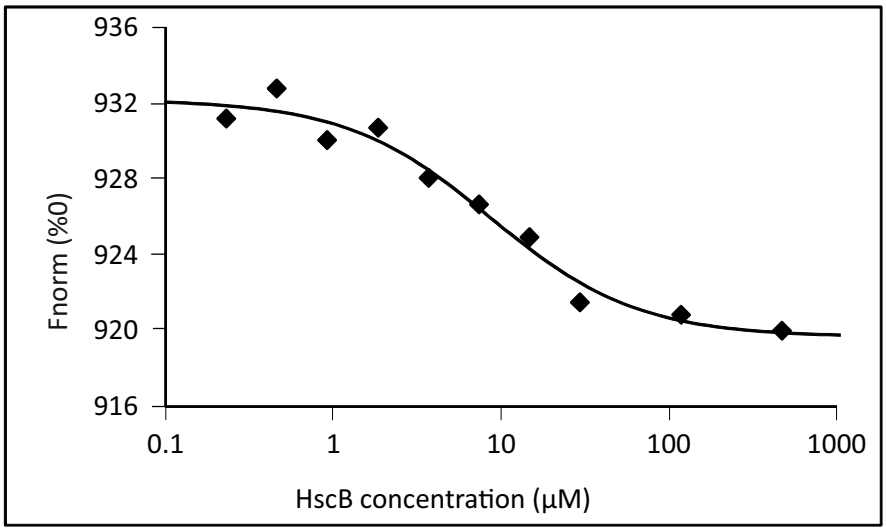

Figure 5.13 MST Data for the IscS and HscB interaction. HscB was dissolved to a final concentration of 473 µM in a buffer containing 20 mM Tris-HCl pH 8, 150 mM NaCl, 0.5 mM TCEP, 0.05% Tween-20 and labelled IscS at a concentration of 50 nM was added. This stock solution was serially diluted 1:1 to give 12 working loaded into hydrophilic capillaries and MST measurement were made at 25 °C using 50% light-emitting diode power and 17% of infrared-laser power. Data are plotted as normalized signal changes as a function of th HscB consentration. The average of three experiments is reported.

The binding curve was obtained by plotting the fluorescence *versus* the logarithm of the progressively diluted concentrations of HscB (figure 5.13). The data obtained with different values of light emitting diode (LED) were directly analysed with the software of the instrument and resulted in a dissociation constant (K_D) of 10 - 30 µM assuming a 1:1 stoichiometry. These affinities are low but comparable to those observed for other components of the Isc machine (Prischi, Konarev et al. 2010) and to that observed for the IscU/HscB interaction (~13 µM) (Hoff, Silberg et al. 2000).

5.4 Discussion

In the first part of my PhD I proved that chaperones, and in particular the co-chaperone HscB, slow down the rate of the overall Fe-S cluster biosynthesis, without differentiating on which level they act. However, several studies have been performed in the past investigating the effect of the chaperones HscA and HscB on

the specific steps of the Fe-S cluster biosynthesis leading to controversial results. Chandramouli and Johnson first studied the second step of the machinery. They showed that chaperones stimulate Fe-S cluster transfer from IscU to apo-Fdx (Chandramouli and Johnson 2006). A few years ago, a study by Bonomi and coworkers investigated the formation of the Fe-S cluster on IscU. They showed that, independently from the initial source of sulfur (chemical or enzymatic), the presence of HscA, HscB and ATP causes as an inhibitory effect (Iametti, Barbiroli et al. 2015).

I decided to probe the inhibitory influence of HscB on the first step of the Fe-S cluster biosynthesis in which the cysteine is converted into alanine by desulfurase IscS. Monitoring by mass spectrometry the amount of these amino acids during the reaction, I demonstrated that HscB slows down also cysteine desulfuration.

Although the inhibitory effect was previously interpretated as to be related to the interaction between HscB and IscU (Iametti, Barbiroli et al. 2015), in my assay IscU was absent. I thus explored the possibility of a previously unidentified direct binding between the co-chaperone and the desulfurase. I tested the binding with several assays (pull-down, size exclusion chromatography). However, only using crosslinking and NMR techniques, which can detect also weak interactions thanks to their high sensitivity, I could prove that HscB and IscS interact.

The biological relevance of the interaction cannot easily be doubted since the affinity K_D is around 10 μM and thus consistent with the K_D values established for other Isc interactions (~20 μM for IscS-CyaY (Prischi, Konarev et al. 2010); ~13 μM for HscB-IscU (Hoff, Silberg et al. 2000)). However, taking in accont of the different conditions and methods of measurement, it is difficult to establish if the quantitative comparison of the K_Ds reflects the extent of competition of two different proteins for a same site.

5.5 Methods

Mass Spectrometry

Cysteine consumption and alanine formation were obtained with 1 μM IscS, 3 mM DTT and 250 μM cysteine in 20 mM Tris-HCl at pH 8 and 150 mM NaCl. When necessary, 3 μM HscB was added. The reaction was stopped with a mixture of acetic acid (0.1%)/acetonitrile (100%) after 0, 10, 20, 40 and 60 min. Determination of alanine and cysteine was performed by mass spectrometry facility at King's College London with HR-LCMS using a Thermo Accela Pump and Pal Autosampler coupled to a Thermo EXactive. Chromatographic separation was performed on a ODS Hypersil 150x2.1 mm 3u column maintained at room temperature. A 10 min gradient was employed using a mobile phase A with 0.1% formic acid in water and a mobile phase B in 0.1% formic acid in acetonitrile: the composition was maintained at 95% A for the first 5min. A 100% composition of A was held for 0.7 min and then decreased to 95% A over the next 4.3 and held until 10 min. Electrospray (ESI) mass spectrometry measurements were performed operating with a capillary voltage of 4.0 kV in positive ion mode, auxiliary gas flow of 10 Arb., sheat gas flow of 60 Arb., capillary temperature of 320 °C. The instrument was set to acquire over the mass range *m*/*z* 80 - 130 with an acquisition time of 10 min. The mass spectrometer was calibrated with solutions of alanine and cysteine in the concentration range of 0 - 500 ng/ml.

Pull-down assays

Glutathione-Sepharose and Ni-NTA resins were equilibrated in a buffer containing 20 mM Tris-HCl pH 8, 150 mM NaCl, 2 mM DTT. Mixtures of the His, GST-tagged HscB and IscS or His-IscS and HscB in the ratio 1:10 (tagged:untagged protein) were prepared, loaded on a Ni-NTA or on a glutathione sepharose resin and incubated for 30 minutes. After extensive washing with the same buffer and

centrifugation, supernatant and resins were separated and loaded on a SDS PAGE gel.

Size Exclusion Chromatography

Analytical SEC experiments were performed on a Superdex200 Increase 10/300 GL column equilibrated in 20 mM Tris-HCl pH 8, 150 mM NaCl, 2 mM DTT. The eluant was monitored at 280, 250 and 392 nm. Fractions were collected and proteins analysed by SDS PAGE gel.

Crosslinking

A mixture of IscS 5 µM and HscB 30 µM was prepared in PBS buffer. Dimethyl adipimidate or Bis[sulfosuccinimidyl]suberate were added to the protein sample to a final concentration of 1.3 mM. The reaction mixture was incubated at room temperature for 30 minutes and quenched by adding Tris-HCl at pH 8 to a final concentration of 20 mM. The quenching reaction was incubated at room temperature for 15 minutes. SDS PAGE was run to determine crosslinked species.

^{15}N-labelled protein expression

^{15}N-labelled proteins were prepared for T1 relaxation NMR measurements. Plasmids were incorporated by BL21(DE3) *E. coli* cells and these were grown in minimal medium composed by M9 salts with 3 g/L of D-glucose and using 1 g/L of $(^{15}NH_4)_2SO_4$ as the sole source of nitrogen. Proteins were then expressed and purified as previously described.

T1 relaxation NMR measurement

^{15}N T1 values were measured at 298 K, with a Bruker AVANCE III spectrometer at 700 MHz proton frequency, using uniformly ^{15}N-enriched HscB (0.160 mM), alone and in the presence of 0.093 mM IscS. The relaxation series was recorded as a

pseudo 3D experiment with scan-wise interleaving, with parametric T1 relaxation delays of 10, 100, 200, 400, 700, 1000, 1500, 2000 and 2500 ms. An overall T1 relaxation time estimate was obtained by averaging the T1 values after excluding residues with a weighted root mean square (wrms) of fitting lower than 0.75 or higher than 1.25.

Isothermal Titration Calorimetry

ITC experiments were performed on an ITC200 microcalorimeter interfaced with a computer for data acquisition and analysis by Origin 7 software. Before the measurements, proteins were dialysed against 20 mM Tris-HCl pH 8, 150mM NaCl, 2 mM DTT. IscS 40 μM was titrated in the calorimetric cell thermostated at 18 °C with successive injections of a 320 μM stock solution of HscB spaced at 120 s intervals. The titration syringe was continuously stirred at 1000 rpm. For the first injection, only 0.2 μL of HscB were added and the corresponding data point was excluded from analysis. Injections were started after baseline stability had been achieved. A reference titration of dilution was carried out by injecting HscB into the calorimetric cell containing only the buffer. Data obtained were fit using a single-site sequential binding model.

Microscale Thermophoresis

MST measurements were performed using a NanoTemper Monolith NT.115 instrument. IscS samples were labelled with the amine-reactive dye NT-647 using the Monolith NT.115 Protein Labelling Kit RED-NHS. The reactive mixture was incubated overnight at 4 °C. Labelling levels were determined using ε_{280} (IscS)= 41370 $M^{-1}cm^{-1}$ and ε_{650} (dye)= 250000 $M^{-1}cm^{-1}$. HscB was dissolved to a final concentration of 473 μM in a buffer containing 20 mM Tris-HCl pH 8, 150 mM NaCl, 0.5 mM TCEP, 0.05% Tween-20 and labelled IscS at a concentration of 50 nM was added. This stock solution was serially diluted 1:1 to give 12 working solutions with different HscB concentration and mantaining the fluorophore concentration constant.

Solutions were loaded into hydrophilic capillaries and MST measurement were made at 25 °C using 40 - 60% light-emitting diode power and 17% of infrared-laser power.

6. STRUCTURAL APPROACH

A further step in the characterisation of the binding between two proteins is the individuation of their surface of interaction. Since structure is strongly connected with function, it is important to identify which residues are involved. Depending on the site of binding, the activity of a protein could be affected. For this reason, structural studies often lead to relevant conclusion on the biological importance of proteins interactions.

6.1 HscB surface of interaction

NMR is usually used because this is a powerful technique able to detect binding between proteins also if they interact with low affinity (in the uM-mM range). The only limit is the inability of detecting directly proteins above ca. 30 kDa, such as is IscS that has a molecular weight of 90 kDa. When the molecular size increases the tumbling rate of the molecule slows and the slow tumbling will cause the magnetisation to dephase rapidly causing the NMR signal to broaden and decay quickly. For this reason, I first started with the investigation of the binding surface on the HscB site.

6.1.1 NMR-HSQC Spectra

The Heteronuclear Single Quantum Correlation (HSQC) is an example of 2-Dimensional NMR experiment. HSQC-NMR spectra appear as an ensamble of spots corresponding to resonances. They provide a fingerprint of proteins because each resonance corresponds to a N-H group and its position, chemical shift, in the spectrum depends on the chemical environment of the amino acid in the protein. If the assignement is known, it will be possible to correlate each resonance with its residue.

NMR thus allows direct identification of the amino acids involved in the surface of

interaction thanks to the possibility of identifying changes of their chemical environment upon the binding. When two molecules interact, what is expected is a shift of the peaks for which the environment has changed because of an involvement of the corresponding amino acids or a conformational change in the chain. However, since the formation of a complex slows down the tumbling of the two single molecules, it could happen that some resonances disappear because of broadening of the signal due to faster relaxation and longer correlation times.

BOX 9 ***Principle of the NMR-HSQC experiment***

NMR spectroscopy is based on the excitation of a sample upon introduction of it into a magnetic field and irradiation by a radio frequency. The irradiation excites the nuclear spins from the ground to an excited state. The signal obtained can be recorded as a plot of the energy emitted as a function of time. This signal, which contains all the information needed, can successively be Fourier transformed to a plot which reports the energy emitted as a function of frequency, which corresponds to the traditional NMR spectrum. A direct extension of this mono-dimensional spectrum is the two-dimensional NMR spectroscopy, in which the signal is recorded as a function of two time variables, t_1 and t_2, and the resulting data Fourier are transformed twice to yield a spectrum which is a function of two frequency variables.

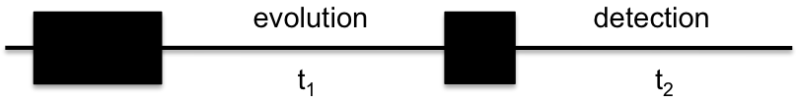

Figure 6.1 General scheme for 2D-NMR pulse sequence.

In the first period, called preparation time, the sample is excited by one or more pulses. The resulting magnetization is allowed to evolve for the first time period, t_1. During the mixing period, coherence is transferred from one spin to another. Mixing sequences use two mechanisms for magnetization transfer: scalar coupling or

dipolar interaction. At the end of the experiment, the signal is recorded as a function of the second time variable t_2.

Apart from protons, proteins contain other magnetically active nuclei, such as ^{15}N and ^{13}C. One particular useful experiment is to record a 2D spectrum in which protons are correlated to the heteroatom to which they are scalarly coupled so that the coordinate of a peak in one dimension is the ^{1}H chemical shift and the coordinate in the other dimension is the chemical shift of the nucleus to which it is coupled. ^{15}N-Heteronuclear Single Quantum Correlation (HSQC) experiments correlate the nitrogen atom of amines with the directly attached proton, so each signal in a HSQC spectrum represents a proton that is bound to a nitrogen atom. Since there is only one H-N per amino acid, each HSQC signal represents one single amino acid. The HSQC also contains signals from the NH_2 groups of the side chains of Asparagine and Glutamine and of the aromatic H-N of Tryptophan and Histidine. Analogous experiment can be performed for ^{13}C and ^{1}H.

In order to obtain HscB selectively enriched in ^{15}N, I expressed it in *E. coli* and I grew cells in minimal medium containing ^{15}N-ammonium. The HSQC Spectrum of free HscB 100 µM in 20 mM Tris-HCl pH8, 150 mM NaCl and 2 mM DTT was recorded at 298 K.

The structure of the co-chaperone HscB has been already studied in literature and depositated in the Protein Data Bank (PDB code: 1FPO). The chemical shifts of its HSQC spectrum are already available in the Biological Magnetic Resonance Database (BMRD) (entry ID 15541). Spectra have been recorded by Fuzery in conditions not completely comparable to mine (Fuzery, Tonelli et al. 2008): buffer contained around 20 mM Tris-HCl, 10 mM DTT and temperature was set at 313 K. Since the major difference can be attributed to the temperature (298 K in my experiments), to use this entry as base for the assignment, I recorded HSQC-NMR

spectra of HscB at different temperature (313, 308, 303 and 298 K) (figure 6.2). For every peak I determined their shift with temperature and their expected position at 298 K.

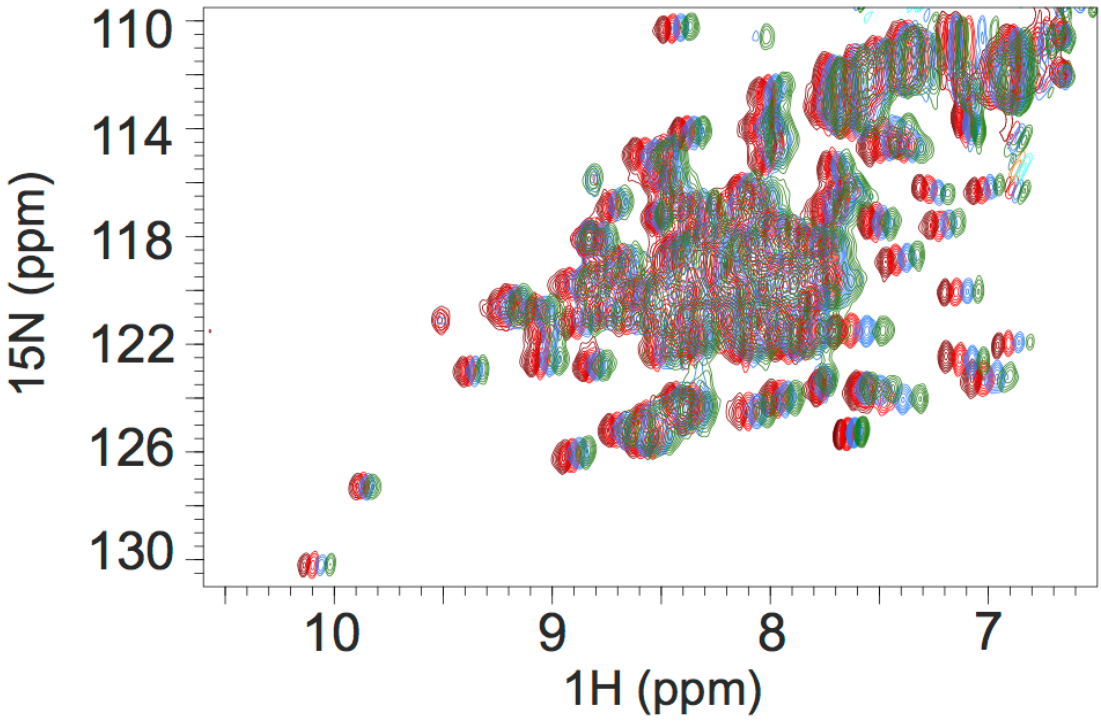

Figure 6.2 ^{15}N HSQC spectra of HscB at different temperatures, recorded at 313 (maroon), 308 (red), 303 (cyan) and 298 K (green) with a protein concentration of 100 μM in 20 mM Tris-HCl pH 8, 150 mM NaCl and 2 mM DTT.

I recorded the ^{15}N HSQC NMR experiments of free HscB (100 μM) and identified all the residues according to the BMR database entry. A ^{15}N labelled HscB sample was then titrated with unlabelled IscS in the 1:1 and 1:2 HscB:IscS molar ratio and ^{15}N HSQC NMR experiments recorded (figure 6.3).

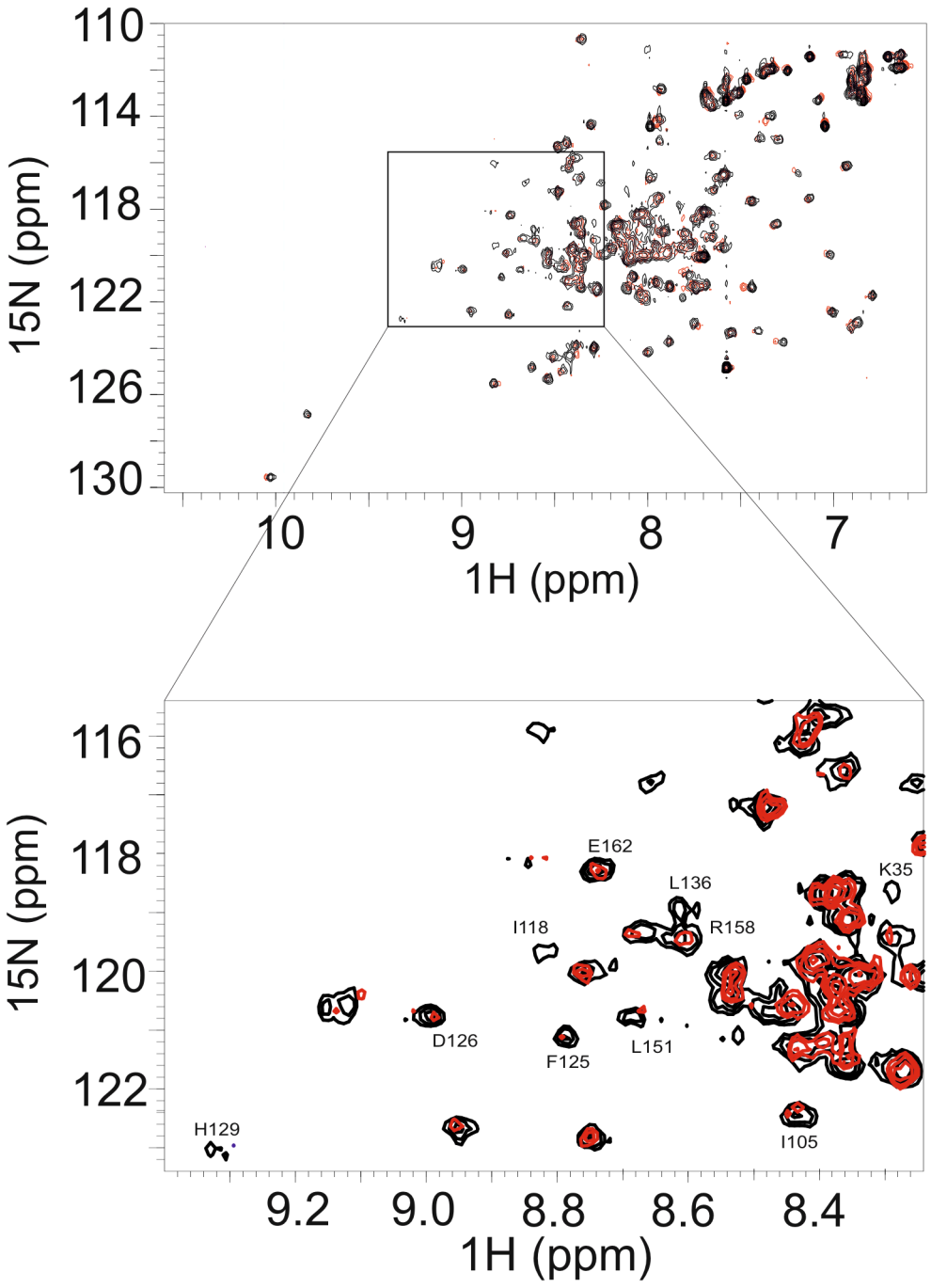

Figure 6.3 HSQC-NMR spectra of ^{15}N-labelled HscB 100 μM (black) and 15N-labelled HscB 100 μM in the presence of IscS 1:1 (red) at 298 K in 20 mM Tris-HCl pH 8, 150 mM NaCl and 2 mM DTT. Bottom: Zoom of a relevant region of the spectrum for the identification of the binding.

The residues of HscB involved in the interaction were mapped. At a 1:1 IscS/HscB molar ratio, many peaks, amongst which those from the J-domain, did not shift. This suggested that IscS has a minimal effect on these regions of HscB. Other resonances (L22, H63, Q95, R99, E104, E106, E111, I118, K119, M124, L157, A161 and D170) had small but detectable chemical shift changes indicative of

environmental changes in the presence of IscS. A third set of residues (I105, I118, F125, H129, L131, L136, E139, L151, D155, R158, E162 and K167) broadened significantly (see appendix I.I for data analysis). At the end of the titration, the HscB spectrum disappeared almost completely as expected for the formation of a complex with molecular weight of 130 kDa (assuming a 1:1 stoichiometry).

Residues with chemical shift		Residues significantly broadened	
L22	H63	Q14	L20
Q95	R99	E104	E106
E104	E106	Q107	D110
E111	I118	E111	F117
K119	M124	I118	L131
L157	A161	Q135	D155
D170		L157	A161
		E162	

Table 6.1 HscB residues affected in the HSQC spectrum after the addition of IscS.

As we can see in figure 6.4, HscB presents a shape similar to a swiss knife made by two domains. Residues affected are mainly located on the C-terminus and map on the internal surface facing the J-domain.

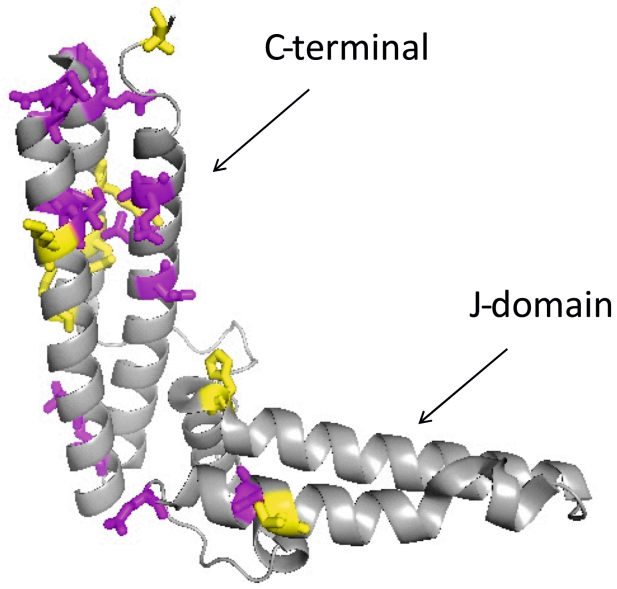

Figure 6.4 Mapping the interaction surface on HscB (PDB code: 1FPO). Residues showing chemical shift perturbation at a 1:1 molar ratio are shown in yellow, those which broaden or disappear in magenta.

6.1.2 NMR-Cross saturation experiments

When two or more molecules interact, part of a chain can rearrange changing its tridimensional position. Thus some amino acids can be affected by a different chemical environment without mapping in the surface of binding and they can present resonance at a different chemical shift comparing with the spectrum of the free protein. Cross saturation is a NMR technique more powerful than the simple chemical shift/disappearance in the HSQC spectra because it is able to distinguish residues that directly interact from those which undergo conformational rearrangements (Takahashi, Nakanishi et al. 2000).

BOX 10 ***Principle of NMR-Cross saturation experiment***

Cross saturation is an NMR measurement technique which can identify the direct interface between molecular complexes. This technique is particularly helpful for weak high molecular complexes in which one component is easily within the smaller NMR size range and the other too large to allow easy detection.

In these experiments, if the two molecules are both proteins, one of the two interacting components (protein I) is uniformly labelled with ^{2}H and ^{15}N and complexed with a non-labelled protein (protein II). The complex is thus composed of molecules with lower (protein I) and higher (protein II) proton densities. In the case of the protein with higher proton density, if the aliphatic proton resonances are irradiated non-selectively using a radio frequency field, not only its aliphatic resonances but also its aromatic and amide protons are instantaneously saturated. This phenomenon is well known as spin diffusion effect. Although the protein uniformly labelled with ^{2}H and ^{15}N is not directly affected by the radio frequency field, it is expected that saturation can be transferred from the target molecule (protein II) to the doubly labelled molecule (protein I) by cross relaxation through the interface of the complex. If the proton density of the doubly labelled molecule is sufficiently low, the saturation transferred is limited to the interface

of interaction. Therefore residues at the interface of protein I can be identified by observing the reductions of the peak intensities in the ^{1}H-^{15}N HSQC spectrum measured by TROSY coherence transfer (Takahashi, Nakanishi et al. 2000).

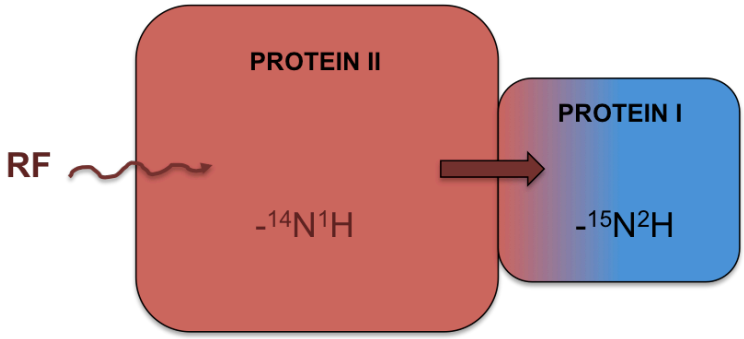

Figure 6.5 Representation of the principles of cross saturation method.

Cross saturation experiments were recorded to discriminate between residues of HscB that are effectively involved in the surface of interaction with IscS and residues which are only affected by a change in conformation. In this experiment HscB was uniformly labelled with ^{2}H and ^{15}N with level of deuteration of around 90%. HscB free (100 µM) was not completely unaffected by cross saturation sequence because some protons were still present in the protein side chains. After the addition of IscS (1:1) the saturation was transferred from IscS to HscB through the interface of the complex by cross relaxation. However, it was transferred only to the directly exposed surface of HscB. I plotted the difference between the TROSY spectrum recorded in the experiment with the aliphatic hydrogen saturated and the spectrum in which the aliphatic radio frequence was off and I compared the experiment performed on HscB in the presence of IscS (1:1) with that on HscB free (figure 6.6).

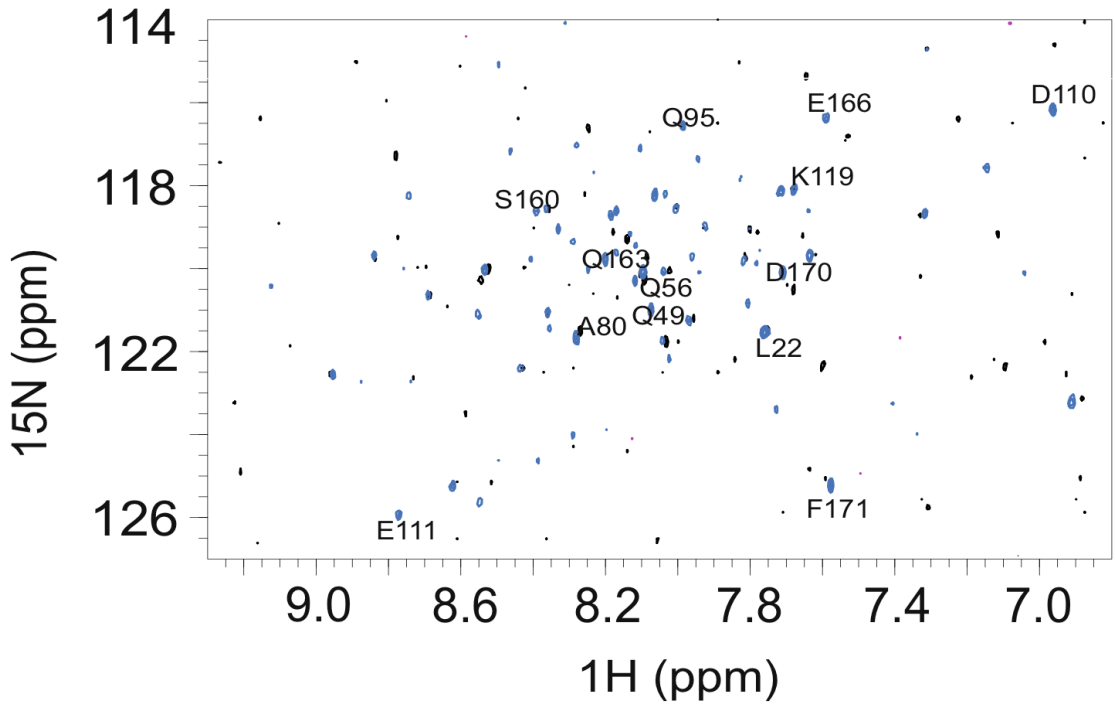

Figure 6.6 Cross saturation experiment on $^{2}H,^{15}N$-labelled HscB 100 μM (black) and in the presence of IscS 1:1 (blue) at 298 K in 20 mM Tris-HCl pH 8, 150 mM NaCl and 2 mM DTT. Saturation of aliphatic resonances was achieved with a pulses centered at 0.5 ppm. The intensity of the amide peaks in the experiment in which the aliphatic hydrogen were saturated was compared with the intensity of the amide peaks in the control off-resonance experiment.

The following residues were observed to be affected: L22, Q49, Q56, A80, Q95, D110, E111, K119, S160, Q163, E166, D170, and F171 (see appendix I.I for data analysis).

Residues affected by Cross saturation	
L22	Q49
Q56	A80
Q95	D110
E111	K119
S160	Q163
E166	D170
F171	

Table 6.2 HscB residues affected by cross saturation after the addition of IscS.

Most of these are close in space and located in the C-terminus of the approximately L-shaped HscB structure and form an exposed patch (figure 6.7).

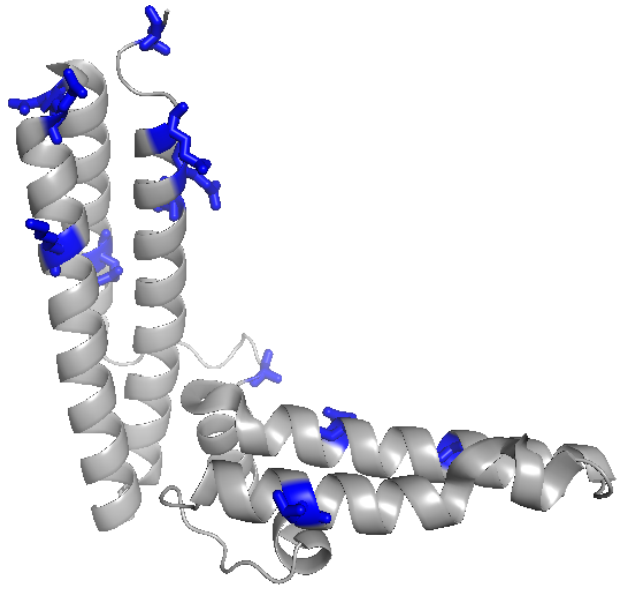

Figure 6.7 Mapping the HscB surface of interaction (PDB code: 1FPO). Cross saturation revealed residues of HscB involved on the surface of interaction with desulfurase IscS at molar ratio 1:1 (evidenced in blue).

6.2 IscS surface of interaction

It is well known in literature that desulfurase IscS is able to bind several proteins (Shi, Proteau et al. 2010). Since it is involved in different pathways (such as tRNA modification and molybdenum cofactor and Fe-S cluster biosynthesis), its possible partners are encoded by different operons. Among the proteins involved in the Fe-S cluster biosynthesis, IscU, ferredoxin, CyaY and YfhJ interact with IscS and these interactions are correlated with a specific role in the machinery. While IscU interacts with only one subunit of the IscS dimer (so two molecules are bound for a dimer) (Urbina, Silberg et al. 2001), CyaY frataxin binds IscS in a pocket between the active site and the IscS dimer interface and touches both the IscS units (Prischi, Konarev et al. 2010). Fdx competes for the same binding site (Yan, Konarev et al. 2013), whereas leaving the interaction with IscU unchanged. In addition, the Fdx binding site overlaps also with the other less known protein YfhJ (Pastore, Adinolfi

et al. 2006). Looking at this information, I was interested in the IscS surface of binding: does the HscB binding site overlap with other proteins?

IscS spontaneously forms a dimer of 90 kDa. Unfortunately, proteins and systems of this dimension are too large to be detectable with standard NMR experiments: peaks broaden to the point that the spectrum completely disappears. To identify the surface of IscS interacting with HscB, I tested the ability of IscS mutants designed *ad hoc* to affect the HscB spectrum: if the mutant is still able to bind, the resulting spectrum is expected to correspond to that obtained in the presence of IscS wild type. On the contrary, if mutations impact residues participating on the binding, the interaction will be at least partially repressed and the spectrum appears as for HscB free. Plasmids expressing variants of IscS which affect different regions of the protein were already available in our laboratory because they had been used in the study of the complex made by IscS and bacterial frataxin, CyaY, (Prischi, Konarev et al. 2010) or ferredoxin, FdX (Yan, Konarev et al. 2013): IscS_R39E/W45E, IscS_K101E/K105E, IscS_R220E/R223E/R225E, IscS_I314E/M315E and IscS_E334S/R340S (figure 6.8). Circular dichroism had been measured in the past and supported that the mutants are all correctly folded as expected from their location in exposed regions of the enzyme.

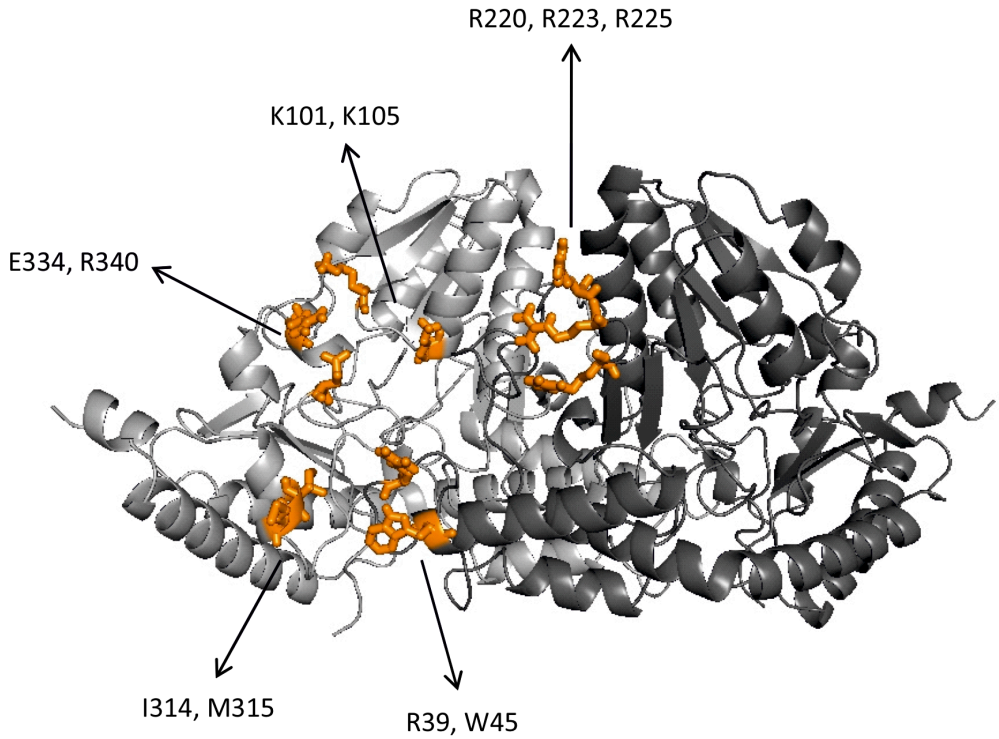

Figure 6.8 Position of the mutations on the structure of IscS (PDB code: 3LVL).

As with the wild type, I recorded the HSQC spectrum of ^{15}N-labelled HscB in the presence of each IscS mutant at molar ratio 1:1. Among them, IscS_R39E/W45E, IscS_R220E/R223E/R225E and IscS_K101E/K105E leave mostly unaffected the spectrum of HscB (figure 6.9 (A, B, C)). This means that mutations of these residues result in complete or partial abolishment of the binding. Conversely, the spectra with IscS_E334S/R340S and IscS_I314E/M315E are affected by IscS addition comparably to wild-type, indicating that these residues are not involved in the interaction (figure 6.9 (D,E)).

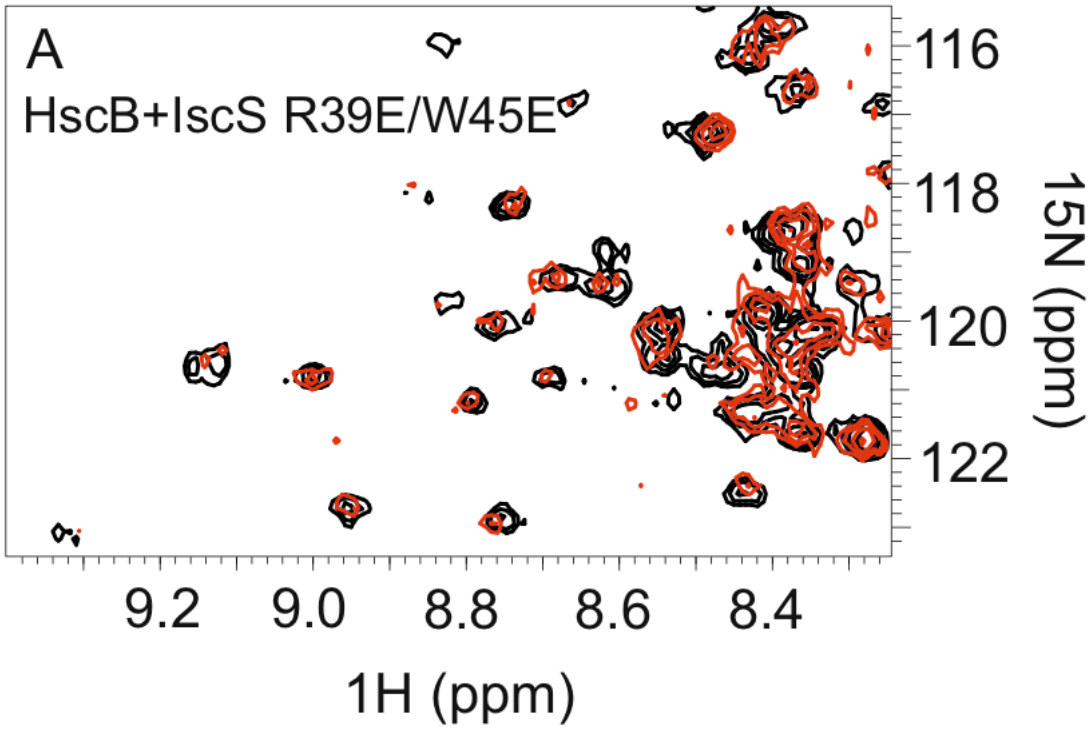

Figure 6.9 (A) Identification of the surface of interaction on IscS by mutagenesis. HSQC-NMR spectra of ^{15}N-labelled HscB 100 μM (black) and in the presence of the IscS_R39E/W45E (1:1) (red) at 298 K in 20 mM Tris-HCl pH 8, 150 mM NaCl and 2 mM DTT.

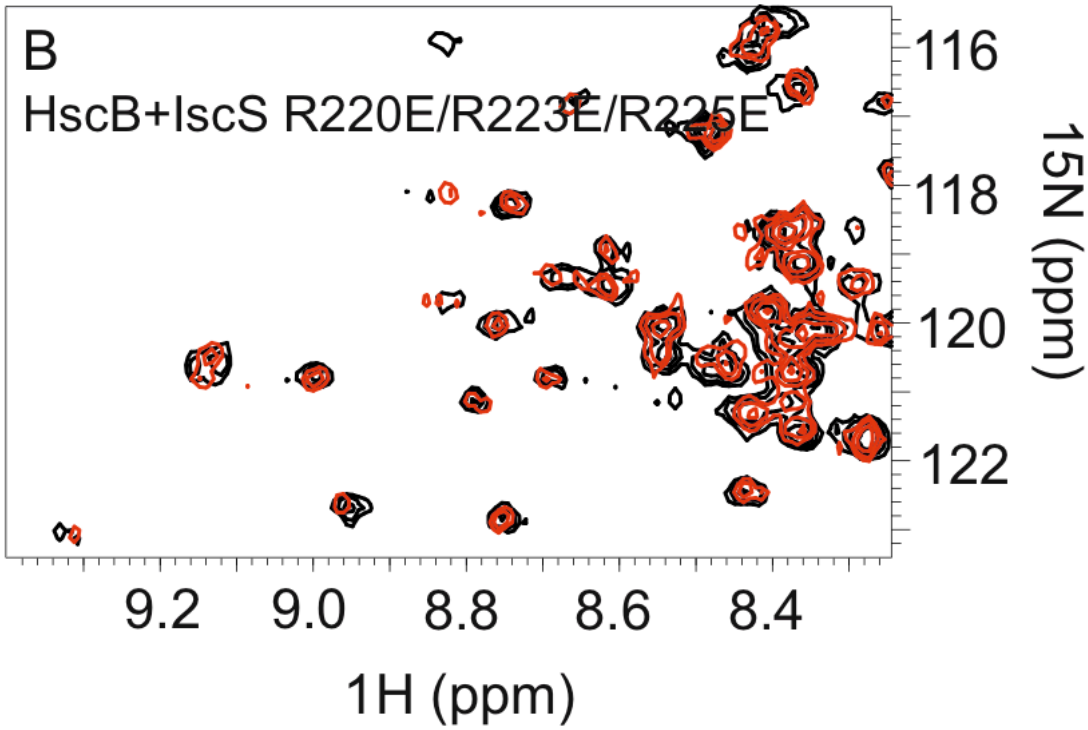

Figure 6.9 (B) Identifiction of the surface of interaction on IscS by mutagenesis. HSQC-NMR spectra of ^{15}N-labelled HscB 100 μM (black) and in the presence of the IscS_R220E/R223E/R225E (1:1) (red) at 298 K in 20 mM Tris-HCl pH 8, 150 mM NaCl and 2 mM DTT.

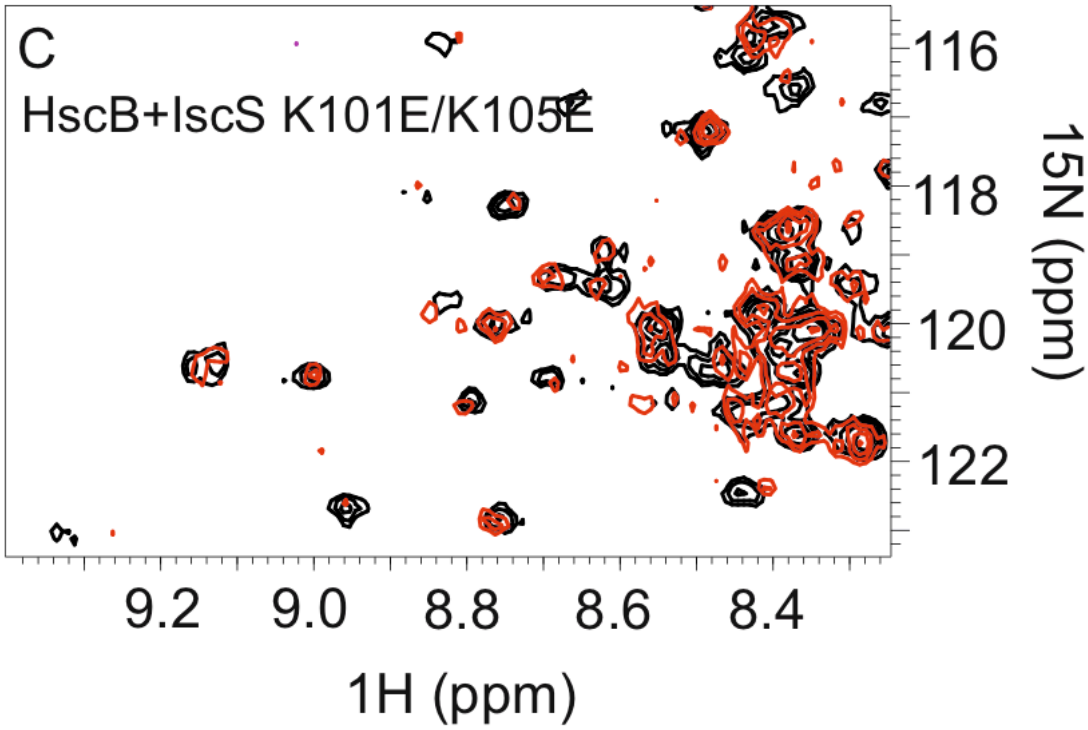

Figure 6.9 (C)Identifiction of the surface of interaction on IscS by mutagenesis. HSQC-NMR spectra of ^{15}N-labelled HscB 100 μM (black) and in the presence of the IscS_K101E/K105E (1:1) (red) at 298 K in 20 mM Tris-HCl pH 8, 150 mM NaCl and 2 mM DTT.

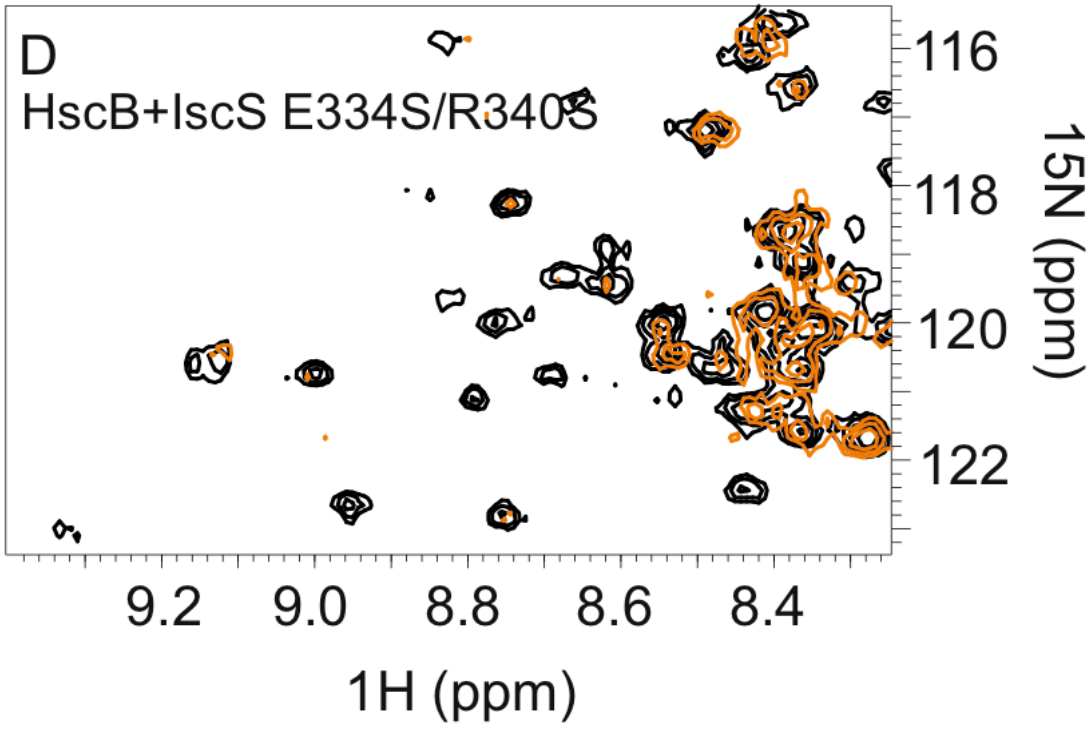

Figure 6.9 (D) Identifiction of the surface of interaction on IscS by mutagenesis. HSQC-NMR spectra of ^{15}N-labelled HscB 100 μM (black) and in the presence of the IscS_E334S/R340S (1:1) (orange) at 298 K in 20 mM Tris-HCl pH 8, 150 mM NaCl and 2 mM DTT.

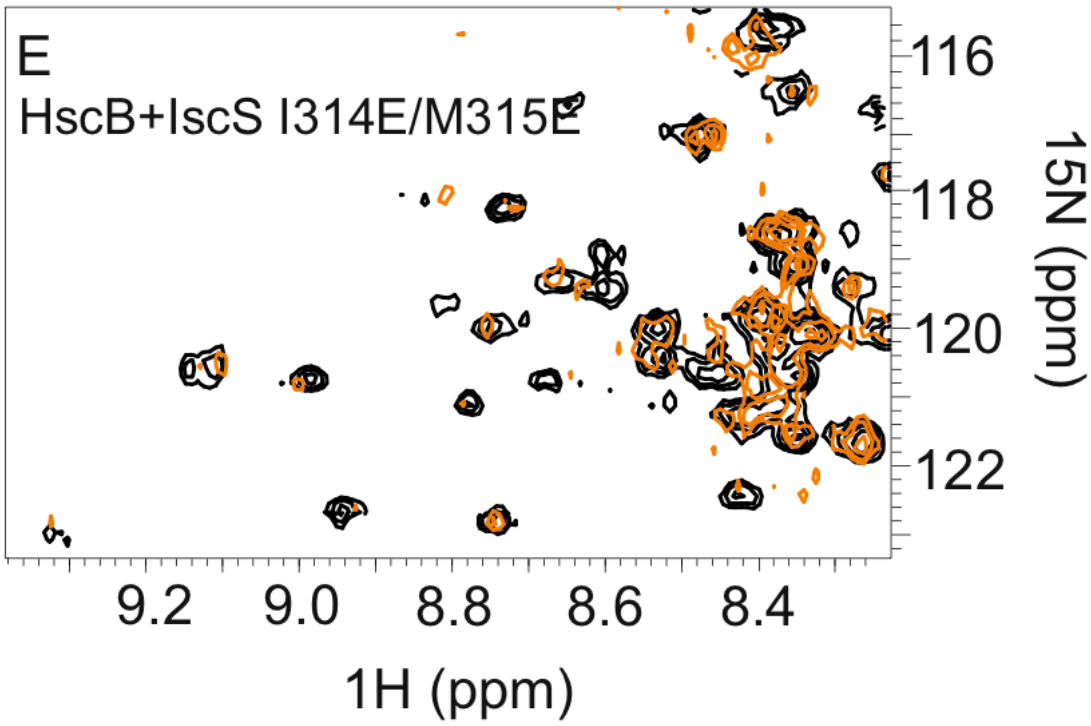

Figure 6.9 (E) Identifiction of the surface of interaction on IscS by mutagenesis. HSQC-NMR spectra of ^{15}N-labelled HscB 100 μM (black) and in the presence of the IscS_I314E/M315E (1:1) (orange) at 298 K in 20 mM Tris-HCl pH 8, 150 mM NaCl and 2 mM DTT.

A similar behaviour was reported with the bacterial frataxin CyaY and for Fdx which also form complexes with IscS.

6.3 Compatibility of HscB binding with other proteins

Both HscB and IscS are involved in binding with several other proteins of the Isc machinery and of other systems. It was thus interesting to investigate if some of these proteins affect the HscB/IscS interaction.

6.3.1 HscB, CyaY and FdX compete for the same site on IscS

The results obtained suggested that HscB binds IscS in a site overlapping with that observed for frataxin, CyaY, (Prischi, Konarev et al. 2010) and ferredoxin, FdX (Yan, Konarev et al. 2013). To validate the hypothesis, I titrated a sample containing the HscB/IscS complex with CyaY (up to a 1:1:3 molar ratio) or Fdx (up to a ratio 1:1:3).

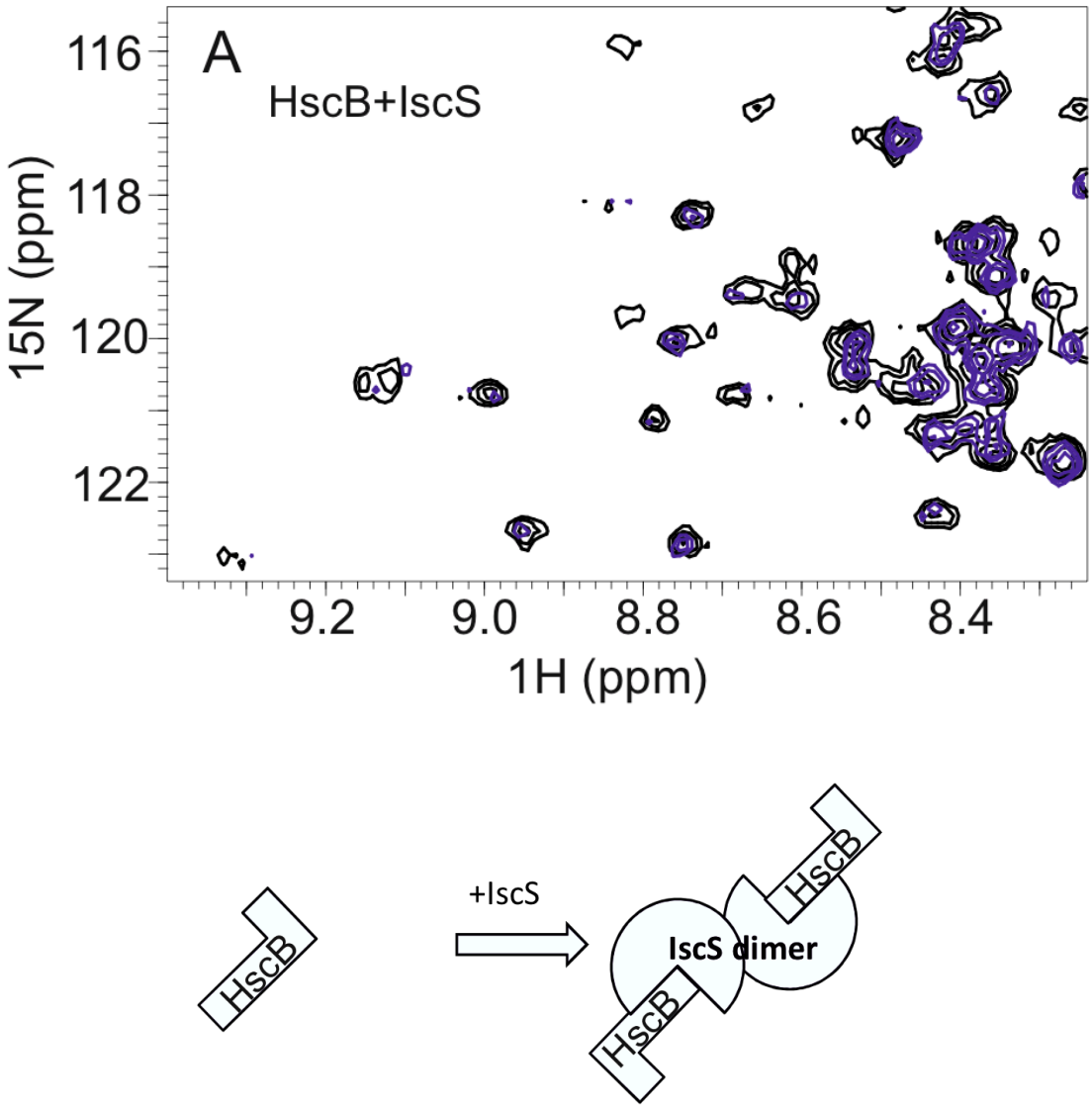

Figure 6.10 (A) Competition experiments of HscB with CyaY and FdX. Superposition of the HSQC spectra of 100 µM free ^{15}N-labelled HscB (black) and in the complex with unlabelled IscS 1:1 (blue) at 298 K in 20 mM Tris-HCl pH 8, 150 mM NaCl and 2 mM DTT. The experiment is summarized schematically below.

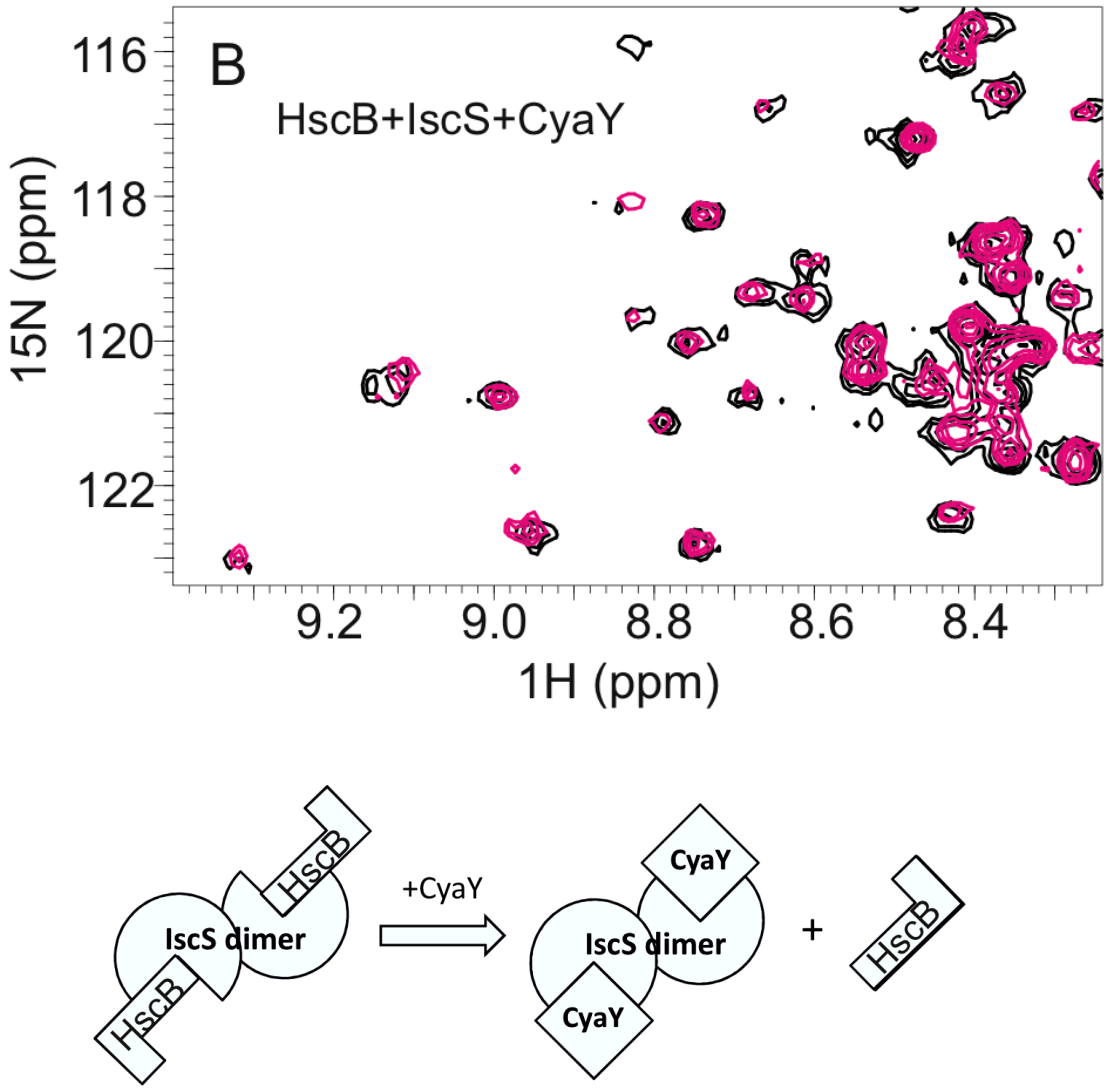

Figure 6.10 (B) Competition experiments of HscB with CyaY and FdX. HSQC spectra of 100 μM ^{15}N-labelled HscB (black) and in complex with IscS with the addition of CyaY (1:1:1) (magenta) at 298 K in 20 mM Tris-HCl pH 8, 150 mM NaCl and 2 mM DTT. The experiment is summarized schematically below.

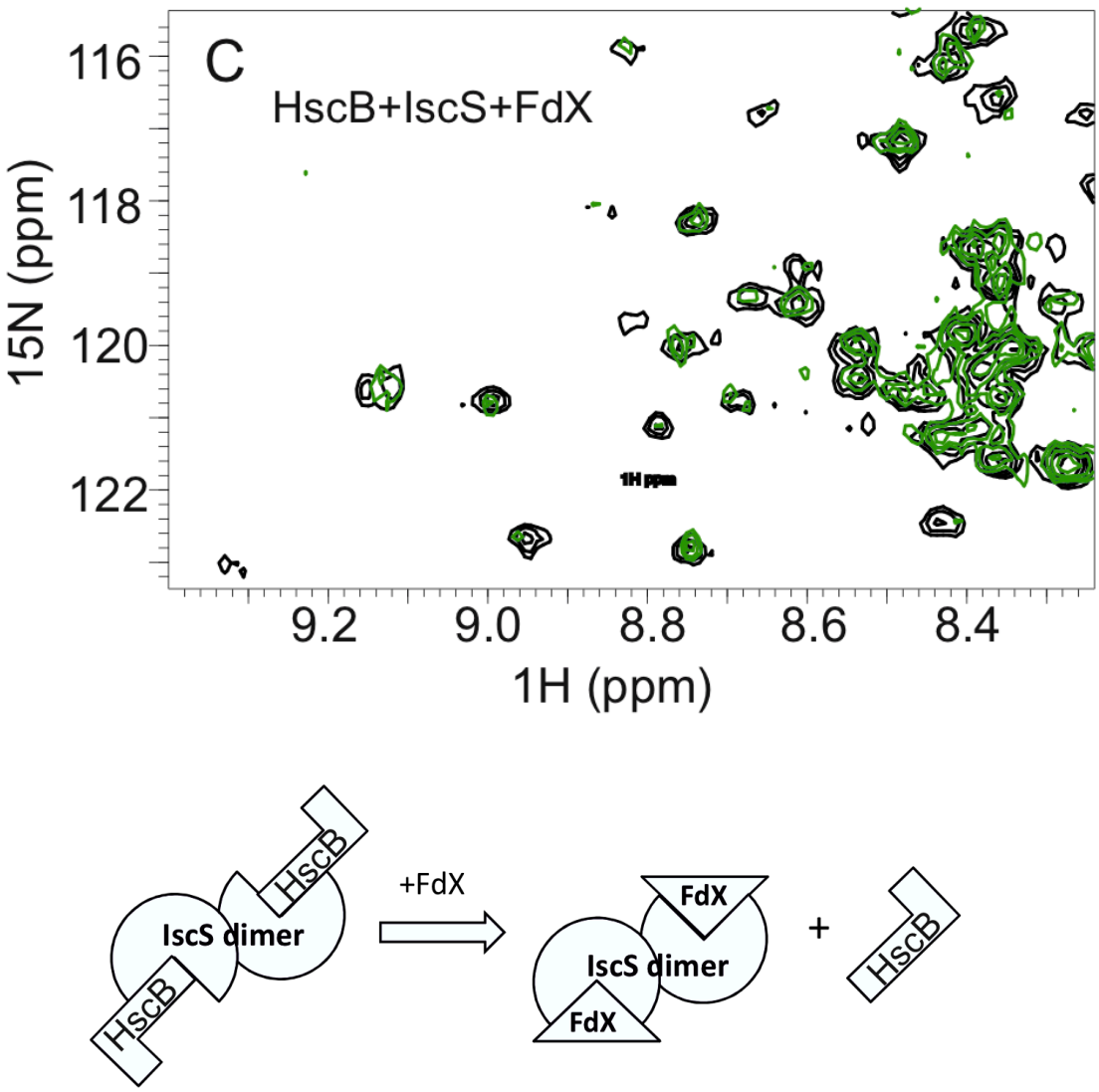

Figure 6.10 (C) Competition experiments of HscB with CyaY and FdX. HSQC spectra of 100 μM ^{15}N-labelled HscB (black) and in the presence of IscS and apo-Fdx (1:1:3) (green) at 298 K in 20 mM Tris-HCl pH 8, 150 mM NaCl and 2 mM DTT. The experiment is summarized schematically below.

I observed that introduction of CyaY causes the progressive reappearance of the spectrum of HscB, consistent with its almost complete displacement from IscS at 1:1:1 (figure 6.10 (B)). Titration of the HscB/IscS complex with Fdx also regenerates the spectrum of HscB but, at a higher molar ratio: at a 1:1:3 ratio of IscS/HscB/Fdx, the spectrum of HscB is only partially restored (figure 6.10 (C)). This confirmed that the interaction between IscS and HscB involves the same site that hosts CyaY and Fdx. The site involves a cleft formed between the two protomers of the IscS dimer and contains PLP and the catalytic centre (Cupp-Vickery, Urbina et al. 2003).

6.3.2 IscU does not compete with IscS/HscB binding

It is well known that HscB is able to bind the scaffold protein IscU and that this interaction enhances the ATPase activity of HscA (Chandramouli and Johnson 2006). Whereas the co-chaperone binds its partner HscA through R152, D155, K156, R158 and Q163, (Fuzery, Tonelli et al. 2008) the binding with IscU involves residues R87, L92, L96, R99, E100 and F153 (Fuzery, Tonelli et al. 2008, Kim, Fuzery et al. 2009, Fuzery, Oh et al. 2011). Both surfaces of interaction belong prevalently to the C-terminus domain (figure 6.11). On the contrary, the interaction with IscS was completely unkown before. NMR allowed the identification of the surface disclosing that residues are close to the surface area responsible for other bindings.

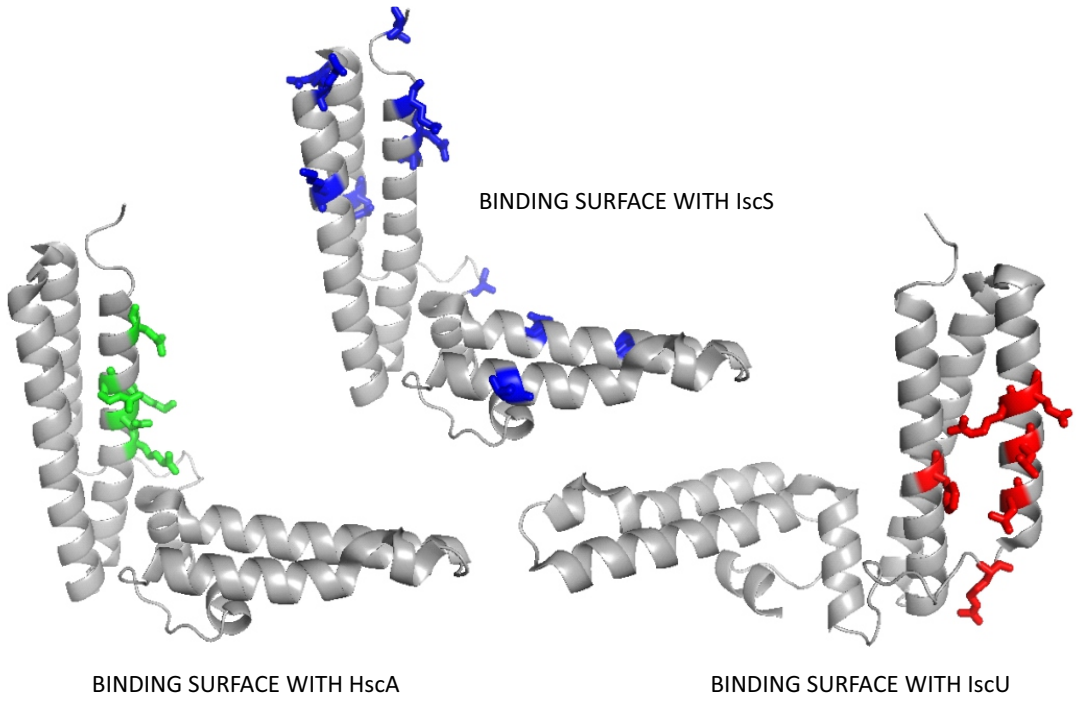

Figure 6.11 Mapping the HscB surface of interaction with HscA (green), IscS (blue) and IscU (red).

Since the scaffold protein IscU is able to bind both the desulfurase IscS and HscB, I checked if the HscB/IscS complex is compatible or mutually exclusive with IscU binding.

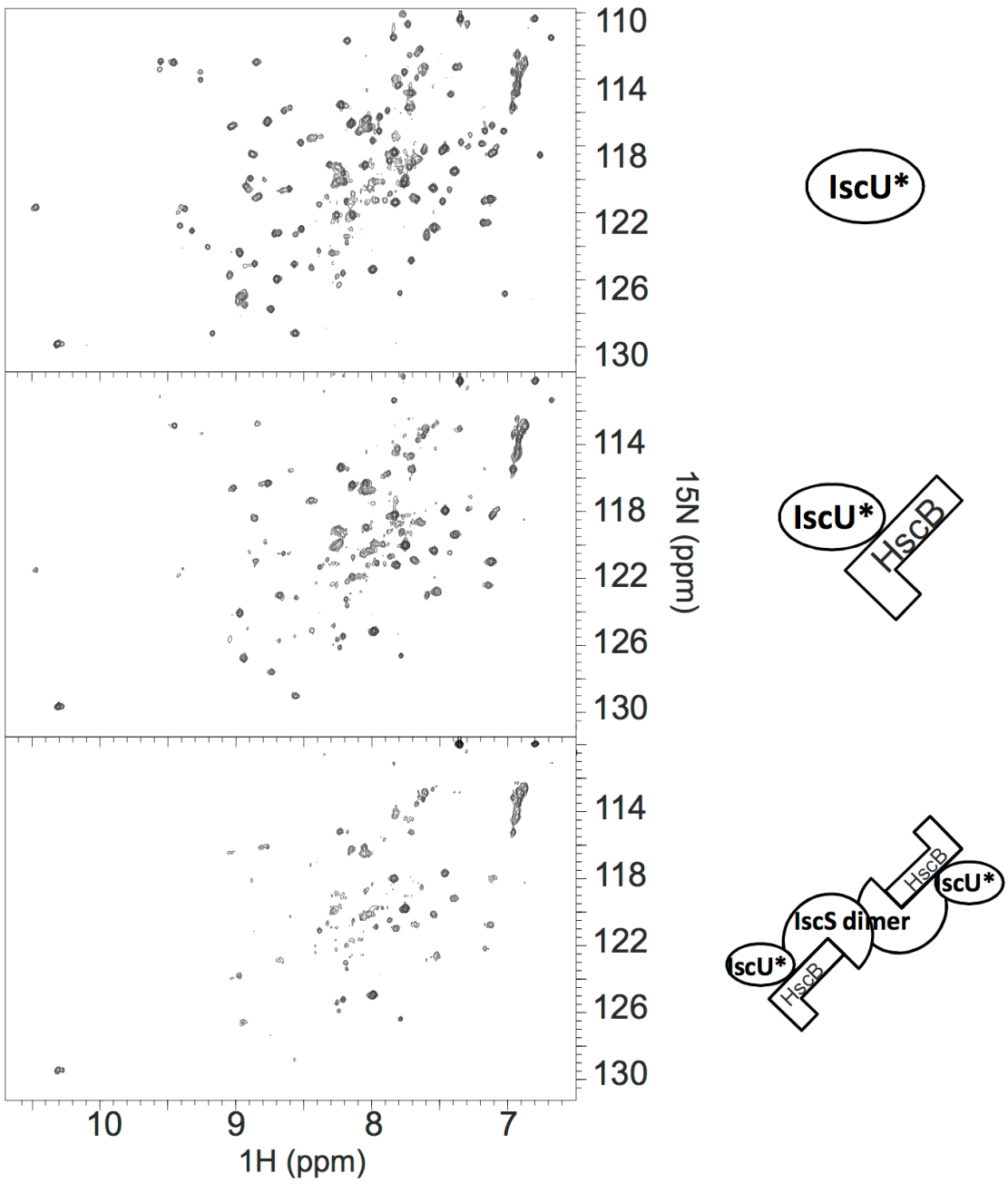

Figure 6.12 (A) IscU does not compete with IscS binding. Comparison of the spectra of ^{15}N-labelled IscU (top), the same but after addition of HscB 1:0.4 (middle) and after the further addition of IscS 1:0.4:0.4 (bottom) at 298 K in 20 mM Tris-HCl pH 8, 150 mM NaCl and 2 mM DTT.

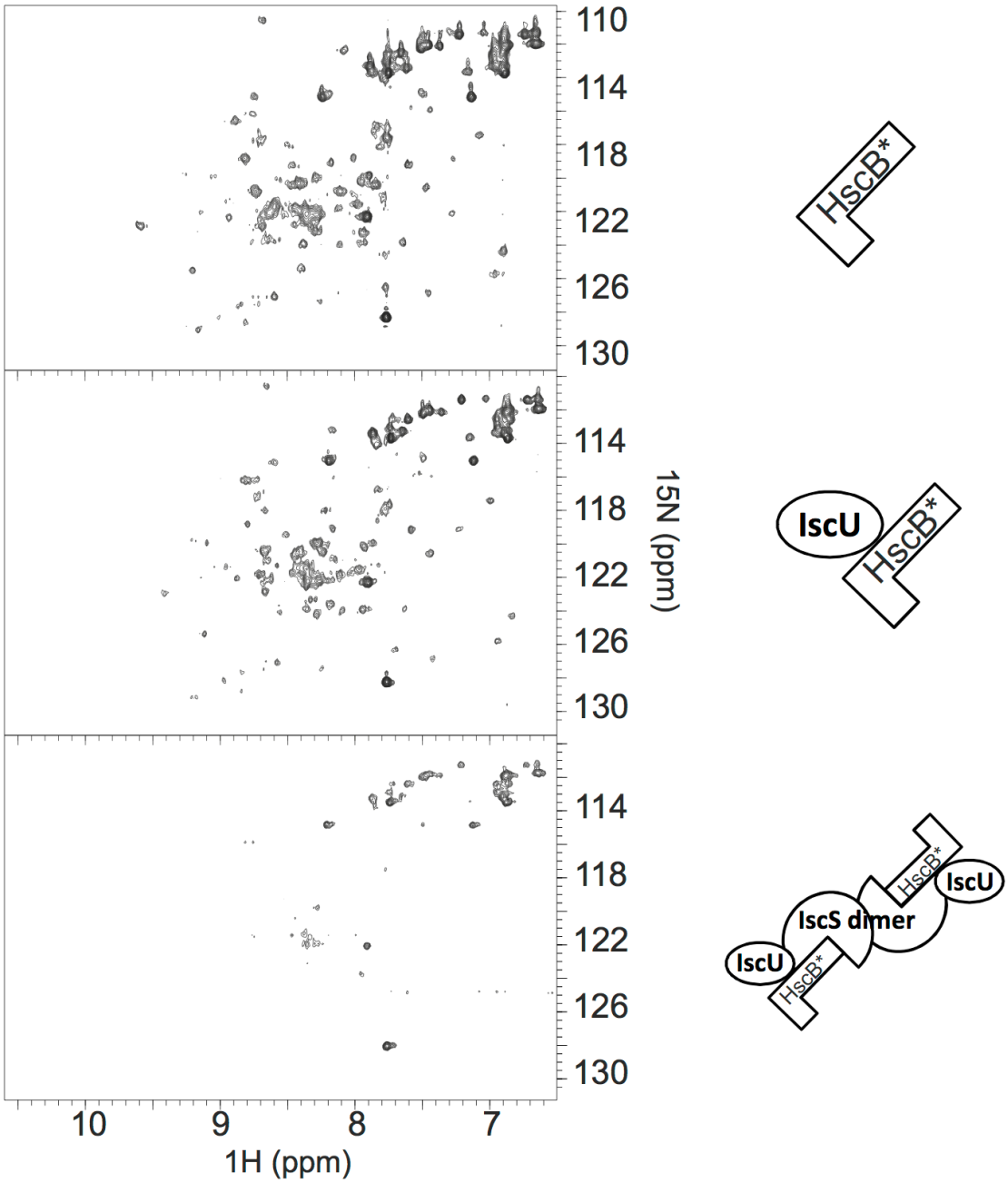

Figure 6.12 (B) IscU does not compete with IscS binding. Comparison of the spectra of ^{15}N-labelled HscB (top), the same but after addition of IscU 1:1 (middle) and after the further addition of IscS 1:1:1 (bottom) at 298 K in 20 mM Tris-HCl pH 8, 150 mM NaCl and 2 mM DTT.

I recorded the HSQC spectrum of a sample of ^{15}N labelled IscU where I added unlabelled HscB (1:0.4 IscU:HscB). I observed the typical chemical shifts expected for binding. I then added unlabelled IscS (1:0.4:0.4) and observed further disappearance of the spectrum (figure 6.12 (A)). Since also the complex composed by IscU and IscS is too big to be detectable with NMR, this result could simply mean

a displacement of HscB. Thus I also titrated labelled HscB with unlabelled IscU, to which I added unlabelled IscS (1:1:1). Also in this case the spectrum disappeared almost completely (figure 6.12 (B)). It can be noted that this result is not due to IscU displacement and HscB/IscS formation because in this last case the ^{15}N-HscB spectrum would have disappeared only partially.

These results conclusively indicate that the interaction between HscB and IscU is compatible with a furter binding with IscS.

6.4 Further evidences about the HscB/IscS interaction

All these studies provided significant information about the structure of HscB-IscS complex. I thus used the power of molecular docking to build models and add indications about the specific contacts between the two proteins. These new hints were then validated.

6.4.1 Molecular docking of the HscB-IscS complex

The software HADDOCK was used to draw and visualise the tridimensional low resolution structure of the HscB-IscS complex. It is a free platform available online which models structures of complexes starting from structures of single constituents, HscB and IscS dimer, and using experimental restraints to guide the molecular docking.

BOX 11 ***Principle of HADDOCK***

HADDOCK (High Ambiguity Driven biomolecular DOCKing) is a docking approach for the modelling of biomolecular complexes (e.g. protein-protein, protein-nucleic acids and protein-small molecule) (Dominguez, Boelens et al. 2003). This is driven by a wide variety of experimental and/or bioinformatics data (Melquiond 2010): usually interface regions are put as restrains of the docking. They could be identified

by mutagenesis, H/D exchange and chemical modifications (e.g. by crosslinkers or oxidative agents) detected by mass spectrometry, nuclear magnetic resonance, chemical shift perturbations and cross saturation. When experimental data are unavailable or scarce, this information can be supplemented by bioinformatics predictions (de Vries 2008). These information sources typically only identify or predict interfacial regions and do not define the contacts across an interface. HADDOCK defines the interfacial regions as ambiguous interaction restraints (AIRs) and it forces the interfaces to come together without imposing a particular orientation.

The docking protocol in HADDOCK consists of three successive steps: rigid-body energy minimization, semi-flexible refinement in torsion angle space and final refinement in explicit solvent refinement. HADDOCK can account for small conformational changes occurring upon binding. The selection of the final models is based on a weighted sum of electrostatics, desolvation and Van der Waals energy terms, along with the energetic contribution of the restraints used to drive the docking.

In the input file, HscB residues L22, Q49, Q56, A80, Q95, D110, E111, K119, S160, Q163, E166 and D170 were imposed as active Ambiguous Interaction Restrains (AIR) because detected by cross saturation experiments, while the IscS residues R220, R223, R225, R39, W45, K101 and K105 were chosen because they are involved in interaction as supported by the mutant studies. Residues directly adiacent to the surface were defined automatically by the program as Passive AIRs. HADDOCK returned 29 structures distributed in 5 clusters (table 6.3).

	Cluster 5	Cluster 2	Cluster 1	Cluster 3	Cluster 4
HADDOCK score	-127.2±6.3	-111.2±8.5	-108.6±13.1	-78.1±13.6	-70.3±15.3
Cluster size	4	7	9	5	4
Root mean square deviation	23.4±0.1	12.3±0.2	18.5±0.1	16.0±0.7	19.6±0.4
VdW energy	-31.9±9.5	-52.2±11.1	-39.0±5.9	-15.6±6.1	-37.5±3.1
Electrostatic energy	-699.5±41.5	-504.5±70.7	-480.0±41.4	-454.4±61.8	-266.5±21.4
Desolvatation energy	29.3±9.4	25.7±12.9	9.0±5.5	18.8±4.1	8.6±9.8
Restraints violation energy	152.1±16.88	162.8±28.36	172.7±38.16	95.5±54.45	100.3±42.15
Buried surfaced area	2179.8±151.9	2341.3±106.8	1591.0±48.7	1193.5±73.5	1232.4±29.1
Z-score	-1.3	-0.6	-0.4	1.0	1.3

Table 6.3 Statistics for the HscB-IscS docking by HADDOCK.

The clusters obtained mainly differed for the orientation of HscB that occupies the cavity centred on the IscS residues R220, R223 and R225 (figure 6.13). Each cluster is associated to a Z-score that indicates how many standard deviations far from the average the cluster is located in terms of score, the more negative being the better. Clusters 5 and 2 were the most energetically favourable with a Z-score of -1.3 and -0.6 respectively that is not significantly lower than the others. Even if cluster 5 produces a better statistic, cluster 2 clearly shows a structure where residues responsible for the binding are better orientated toward IscS. At the same time the binding surface area for IscU is positioned in an exposed area and thus available for a further binding.

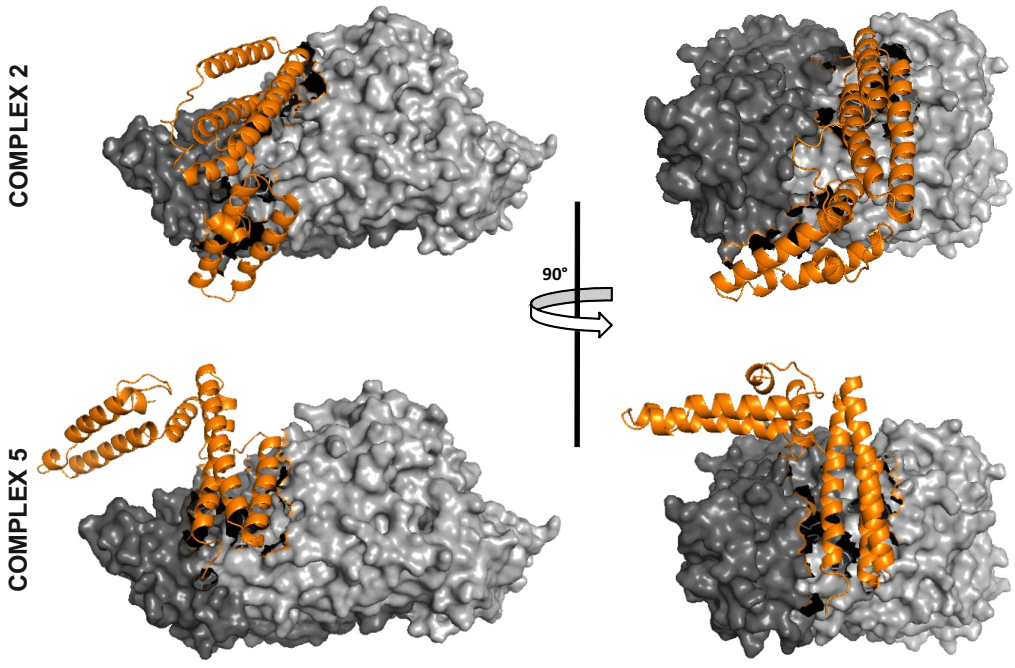

Figure 6.13 Structure of the most energetically favourable clusters (cluster 2 and 5) obtained with HADDOCK for the molecular docking of the HscB-IscS complex using 1FPO and 1P3W as PDB

starting structures. For IscS active ambiguous interaction restraints (AIRs) were defined as R220, R223, R225, R39, and W45, for the first protomer and K101 and K105 for the second promoter; for HscB, residues detected by cross saturation experimentsactive were defined as AIRs. Passive AIRs were defined automatically.

Several polar contacts were identified in the predicted structures and it could be elicited that HscB and desulfurase IscS bind through electrostatic interaction (table 6.4).

Cluster 5		Cluster 2	
HscB	**IscS**	**HscB**	**IscS**
E82	R340(B)	Q56	K318(B)
E97	R220(A), R223(A)	R62	E49(A)
E100	R237(A)	D110	R225(A)
D103	R39(A)	E111	R223(A)
E104	R67(A)	E115	R220(A),R223(A)
E106	R39(A)	E165	R220(A),R237(A)
K156	E334(B)	E166	R237(A)
K167	E311(B)		
D170	K318(B)		

in bracket the chain to which the residue belongs

Table 6.4 Polar contacts between HscB and IscS in the formation of the complex as identified in HADDOCK clusters 5 and 2.

Observing the HADDOCK models, it was evident that HscB approaches the desulfurase to its exposed positive patch through a negative surface (figure 6.14).

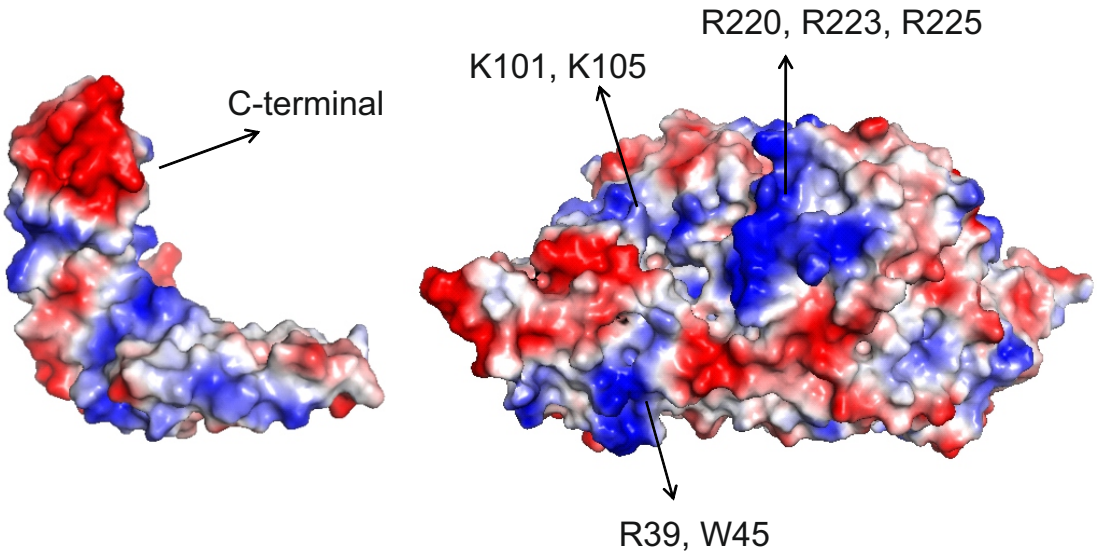

Figure 6.14 Electrostatic surfaces of HscB (left) and IscS (right). The two proteins interact through charged patches.

6.4.2 HscB binds IscS through negatevely charged residues

The surface of interaction on HscB was validated by designing acid-to-base mutations chosen among target residues that could potentially affect the interaction: E100, E111, E115, E165 and E166 from the C-terminal and E134, D137 from the region at the interface with the J-domain. I mutated acidic residues into lysines to invert the charge of the patch close to the surface involved. HscB_E100K, HscB_E111K/E115K, HscB_E134K/D137K and HscB_E165K/E166K mutants were designed to affect solvent exposed residues without altering the stability of the protein (figure 6.15).

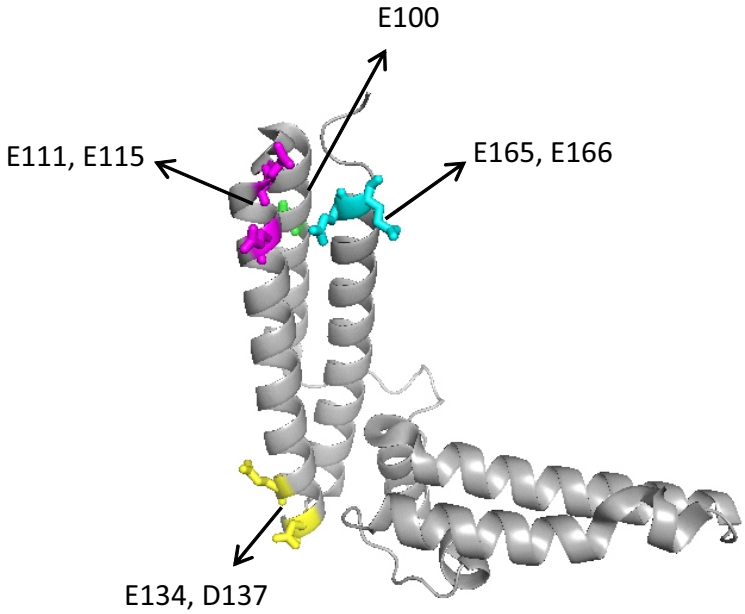

Figure 6.15 Position of the mutations on the structure of HscB (PDB code: 1FPO)

In order to introduce point mutations on HscB, the plasmid encoding for the wild-type protein was amplified by polymerase chain reaction using oligonucleotide primers carrying the desired mutations.

BOX 12 *Principle of site-directed mutagenesis*

A polymerase Chain Reaction (PCR) is a rapid method for cloning genes and duplicate DNA sequence in large amount. The DNA polymerase used is a heat stabile enzyme that synthesises strands of DNA complementary to the DNA template, the sequence of interest to be amplified. Primers, short pieces of single-stranded DNA, bind specifically to the complementary 3' end of the target sequence and allow the polymerase to synthese new DNA in the presence of nucleotides.

When a substitution mutation is desired, one of the primers must contain the desired mutation thus forming a mismatch with the template strand on the plasmid. The product of the PCR is a linearized plasmid containing the mutation at one end. Every PCR cycle consists in three steps: separation, annealing and synthesis.

Separation of the two strands of the DNA double helix to create single strands occurs at very high temperature, 94 - 96 °C. The temperature is then lowered to allow primers to bind the DNA. Optimal binding temperatures can vary because different primers anneal at different temperatures, but they are usually around 60°C. Then the temperature is raised to 72 °C to allow the DNA polymerase enzyme to synthesis new strands of complementary DNA using free nucleotides in solution. The reaction may be cycled 20 - 40 times depending on the number of copies of DNA required, the purity and amount of the sample. The number of mutated DNA sequence increase exponentially every cycle.

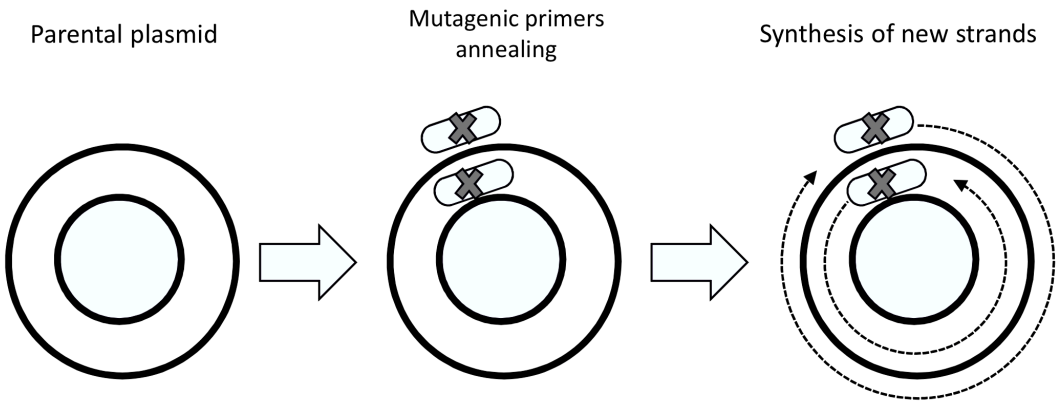

Figure 6.16 Overview of site-directed mutagenesis method.

After amplification, the parental plasmid must be degradated using DpnI to prevent false positive that may occur due to the higher transformation efficiency with the template plasmid. When PCR reaction yields a highly contaminated product, it may be convenient to purify the DNA. A ligation step is used to recircularize the mutagenized plasmid. If 5'-phosphorylated primers are used, the ligation step can be performed directly after DpnI digestion. In contrast if unmodified oligonucleotides are used, a preliminary step of phosphorylation of free 5' ends of the linearized plasmid must be performed. Re-circularization is achieved by incubating the mix with a ligase (Dominy and Andrews 2003).

Primers were designed according to the desired mutation and satisfying the following characteristics: possibly only one of the two primers contained the desired mutation; they annealed to adjacent and opposite strands of the plasmid; primers were between 25 and 45 bases length, with a melting temperature (T_m) of around 60 °C (see appendix II). Primers longer than 45 bases were avoided because of the increase of the likelihood of secondary structure formation, which may affect the efficiency of the mutagenesis reaction. T_m was calculated as below

$$T_m = 4°C \cdot (G + C) + 2°C \cdot (A + T)$$

where G is the number of guanine present in the primer, C cytosine, A adenine and T thymine. Primers optimally should have a minimum GC content of 40% and should terminate in one or more C or G bases.

In the genetic code, glutamate could be encoded by the triplet of nucleic bases *gaa* or *gag*, Aspartate by *gac* or *gat* and Lysine by *aaa* or *aag*. Primers were designed trying to minimase the mismatches: triplet *gaa* was mutated in *aaa*, *gag* and *gac* in *aag* (figure 6.17).

```
5'-atggattacttcaccctctttggcttgcctgcccgctatcaactcgatacccaggcgctg-3'
    M  D  Y  F  T  L  F  G  L  P  A  R  Y  Q  L  D  T  Q  A  L
5'-agcctgcgttttcaggatctacaacgtcagtatcatcctgataaattcgccagcggaagc-3'
    S  L  R  F  Q  D  L  Q  R  Q  Y  H  P  D  K  F  A  S  G  S
5'-caggcggaacaactcgccgccgtacagcaatctgcaaccattaaccaggcctggcaaacg-3'
    Q  A  E  Q  L  A  A  V  Q  Q  S  A  T  I  N  Q  A  W  Q  T
5'-ctgcgtcatccgttaatgcgcgcggaatatttgctttctttgcacggctttgatctcgcc-3'
    L  R  H  P  L  M  R  A  E  Y  L  L  S  L  H  G  F  D  L  A
5'-agcgagcagcatactgtgcgcgacaccgcgttcctgatggaacagttggagctgcgcgaa-3'
    S  E  Q  H  T  V  R  D  T  A  F  L  M  E  Q  L  E  L  R  E
5'-gagctggacgagatcgaacaggcgaaagatgaagcgcggctggaaagctttatcaaacgt-3'
    E  L  D  E  I  E  Q  A  K  D  E  A  R  L  E  S  F  I  K  R
5'-gtgaaaaagatgtttgatacccgccatcagttgatggttgaacagttagacaacgagacg-3'
    V  K  K  M  F  D  T  R  H  Q  L  M  V  E  Q  L  D  N  E  T
5'-tgggacgcggcggcggataccgtgcgtaagctgcgttttctcgataaactgcgaagcagt-3'
    W  D  A  A  A  D  T  V  R  K  L  R  F  L  D  K  L  R  S  S
5'-gccgaacaactcgaagaaaaactgctcgatttttaataa-3'
    A  E  Q  L  E  E  K  L  L  D  F  -  -
```

Figure 6.17 DNA sequence coding for HscB. Positions of the point mutations are evidenced in colour.

The PCR program was set with the following parameters. For the annealing step a temperature gradient of 10 °C was set in the PCR machine grid. This allowed performing reactions at different temperature at the same time.

Preheat lid	105°C	
Initial denaturation	95°C	2min
30 cycles	98°C	15s
	65-55°C	30s
	72°C	4.5min
Final extension	72°C	10min

Table 6.5 PCR program used for the site-directed mutagenesis of HscB to produce HscB_E100K, HscB_E111K/E115K, HscB_E134K/D137K and HscB_E165K/E166K mutants.

The PCR products were purified, the plasmids purity was checked on an agar gel and their sequence checked. Proteins were then expressed and purified following the same protocol as the wild-type HscB. I probed the fold of mutants by circular dichroism. CD spectra were recordeded in the range between 195 and 260nm and compared with the wild-type curve.

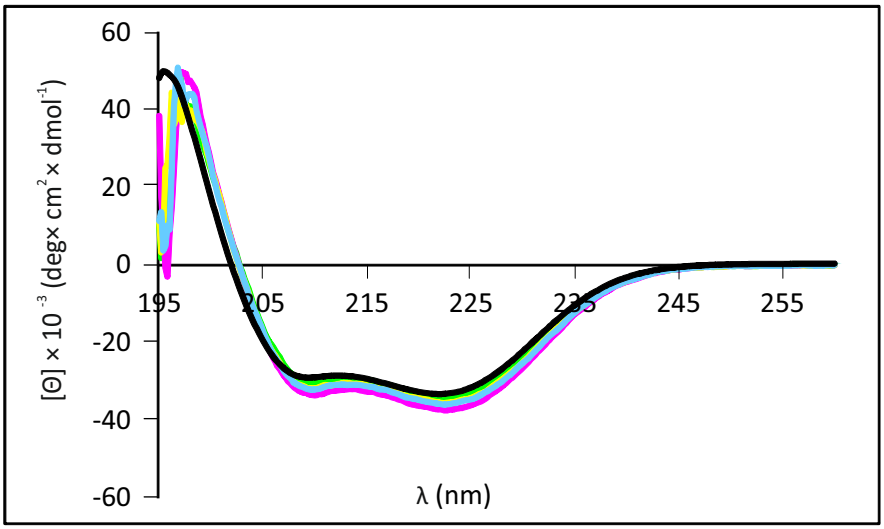

Figure 6.18 CD spectra of HscB mutants: HscB_E100K (green), HscB_E111KE115K (magenta), HscB_E134K/D137K (yellow), HscB_E165K/E166K (cyan) and HscB wt (black) with a protein concentration of 10 μM in 20 mM Tris-HCl pH 8, 150 mM NaCl and 2 mM DTT, at room temperature, in cuvettes of 1 cm path length with 0.1 nm of resolution, a band width of 2 nm and a scan speed of 200 nm/min and accumulated 30 times. The baseline correction was obtained by subtraction of the buffer spectrum.

The spectra of HscB mutants are all superposable on that of the wild-type proving that they retain the fold and do not present alterations, as it was expected since the mutations affect exposed residues (figure 6.18).

The ability of these mutants to bind IscS was tested by NMR and compared with that of HscB wild-type. If the spectrum of the mutant is not affected by addition of IscS the binding has been suppressed confirming that residues mutated belong to the surface of interaction.

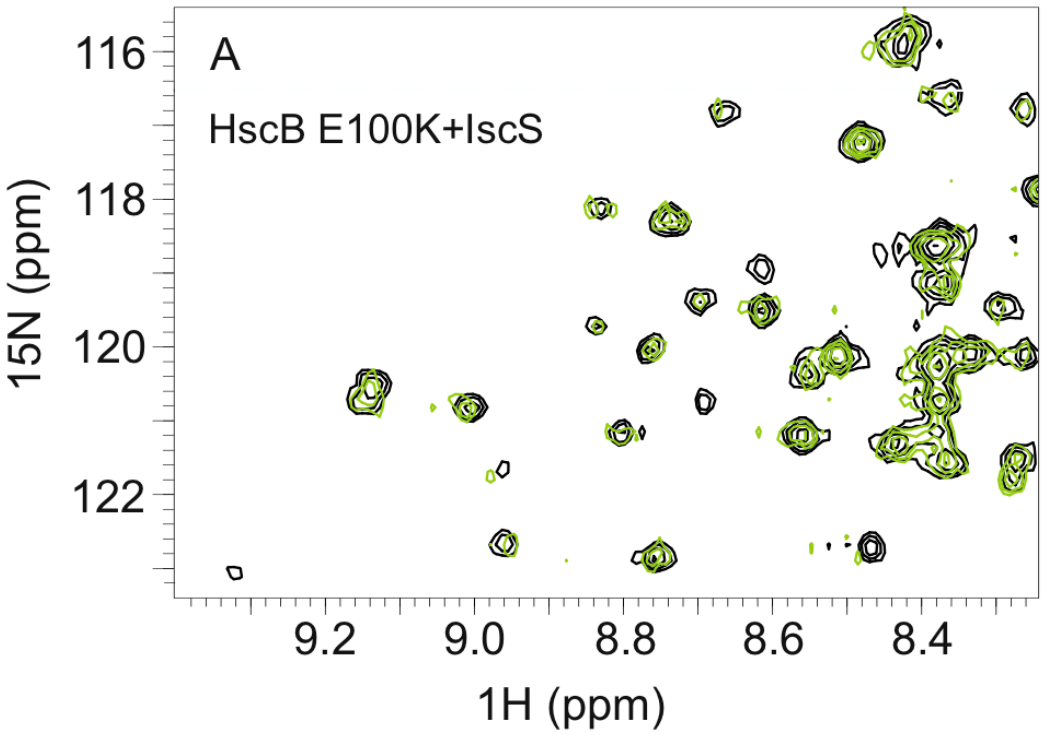

Figure 6.19 (A) HSQC-NMR spectra of HscB mutants. ^{15}N-labelled HscB_E100K 100 μM (black) and ^{15}N-labelled HscB_E100K in the presence of the IscS (1:1) (green) at 298 K in 20 mM Tris-HCl pH 8, 150 mM NaCl and 2 mM DTT.

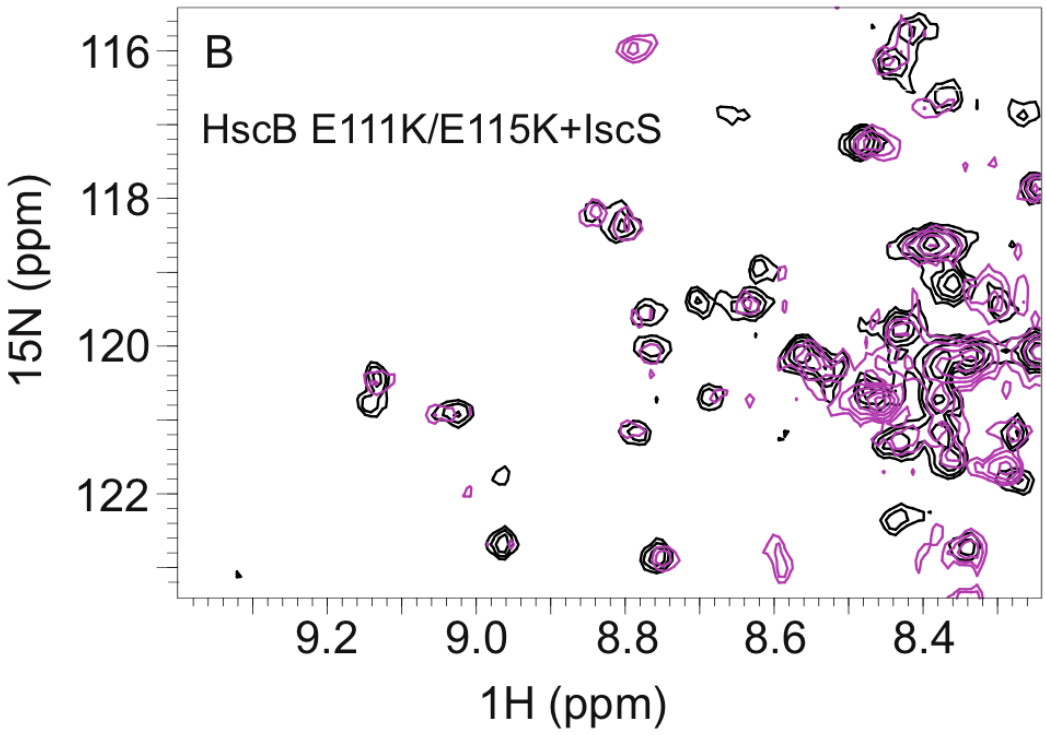

Figure 6.19 (B) HSQC-NMR spectra of HscB mutants. ^{15}N-labelled HscB_E111K/E115K 100 μM (black) and ^{15}N-labelled HscB_E111K/E115K in the presence of the IscS (1:1) (magenta) at 298 K in 20 mM Tris-HCl pH 8, 150 mM NaCl and 2 mM DTT.

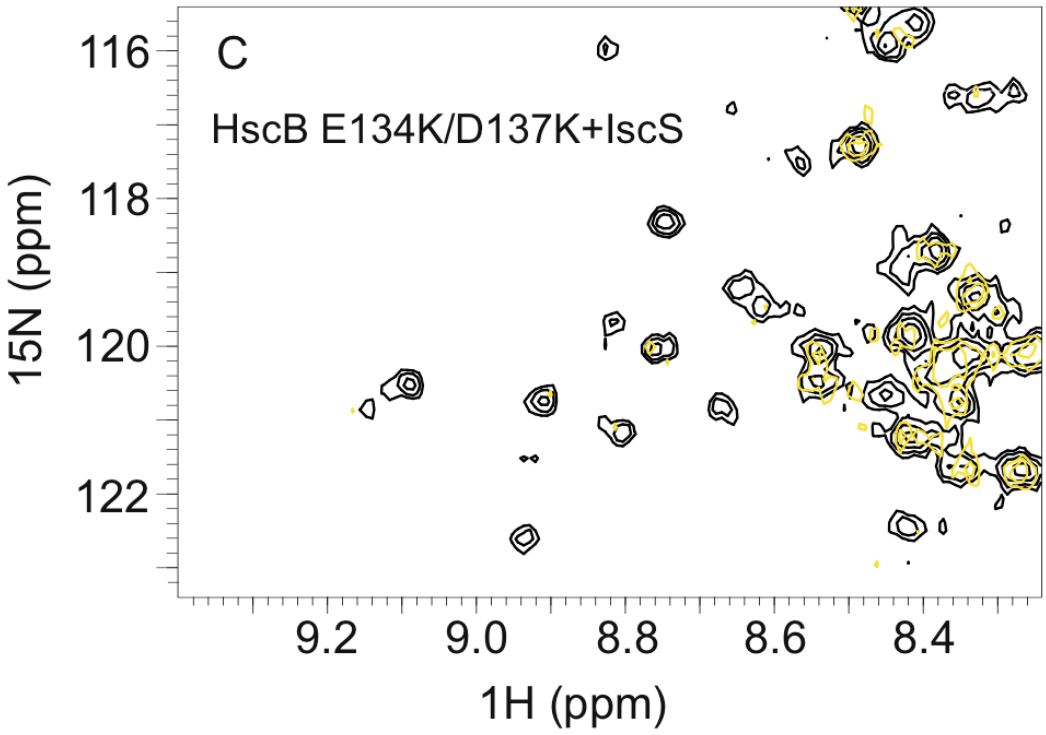

Figure 6.19 (C) HSQC-NMR spectra of HscB mutants. ^{15}N-labelled HscB_E134K/D137K 100 μM (black) and ^{15}N-labelled HscB_E134K/D137K in the presence of the IscS (1:1) (yellow) at 298 K in 20 mM Tris-HCl pH 8, 150 mM NaCl and 2 mM DTT.

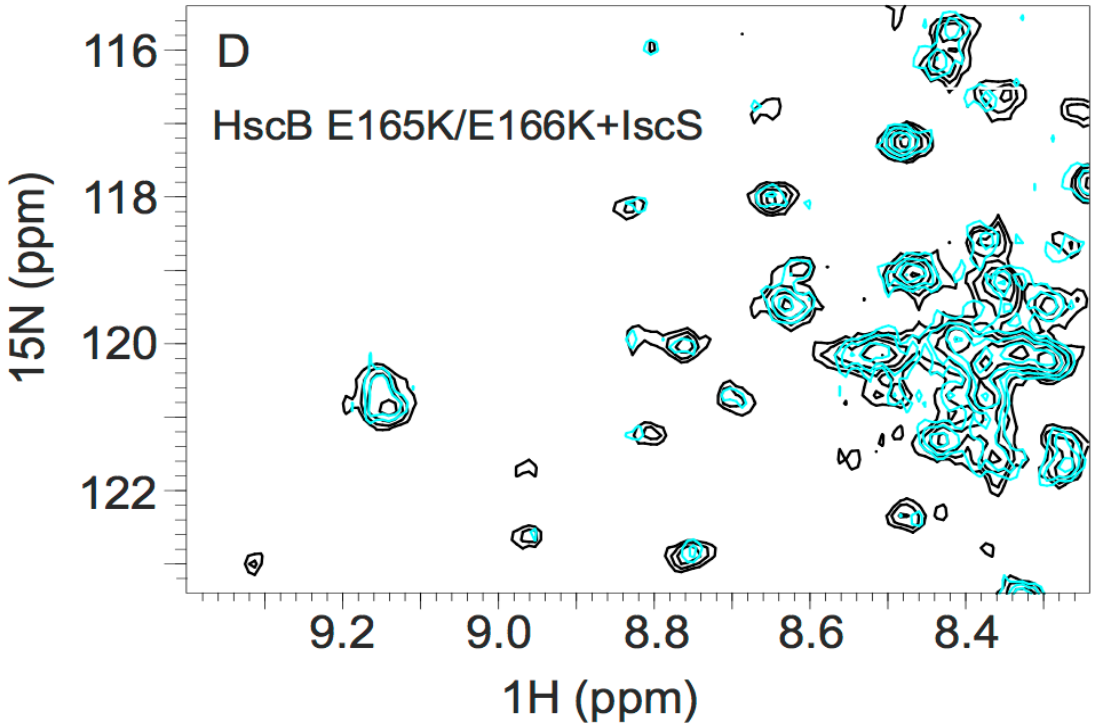

Figure 6.19 (D) HSQC-NMR spectra of HscB mutants. ^{15}N-labelled HscB_E165K/E166K 100 μM (black) and ^{15}N-labelled HscB_E165K/E166K in the presence of the IscS (1:1) (cyan) at 298 K in 20 mM Tris-HCl pH 8, 150 mM NaCl and 2 mM DTT.

With the only exception of HscB_E134K/D137K (figure 6.19 (C)), addition of IscS to the HscB mutants had effects visibly milder than the wild-type, with HscB_E100K showing the smaller effect (figure 6.19 (A, B, D).

To conclude the study, I performed the enzymatic kinetic assay: I checked the effect of the mutants on the ability of the system made by desulfurase IscS and the scaffold IscU to compose the Fe-S cluster. Kinetics were carried out in the presence of the individual mutants, with aconitase2 as protein reporter and under the same conditions used above (see chapter 4).

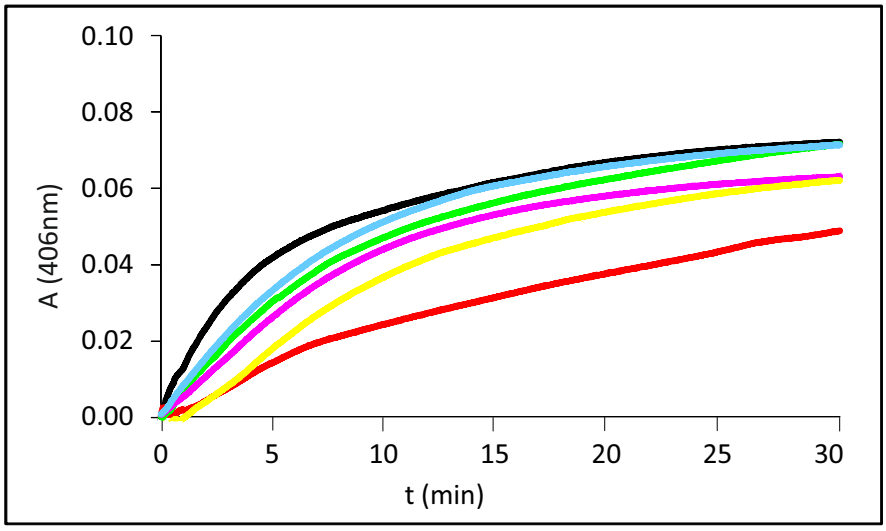

Figure 6.20 Effect of HscB mutants on the kinetics of Fe-S cluster formation on Aco2 (50 μM) in the presence of 1 μM IscS, 8μM IscU and 10 μM HscB wt (red) or HscB_E100K (green) or HscB_E111KE115K (magenta) or HscB_E134K/D137K (yellow) or HscB_E165K/E166K (cyan) in 20 mM Tris-HCl pH 8, 150 mM NaCl, 3 mM DTT, 250 μM Cys and 25 μM Fe^{2+}. The control in the absence of HscB is reported in black.

Accordingly with what was expected, all the HscB mutants led to effects comparable with the control assay in the absence of HscB. I observed inhibition only for the mutant HscB_E134K/D137K (figure 6.20).

Overall, these results confirm the interaction between IscS and HscB and validate the binding interface. It can thus be concluded that HscB binds weakly but specificly to IscS and prevalently through polar contacts involving its C-terminus domain.

6.5 Discussion

HscB presents a L-shaped structure with two arms, one spanning the C-terminus, the other the J-domain, with different length. NMR HSQC spectra and then cross saturation experiments confirmed that HscB is able to bind IscS and revealed that the binding involves a side of the long stem and causes a conformational rearrangement of part of the chain.

Some residues of IscS, belonging to specific and strategic positions for its function or for the interaction with other proteins, were mutated by previously researcher in Pastore's lab (Prischi, Konarev et al. 2010, Yan, Konarev et al. 2013). Investigating their effect on the HSQC spectrum of HscB, I identified some of the sites of IscS implicated in the binding. The surface of interaction seems to involve the cavity of IscS in the interface between the two protomers and the active site. This surface is already involved in the interaction with other components of the Isc machine, which binds with similar weak affinity, as frataxin CyaY and ferredoxin (Prischi, Konarev et al. 2010, Yan, Konarev et al. 2013). For this reason I tested the ability of CyaY and FdX to abolish binding of of HscB to IscS. I observed that frataxin replaces HscB to form a more stable complex with IscS. On the other side a higher amount of FdX was needed. As the same surface of interaction is involved in the binding with different proteins, it is interesting to suppose the requirement of a tight regulation which establishes which protein is bound at a specific time.

Interestingly the proposed binding sites on HscB for IscU involve residues that are close to the region that binds to IscS (Fuzery, Tonelli et al. 2008, Kim, Fuzery et al. 2009, Fuzery, Oh et al. 2011). According to what I observed experimentally, contemporaneus binding is still possible and they could form a complex formed by HscB, IscU and IscS, a hypothesis not previously considered. The Isc machinery is supposed to work forming different complexes at time made by proteins with a specific function relevant for each specific step of the Fe-S cluster synthesis. On the contrary, these last results opened to the possibility of a different mechanism in which IscS acts as template of a multicomplex system.

Finally, NMR-HSQC experiments and kinetic assays with specificly designed acid-to-base mutants of HscB confirmed that the two proteins interact through an electrostatic binding, as was suggested by the HADDOCK models.

6.6 Methods

^{15}N-labelled and ^{2}H, ^{15}N-labelled protein expression

^{15}N and ^{2}H,^{15}N-labelled proteins were prepared for NMR HSQC and Cross saturation experiments. Plasmids were inserted into BL21(DE3) *E. coli* cells by transformation and these were grown in minimal medium composed by M9 salts with 3 g/L of D-glucose and using 1 g/L of $(^{15}NH_4)_2SO_4$ as the sole source of nitrogen. To obtain the ^{2}H-labelling, minimal medium contained D_2O instead of water. Proteins were then expressed and purified as previously described.

NMR spectroscopy

NMR spectra were acquired on Bruker AVANCE spectrometers operating at 600, 700 and 800 MHz proton frequencies. Typically, measurements were carried out at 298K in 20 mM Tris-HCl pH 8, 150 mM NaCl and 2 mM DTT using a 0.1 mM uniformly ^{15}N-enriched HscB free and titrated with 0.1 and 0.2 mM of IscS. Water suppression was achieved by using WATERGATE (Piotto, Saudek et al. 1992). Spectra were processed by using the NMRPipe program (Delaglio, Grzesiek et al. 1995) and analyzed by Ccpnmr (Vranken, Boucher et al. 2005). Spectral assignment of HscB was based was based on the BMRB deposition (entry ID 15541).

Cross Saturation transfer NMR experiment

Cross saturation experiments were performed on a Bruker AVANCE III spectrometer at 950 MHz at 298 K, using TROSY detection on a sample of 0.100 mM ^{2}H,^{15}N-labelled HscB alone or in the presence of 0.100 mM IscS. Saturation of aliphatic resonances was achieved using a train of hyperbolic secant pulses of 50ms duration, giving a saturation bandwidth of +/-200 Hz, centered at 0.5 ppm. The overall duration of the saturation was 1s. The intensity of the amide peaks in the experiment in which the aliphatic hydrogen were saturated (on-resonance

experiment) was compared with the intensity of the amide peaks in the control off-resonance experiment.

HADDOCK Model building

Docking of the complex between HscB and dimer IscS was computed using the HADDOCK webserver interface service (*http://haddock.chem.uu.nl*) (de Vries 2010) using 1FPO and 1P3W as starting structures respectively. For IscS active ambiguous interaction restraints (AIRs) were defined as R220, R223, R225, R39, and W45, for the first protomer and K101 and K105 for the second promoter; passive AIRs were defined automatically. For HscB, active AIRs were defined as residues L22, Q49, Q56, A80, Q95, D110, E111, K119, S160, Q163, E166, D170 and passive AIRs were defined automatically by HADDOCK.

Site-directed mutagenesis and plasmids amplification

HscB mutants HscB_E100K, HscB_E111K/E115K, HscB_E134K/D137K and HscB_E165K/E166K were prepared by site-directed mutagenesis of the construct pET-24 HscB (already available in Pastore's lab) by amplification with KAPA HiFi PCR Kit and using primers ordered on Integrated DNA Techonology. PCR mixture was prepared with 1 µL of dNTP 2 mM, primers 0.25 µM, pET-24 template plasmid 0.2 µM and KAPA HiFi polymerase. After a pre-heat of the lid at 105 °C, the PCR program started reaching 98 °C for 2 min. The grid maintained a temperature of 98 °C for 15 s, reached the different annealing temperature (55.8, 57.9, 59.6, 61.6 or 63.6 °C) for 30 s and 72 °C for 4.5 s. The reaction ended with 5 min at 72 °C. The PCR product was incubated for 30 min at 37 °C with 1 µL of DpnI and purified with a Zymo Research PCR cleanup Kit. The plasmid purity was checked on an agar gel. After incubation at 37 °C for 30 min with 1 µL of T4 PNK, 1 µL of Quick ligase was added at room temperature for 10 min. Plasmid sequences was checked through the GATC service with T7 primers.

HscB mutants were expressed and purified from *E. coli* strain BL21(DE3) as

previously described. To prepare ^{15}N-labelled proteins for NMR HSQC experiments, BL21(DE3) *E. coli* cells were grown in minimal medium composed by M9 salts with 3 g/L of D-glucose and using 1 g/L using $(^{15}NH_4)_2SO_4$ as the sole source of nitrogen.

CD spectrum

Far-UV CD spectra were recorded on a Jasco J-815 CD Spectrometer. Measurements were repeated at least twice on independent protein preparations to ensure reproducibility of the results. Samples were prepared using a protein concentration of 10 µM in 20 mM Tris-HCl pH 8, 150 mM NaCl and 2 mMDTT. Measurements were carried out at room temperature in fused silica cuvettes of 1 cm path length (Hellma). Typically CD spectra were recorded between 195 and 260 nm, accumulated 30 times, with 0.1 nm of resolution, a band width of 2 nm and a scan speed of 200 nm/min. A nitrogen flow assured anaerobic conditions and a baseline correction was obtained by subtraction of the appropriate buffer spectrum.

Reconstitution experiments

Enzymatic cluster formation was achieved under strict anaerobic conditions in a Belle chamber kept under nitrogen atmosphere. The reaction was followed by absorbance spectroscopy using a Cary 50 Bio Spectrophotometer (Varian). Absorbance variations at 406 nm were measured as a function of time. A solution of 50 µM of Aco2 was incubated in sealed cuvettes typically using 3 mM DTT, 8µM IscU, 3µM HscB (wild type or mutant), 1 µM IscS and 25 µM $Fe(NH_4)_2(SO_4)_2$ for 30 minutes in 20 mM Tris-HCl pH 8 and 150 mM NaCl. The reaction was initiated by adding 250 µM of the substrate L-cysteine. Each experiment was repeated at least 3 times on different batches of proteins.

CONCLUSION

Friedreich's ataxia is a neurodegenerative disease caused by the deficiency of frataxin, an iron binding protein present in mitochondrial matrix (Pandolfo and Pastore 2009). Patients affected by this pathology show abnormalities in the iron metabolism and damage caused by oxidative stress (Pandolfo and Pastore 2009). Thus, although frataxin function is still unclear it seems to be involved in Fe-S cluster biogenesis (Pandolfo and Pastore 2009). To understand the functioning of the machinery of Fe-S cluster formation became thus of extreme importance in order to get new insights about the mechanism of neurodegenerative diseases such as Friedreich ataxia. Since frataxin is extremely conserved between species (Gibson, Koonin et al. 1996), bacterial cells are a simpler system suitable to characterize protein functions. In bacteria Fe-S clusters are synthesised by a relatively complex machinery that involves several proteins expressed by the same operon *isc* (Tokumoto and Takahashi 2001).

For the first time I investigated the Fe-S cluster formation in the presence of the chaperones HscA, HscB and ATP in addition to desulfurase IscS and scaffold protein IscU. For each component I found the best concentration for which the effect is maximum. Usually chaperones are intended as "helpers of folding" and so are expected to activate the enzyme activity (Chandramouli and Johnson 2006), conversely, I observed that HscB, alone and in the co-presence of HscA, causes a decrease in the rate of cluster formation as it was already showed by Iametti et al. (Iametti, Barbiroli et al. 2015). The inhibitory effect of HscB is independent from the Fe-S cluster acceptor used. Iametti et al. affirmed its independency also from the source of sulfur and explained the effect with the interaction between IscU and the chaperones (Iametti, Barbiroli et al. 2015). However, I demonstrated that HscB slows down also cysteine desulfuration.

I demonstrated the inhibition of the IscS activity proving a previously unidentified interaction between HscB and the desulfurase. They bind with an affinity constant K_D of around 10 μM comparable with K_D values established for interactions of others Isc proteins (~20 μM for IscS-CyaY (Prischi, Konarev et al. 2010); ~13 μM for HscB-IscU (Hoff, Silberg et al. 2000)) .

The HscB surface of interaction maps into a side of the C-terminus of its L-shaped structure. On the other hand, IscS binds the co-chaperone through the cleft in the interface between the two protomers and the active site. This is the site where also YfhJ, ferredoxin and CyaY, the bacterial otholog of frataxin, bind (Pastore, Adinolfi et al. 2006, Prischi, Konarev et al. 2010, Yan, Konarev et al. 2013). It was previously demonstrated by molecular dynamics that the binding of CyaY in this site can restrict the motions of the catalytic loop which is thought to transfer persulfide, bound to Cys238, to the nearby IscU (di Maio, Chandramouli et al. 2017). Similarly, the interaction with HscB could interfere with the loop movement by steric hindrance explaining the inhibitory effect on Fe-S cluster formation.

My studies have suggested a competition between HscB and CyaY and between HscB and ferredoxin for the same binding surface of IscS. This competition could suggest a link between these proteins with a functional significance. It is intriguing how multiple interactions of IscS with very different proteins involve the same surface of binding and suggest the requirement of a tight regulation on which specific protein is bound at the different time points. A possible way to explain my findings is to remember that IscS is a dimer. This means that, in the presence of suitable different effectors, different interactions may in principle be possible on the two IscS protomers leading to a complex but efficient regulation according to an allosteric mechanism (figure 7).

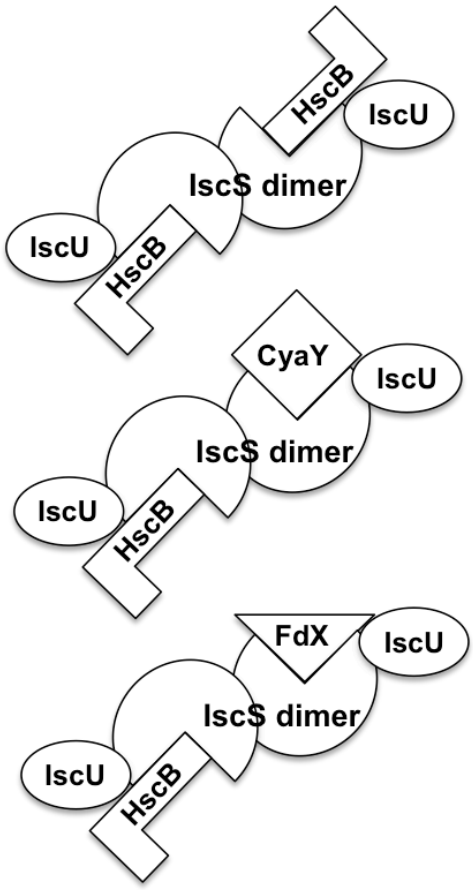

Figure 7 Scheme to illustrate the possible regulation of the IscS interactions. Different effectors may signal which components are bound to IscS at any time point keeping in mind that IscS is a dimer. The possibility of occupying two independent binding sites also makes room to the possibility that allosteric mechanisms may operate.

At the same time, the possibility of HscB to bind concomitantly IscU and IscS was probed and suggests the possibility that IscS acts as the template and mediates the interaction of the chaperones with its preferential partner IscU. An IscS-mediated interaction with IscU was also observed for the bacterial frataxin CyaY which does not interact directly with IscU at variance with the longer eukaryotic orthologue (Layer, Ollagnier-de Choudens et al. 2006, Adinolfi, Iannuzzi et al. 2009).

My unexpected results may change completely the perspective of the events involved in the Isc machine: the whole scene of action for Fe-S cluster formation seems now to gravitate around IscS rather than involving two different machines, one on IscS and the other on the two chaperones. It also proposes a potentially

different role of the two chaperones: they may not be just passive players able to "help" folding but more active components of the cellular machine. A similar view was also put forward in a recent comprehensive review in which it is proposed that chaperones are unfoldases (Finka, Mattoo et al. 2016). This hypothesis could represent a further explaination of the inhibitory effect of HscB and HscB/HscA on cluster formation and on desulfuration. It would also explain evidence suggesting that HscB binds preferentially the structured state of IscU (Kim, Tonelli et al. 2012). However, the exact role of HscB on IscS is still open.

While much more needs to be done to completely unveil the structural and functional understanding of the Fe-S cluster biogenesis, my studies add up a new tessera to the comprehension of the *isc* machine and its regulation and open new avenues to the perception of the role of chaperones.

APPENDIX I – NMR ANALYSIS

I.I Chemical shift perturbation and spectrum broadening

In principle, a good analysis of variation of a protein HSQC spectrum after the binding with a ligand, allows the determination of the surface of interaction. I tried to identify the region of HscB responsible for the interaction with IscS with a molar ratio of 1:1. Unfortunately the binding causes the formation of a complex of around 130 kDa that increases the correlation time with a significant broadening in the spectrum. This made the analysis hard and the precise identification of the residues involved difficult.

First, for each resonance, I plotted the chemical shift perturbation upon IscS addition calculated directly by CcpNmr as $\sqrt{\frac{1}{2}(\delta_H^2 + 0.15\delta_N^2)}$ and I selected those with $\Delta\delta \geq 0.018 ppm$ (L22, H63, Q95, R99, E104, E106, E111, I118, K119, M124, L157, A161 and D170) (figure I.I).

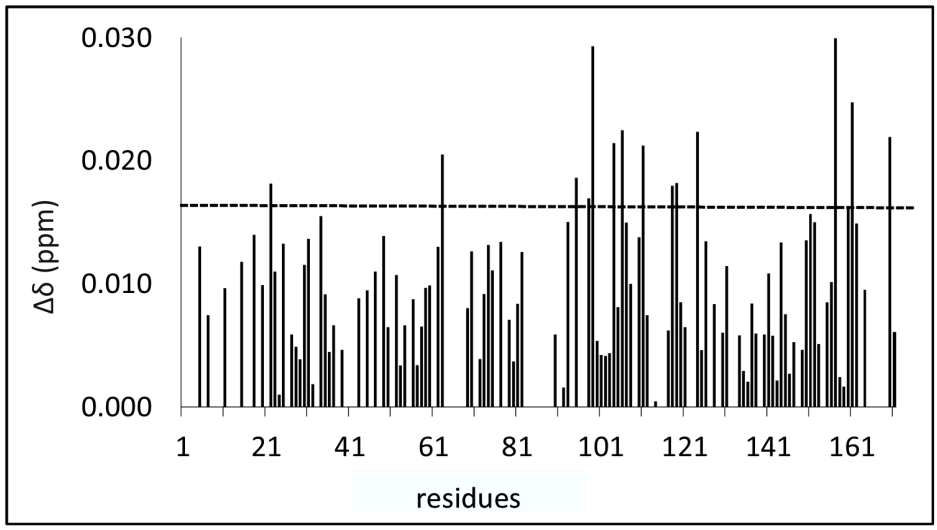

Figure I.I Chemical shift perturbation in the HSQC spectrum of 100 μM HscB after the addition of IscS (1:1) at 298K in 20 mM Tris-HCl pH 8, 150 mM NaCl and 2 mM DTT.

To estimate the region that is more affected by the broadening, for each peak I measured the variation in height and in volume compared with the values in the free

protein spectrum. I identified residues for which both values exceed 90% of variation (Q14, L20, E104, E106, Q107, D110, E111, F117, I118, L131, Q135, D155, L157, A161, E162) (figure I.II).

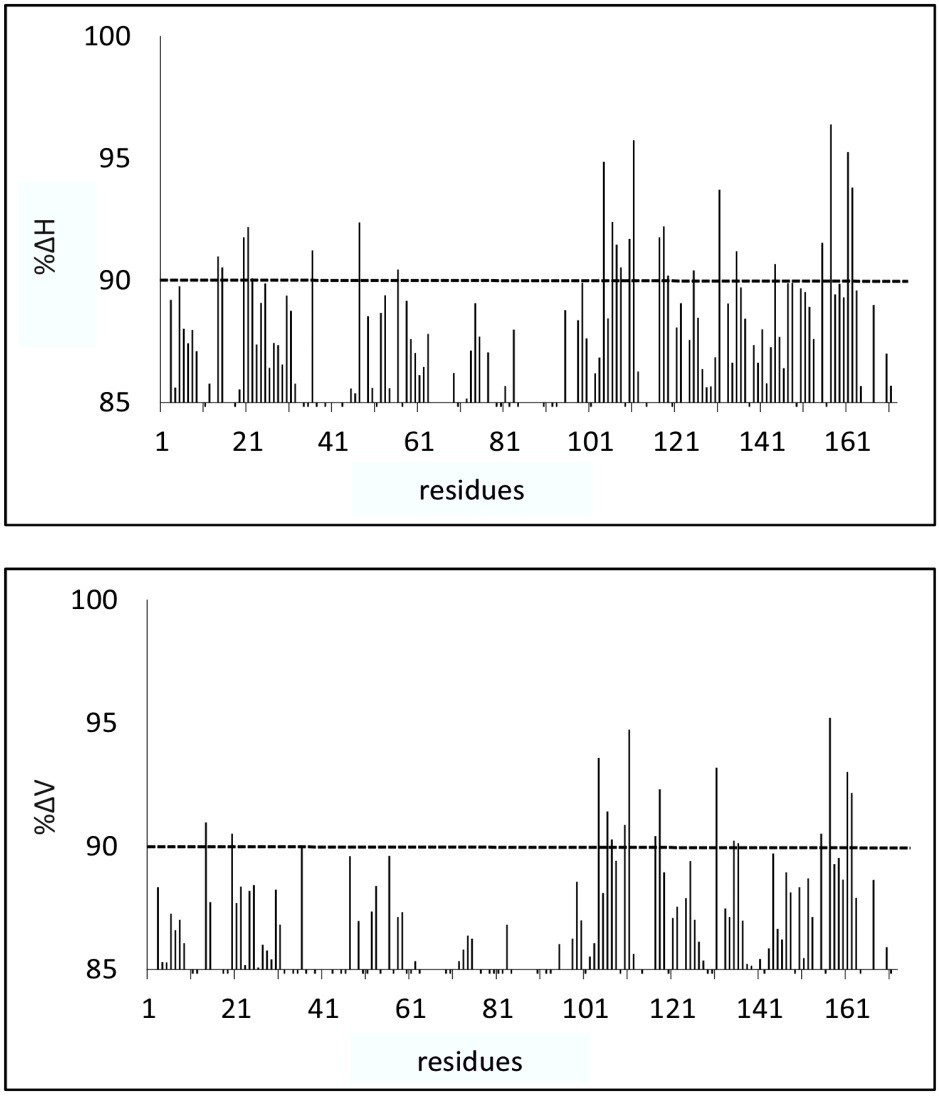

Figure I.II Peaks broadening determination. Variations of height and volume of peaks in the HSQC spectrum of 100 µM HscB after the addition of IscS (1:1) at 298K in 20 mM Tris-HCl pH 8, 150 mM NaCl and 2 mM DTT.

I.II Analysis of cross saturation experiment

To perform the cross saturation experiment, HscB was expressed and purified as uniformly labelled with ^{2}H and ^{15}N. Levels of deuteration of around 90% were obtained and, since some protons were still present in the protein side chains, HscB free spectrum was not completely aneffected by cross saturation sequence. I then recorded the spectrum after the addition of IscS (1:1).

For both the samples (HscB and HscB:IscS mixture), I plotted the difference between the TROSY spectrum recorded in the experiment with the aliphatic hydrogen saturated and the spectrum in which the aliphatic radio frequence was off. The spectra obtained presented high levels of noise and weak signals. In order to avoid artifacts due to the not perfect deuteration of HscB, height and volume values of peaks in the free protein sample were subtracted from the values in the mixture. I finally identified residues for which both values of heigh and volume overseeded the average value of variation plus one standard deviation (L22, Q49, Q56, A80, Q95, D110, E111, K119, S160, Q163, E166, D170, and F171) (figure I.III).

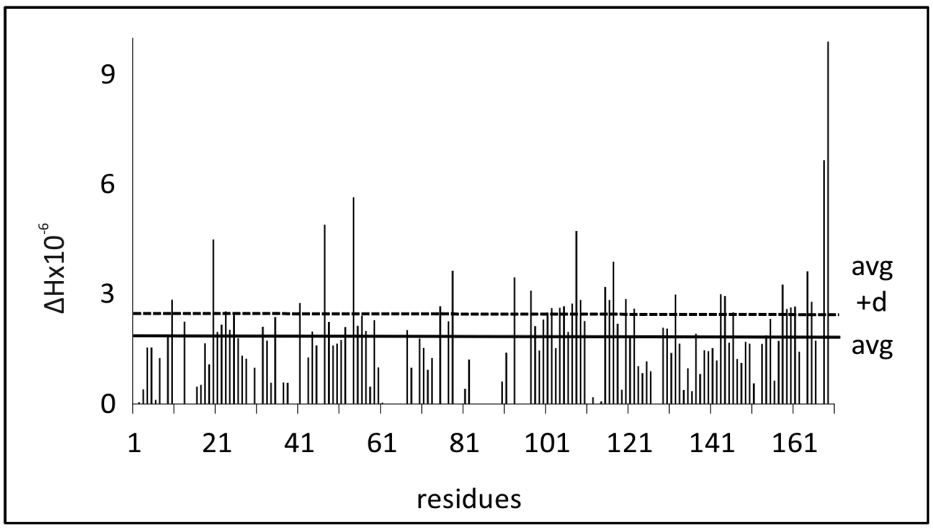

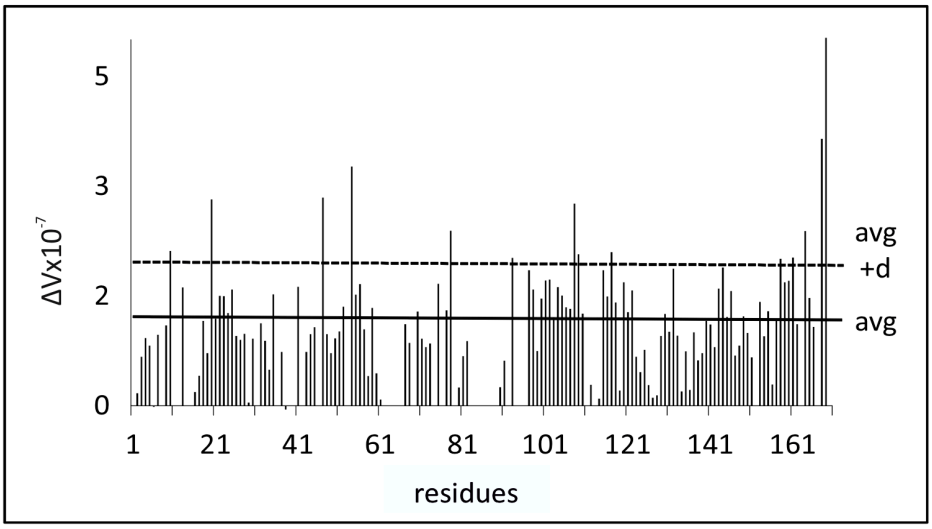

Figure I.III Determination of residues affected by cross saturation. Variations of height and volume in the TROSY spectrum of 100 μM HscB after the addition of IscS (1:1) at 298 K in 20 mM Tris-HCl pH 8, 150 mM NaCl and 2 mM DTT. Saturation of aliphatic resonances was achieved with a pulses centered at 0.5 ppm.

APPENDIX II – PRIMERS DESIGN

Below are reported the schemes of the primers designed and ordered from Integrated DNA Techonology (IDT) for the HscB site-directed mutagenesis. Mutatated residues are indicated. Forward primers, in the 5'-3' direction, are reported in bold. Reverse primers, in the 3'-5' direction, are underlined. They were ordered in their reverse complementary form.

HscB E100K sequence

```
5'-atggattacttcaccctctttggcttgcctgcccgctatcaactcgatacccaggcgctg-3'
    M  D  Y  F  T  L  F  G  L  P  A  R  Y  Q  L  D  T  Q  A  L
5'-agcctgcgttttcaggatctacaacgtcagtatcatcctgataaattcgccagcggaagc-3'
    S  L  R  F  Q  D  L  Q  R  Q  Y  H  P  D  K  F  A  S  G  S
5'-caggcggaacaactcgccgccgtacagcaatctgcaaccattaaccaggcctggcaaacg-3'
    Q  A  E  Q  L  A  A  V  Q  Q  S  A  T  I  N  Q  A  W  Q  T
5'-ctgcgtcatccgttaatgcgcgcggaatatttgctttctttgcacggctttgatctcgcc-3'
    L  R  H  P  L  M  R  A  E  Y  L  L  S  L  H  G  F  D  L  A
5'-agcgagcagcatactgtgcgcgacaccgcgttcctgatggaacagttgGAGCTGCGCAAA-3'
    S  E  Q  H  T  V  R  D  T  A  F  L  M  E  Q  L  E  L  R  K
5'-GAGCTGGacgagatcgaacaggcgaaagatgaagcgcggctggaaagctttatcaaacgt-3'
    E  L  D  E  I  E  Q  A  K  D  E  A  R  L  E  S  F  I  K  R
5'-gtgaaaaagatgtttgatacccgccatcagttgatggttgaacagttagacaacgagacg-3'
    V  K  K  M  F  D  T  R  H  Q  L  M  V  E  Q  L  D  N  E  T
5'-tgggacgcggcggcggataccgtgcgtaagctgcgttttctcgataaactgcgaagcagt-3'
    W  D  A  A  A  D  T  V  R  K  L  R  F  L  D  K  L  R  S  S
5'-gccgaacaactcgaagaaaaactgctcgatttttaataa-3'
    A  E  Q  L  E  E  K  L  L  D  F  -  -
```

Primers sequence

E100K_forward `5'-gagctgcgcAaagagctgg-3'`

%GC: 58 and T_m: 66°C

E100K_reverse `5'-caactgttccatcaggaacgc-3'`

%GC: 52 and T_m: 65°C

HscB E111,115K sequence

```
5'-atggattacttcaccctctttggcttgcctgcccgctatcaactcgatacccaggcgctg-3'
    M  D  Y  F  T  L  F  G  L  P  A  R  Y  Q  L  D  T  Q  A  L
5'-agcctgcgttttcaggatctacaacgtcagtatcatcctgataaattcgccagcggaagc-3'
    S  L  R  F  Q  D  L  Q  R  Q  Y  H  P  D  K  F  A  S  G  S
5'-caggcggaacaactcgccgccgtacagcaatctgcaaccattaaccaggcctggcaaacg-3'
    Q  A  E  Q  L  A  A  V  Q  Q  S  A  T  I  N  Q  A  W  Q  T
5'-ctgcgtcatccgttaatgcgcgcggaatatttgctttctttgcacggctttgatctcgcc-3'
    L  R  H  P  L  M  R  A  E  Y  L  L  S  L  H  G  F  D  L  A
5'-agcgagcagcatactgtgcgcgacaccgcgttcctgatggaacagttggagctgcgcgaa-3'
    S  E  Q  H  T  V  R  D  T  A  F  L  M  E  Q  L  E  L  R  E
5'-gagctggacgagatcgaacaggcgaaagatAaagcgcggctgAaaagctttatcaaacgt-3'
    E  L  D  E  I  E  Q  A  K  D  K  A  R  L  K  S  F  I  K  R
5'-gtgaaaaagatgtttgatacccgccatcagttgatggttgaacagttagacaacgagacg-3'
    V  K  K  M  F  D  T  R  H  Q  L  M  V  E  Q  L  D  N  E  T
5'-tgggacgcggcggcggataccgtgcgtaagctgcgttttctcgataaactgcgaagcagt-3'
    W  D  A  A  A  D  T  V  R  K  L  R  F  L  D  K  L  R  S  S
5'-gccgaacaactcgaagaaaaactgctcgatttttaataa-3'
    A  E  Q  L  E  E  K  L  L  D  F  -  -
```

Primers sequence

E111,115K_forward `5'-cggctgAaaagctttatcaaac-3'`

%GC: 41 and T_m: 61°C

E111,115K_reverse `5'-cgcttTatctttcgcctgt-3'`

%GC: 47 and T_m: 61°C

HscB E134K, D137K sequence

```
5'-atggattacttcaccctctttggcttgcctgcccgctatcaactcgatacccaggcgctg-3'
    M  D  Y  F  T  L  F  G  L  P  A  R  Y  Q  L  D  T  Q  A  L
5'-agcctgcgttttcaggatctacaacgtcagtatcatcctgataaattcgccagcggaagc-3'
    S  L  R  F  Q  D  L  Q  R  Q  Y  H  P  D  K  F  A  S  G  S
5'-caggcggaacaactcgccgccgtacagcaatctgcaaccattaaccaggcctggcaaacg-3'
    Q  A  E  Q  L  A  A  V  Q  Q  S  A  T  I  N  Q  A  W  Q  T
5'-ctgcgtcatccgttaatgcgcgcggaatatttgctttctttgcacggctttgatctcgcc-3'
    L  R  H  P  L  M  R  A  E  Y  L  L  S  L  H  G  F  D  L  A
5'-agcgagcagcatactgtgcgcgacaccgcgttcctgatggaacagttggagctgcgcgaa-3'
    S  E  Q  H  T  V  R  D  T  A  F  L  M  E  Q  L  E  L  R  E
5'-gagctggacgagatcgaacaggcgaaagatgaagcgcggctggaaagctttatcaaacgt-3'
    E  L  D  E  I  E  Q  A  K  D  E  A  R  L  E  S  F  I  K  R
5'-gtgaaaaagatgtttgatacccgccatcagttgatggttAaacagttaAaGaacgagacg-3'
    V  K  K  M  F  D  T  R  H  Q  L  M  V  K  Q  L  K  N  E  T
5'-tgggacgcggcggcggataccgtgcgtaagctgcgttttctcgataaactgcgaagcagt-3'
    W  D  A  A  A  D  T  V  R  K  L  R  F  L  D  K  L  R  S  S
5'-gccgaacaactcgaagaaaaactgctcgatttttaataa-3'
    A  E  Q  L  E  E  K  L  L  D  F  -  -
```

Primers sequence:

E134K, D137K_forward `5'-ttaAaGaacgagacgtgggac-3'`

%GC: 48 and T_m: 61°C

E134K, D137K_reverse `5'-ctgttTaaccatcaactgatgg-3'`

%GC: 41 and T_m: 60°C

HscB E165,166K sequence

```
5'-atggattacttcaccctctttggcttgcctgcccgctatcaactcgatacccaggcgctg-3'
    M  D  Y  F  T  L  F  G  L  P  A  R  Y  Q  L  D  T  Q  A  L
5'-agcctgcgttttcaggatctacaacgtcagtatcatcctgataaattcgccagcggaagc-3'
    S  L  R  F  Q  D  L  Q  R  Q  Y  H  P  D  K  F  A  S  G  S
5'-caggcggaacaactcgccgccgtacagcaatctgcaaccattaaccaggcctggcaaacg-3'
    Q  A  E  Q  L  A  A  V  Q  Q  S  A  T  I  N  Q  A  W  Q  T
5'-ctgcgtcatccgttaatgcgcgcggaatatttgctttctttgcacggctttgatctcgcc-3'
    L  R  H  P  L  M  R  A  E  Y  L  L  S  L  H  G  F  D  L  A
5'-agcgagcagcatactgtgcgcgacaccgcgttcctgatggaacagttggagctgcgcgaa-3'
    S  E  Q  H  T  V  R  D  T  A  F  L  M  E  Q  L  E  L  R  E
5'-gagctggacgagatcgaacaggcgaaagatgaagcgcggctggaaagctttatcaaacgt-3'
    E  L  D  E  I  E  Q  A  K  D  E  A  R  L  E  S  F  I  K  R
5'-gtgaaaaagatgtttgatacccgccatcagttgatggttgaacagttagacaacgagacg-3'
    V  K  K  M  F  D  T  R  H  Q  L  M  V  E  Q  L  D  N  E  T
5'-tgggacgcggcggcggataccgtgcgtaagctgcgttttctcgataaactgcgaagcagt-3'
    W  D  A  A  A  D  T  V  R  K  L  R  F  L  D  K  L  R  S  S
5'-gccgaacaactcAaaAaaaaactgctcgattttaataagcg-3'
    A  E  Q  L  K  K  K  L  L  D  F  -  -
```

Primers sequence

E165,166K_forward `5'-cgaacaactcAaaAaaaaactgctcg-3'`

%GC: 42 and T_m: 65°C

E165,166K_reverse `5'-gcactgcttcgcagtttatcg-3'`

%GC: 52 and T_m: 66°C

APPENDIX III – ISC PROTEINS STRUCTURAL REVIEW

Three-dimensional structures of Isc proteins and their complexes provided important insight into the process of Fe-S cluster biosynthesis and transfer. The scheme below summarizes the relevant information about all the Isc protein structures deposited in PDB.

Protein	Comment	Organism	PDB code (method)
IscU	Scaffold protein	E. coli	2l4x (NMR)
IscU(D39A)	Scaffold protein variant with stabilized S-state	E. coli	2kqk (NMR)
IscU(D39A)-[2Fe-2S]	Holo scaffold protein	Aquifex aeolicus	2z7e (X-ray)
IscU-Zn	Inhibited form of IscU	Haemophilus influenzae	1rp9 (NMR)
IscU-Zn	Inhibited form of IscU	Thermus thermophilus	2qq4 (X-ray)
IscU-Zn	Inhibited form of IscU	Streptococcus pyogenes	1su0 (X-ray)
IscS	Cysteine desulfurase; $(IscS)_2$ homodimer	E. coli	1p3w (X-ray)
IscU-IscS complex	$(IscU)_2$-$(IscS)_2$	E. coli	3lvl (X-ray)
IscU(D39A)-[2Fe-2S] complex	$(IscU\text{-}[2Fe\text{-}2S])_2$-$(IscS)_2$	Archaeoglobus fulgidus	4eb5 (X-ray)
IscU(D39A)-[2Fe-2S] complex	Oxydatively degraded	Archaeoglobus fulgidus	4eb7 (X-ray)
IscA(1-105)	Iron delivery, alternative scaffold; homo-tetramer, Hg derivative	E. coli	1r94 (X-ray)
IscA(1-107)	Iron delivery, alternative scaffold; homo-tetramer, apo-protein	E. coli	1s98 (X-ray)
IscA(1-116)	Iron delivery, alternative scaffold; monomer	Aquifex aeolicus	1nwb (NMR)
YfhJ	Iron delivery or frataxin-like regulator of cluster assembly?	E. coli	1uj8 (X-ray)
YfhJ	Iron delivery or frataxin-like regulator of cluster assembly?	E. coli	2bzt (NMR)
CyaY	Inhibitor of cluster assembly	E. coli	1ew4 (X-ray)
CyaY-Fe complex	Iron delivery protein?	E. coli	1soy (NMR)
Yfh1	Iron delivery protein	Saccharomyces cerevisiae	1xaq (NMR)
Yfh1 (trimeric)	Iron delivery protein	Saccharomyces cerevisiae	2fql (X-ray)
Yfh1 (trimeric)	Iron delivery protein	Saccharomyces cerevisiae	3oeq (X-ray)
Yfh1 (trimeric, Co complex)	Iron delivery protein	Saccharomyces cerevisiae	3oer (X-ray)
Yfh1 (trimeric, Fe^{2+} complex)	Iron delivery protein	Saccharomyces cerevisiae	4ec2 (X-ray)
frataxin	Enhances desulfurase activity	Homo sapiens	1ekg (X-ray)
frataxin	Enhances desulfurase activity	Homo sapiens	1ly7 (NMR)
HscA(390-615)- peptide complex	Chaperone (DnaK-type protein) substrate binding domain with bound IscU peptide	E. coli	1u00 (X-ray)
HscB	Co-chaperone (DnaJ-type protein)	E. coli	1fpo (X-ray)
Hsc20	Co-chaperone (DnaJ-type protein)	Homo sapiens	3bvo (X-ray)
FdX	Electron transfer	E. coli	1i7h (X-ray)
IscR	Apo-repressor protein; homodimer	E. coli	4hf0 (X-ray)
IscR-DNA complex	Homodimer with bound HYA promotor fragment	E. coli	4chu (X-ray)

Table IV Proteins involved in iron-sulfur cluster assembly and relevant structural information (Kim, Bothe et al. 2015).

APPENDIX IV - PUBLICATIONS

Papers published during my PhD course of which I am one of the author:

Puglisi R., Yan R., Adinolfi S. and Pastore A., (2016). *A new tessera into the interactome of the isc operon: A novel interaction between HscB and IscS*. Front. Mol. Biosci. 3:48.

Faggianelli N., **Puglisi R.**, Veneziano L., Romano S., Frontali M., Vannocci T., Fortuni S., Testi R. and Pastore A. (2015). Analyzing the Effects of a G137V Mutation in the *FXN* Gene. *Frontiers in Molecular Neuroscience*, *8*, 66.

Iannuzzi C., Adrover M., **Puglisi R.**, Yan R., Temussi P. A., & Pastore A. (2014). The role of zinc in the stability of the marginally stable IscU scaffold protein. *Protein Science : A Publication of the Protein Society*, *23*(9), 1208–1219.

Sanfelice D., **Puglisi R.**, Martin S. R., Di Bari L., Pastore A., & Temussi P. A. (2014). Yeast Frataxin Is Stabilized by Low Salt Concentrations: Cold Denaturation Disentangles Ionic Strength Effects from Specific Interactions. *PLoS ONE*, *9*(5), e95801.

BIBLIOGRAPHY

Adinolfi, S., C. Iannuzzi, F. Prischi, C. Pastore, S. Iametti, S. R. Martin, F. Bonomi and A. Pastore (2009). "Bacterial frataxin CyaY is the gatekeeper of iron-sulfur cluster formation catalyzed by IscS." Nat Struct Mol Biol **16**(4): 390-396.

Adinolfi, S., M. Nair, A. Politou, E. Bayer, S. Martin, P. Temussi and A. Pastore (2004). "The factors governing the thermal stability of frataxin orthologues: how to increase a protein's stability." Biochemistry **43**(21): 6511-6518.

Adinolfi, S., F. Rizzo, L. Masino, M. Nair, S. R. Martin, A. Pastore and P. A. Temussi (2004). "Bacterial IscU is a well folded and functional single domain protein." Eur J Biochem **271**(11): 2093-2100.

Adinolfi, S., M. Trifuoggi, A. S. Politou, S. Martin and A. Pastore (2002). "A structural approach to understanding the iron-binding properties of phylogenetically different frataxins." Hum Mol Genet **11**(16): 1865-1877.

Agar, J. N., C. Krebs, J. Frazzon, B. H. Huynh, D. R. Dean and M. K. Johnson (2000). "IscU as a scaffold for iron-sulfur cluster biosynthesis: sequential assembly of [2Fe-2S] and [4Fe-4S] clusters in IscU." Biochemistry **39**(27): 7856-7862.

Ashley, C. N., K. D. Hoang, D. R. Lynch, S. L. Perlman and B. L. Maria (2012). "Childhood ataxia: clinical features, pathogenesis, key unanswered questions, and future directions." J Child Neurol **27**(9): 1095-1120.

Ayala-Castro, C., A. Saini and F. W. Outten (2008). "Fe-S cluster assembly pathways in bacteria." Microbiol Mol Biol Rev **72**(1): 110-125, table of contents.

Beinert, H. (2000). "Iron-sulfur proteins: ancient structures, still full of surprises." J Biol Inorg Chem **5**(1): 2-15.

Beinert, H., R. H. Holm and E. Munck (1997). "Iron-sulfur clusters: nature's modular, multipurpose structures." Science **277**(5326): 653-659.

Beinert, H., M. C. Kennedy and C. D. Stout (1996). "Aconitase as Ironminus signSulfur Protein, Enzyme, and Iron-Regulatory Protein." Chem Rev **96**(7): 2335-2374.

Beinert, H. and P. J. Kiley (1999). "Fe-S proteins in sensing and regulatory functions." Curr Opin Chem Biol **3**(2): 152-157.

Bertini, I., J. A. Cowan, C. Del Bianco, C. Luchinat and S. S. Mansy (2003). "Thermotoga maritima IscU. Structural characterization and dynamics of a new class of metallochaperone." J Mol Biol **331**(4): 907-924.

Bilder, P. W., H. Ding and M. E. Newcomer (2004). "Crystal structure of the ancient, Fe-S scaffold IscA reveals a novel protein fold." Biochemistry **43**(1): 133-139.

Bonomi, F., S. Iametti, A. Morleo, D. Ta and L. E. Vickery (2008). "Studies on the mechanism of catalysis of iron-sulfur cluster transfer from IscU[2Fe2S] by HscA/HscB chaperones." Biochemistry **47**(48): 12795-12801.

Bonomi, F., S. Iametti, A. Morleo, D. Ta and L. E. Vickery (2011). "Facilitated transfer of IscU-[2Fe2S] clusters by chaperone-mediated ligand exchange." Biochemistry **50**(44): 9641-9650.

Bonomi, F., S. Iametti, D. Ta and L. E. Vickery (2005). "Multiple turnover transfer of [2Fe2S] clusters by the iron-sulfur cluster assembly scaffold proteins IscU and IscA." J Biol Chem **280**(33): 29513-29518.

Bonomi, F., S. Pagani and D. M. Kurtz, Jr. (1985). "Enzymic synthesis of the 4Fe-4S clusters of Clostridium pasteurianum ferredoxin." Eur J Biochem **148**(1): 67-73.

Brahms, S. and J. Brahms (1980). "Determination of protein secondary structure in solution by vacuum ultraviolet circular dichroism." J Mol Biol **138**(2): 149-178.

Bridwell-Rabb, J., C. Iannuzzi, A. Pastore and D. P. Barondeau (2012). "Effector role reversal during evolution: the case of frataxin in Fe-S cluster biosynthesis." Biochemistry **51**(12): 2506-2514.

Bulteau, A. L., H. A. O'Neill, M. C. Kennedy, M. Ikeda-Saito, G. Isaya and L. I. Szweda (2004). "Frataxin acts as an iron chaperone protein to modulate mitochondrial aconitase activity." Science **305**(5681): 242-245.

Chandramouli, K. and M. K. Johnson (2006). "HscA and HscB stimulate [2Fe-2S] cluster transfer from IscU to apoferredoxin in an ATP-dependent reaction." Biochemistry **45**(37): 11087-11095.

Correia, A. R., S. Adinolfi, A. Pastore and C. M. Gomes (2006). "Conformational stability of human frataxin and effect of Friedreich's ataxia-related mutations on protein folding." Biochem J **398**(3): 605-611.

Correia, A. R., C. Pastore, S. Adinolfi, A. Pastore and C. M. Gomes (2008). "Dynamics, stability and iron-binding activity of frataxin clinical mutants." FEBS J **275**(14): 3680-3690.

Cowan, J. A. (2009). Iron Sulfur Cluster Biosynthesis. Bioinorganic Chemistry**:** 3-16.

Crack, J. C., J. Green, A. J. Thomson and N. E. Le Brun (2012). "Iron-sulfur cluster sensor-regulators." Curr Opin Chem Biol **16**(1-2): 35-44.

Cupp-Vickery, J. R., J. C. Peterson, D. T. Ta and L. E. Vickery (2004). "Crystal structure of the molecular chaperone HscA substrate binding domain complexed with the IscU recognition peptide ELPPVKIHC." J Mol Biol **342**(4): 1265-1278.

Cupp-Vickery, J. R., H. Urbina and L. E. Vickery (2003). "Crystal structure of IscS, a cysteine desulfurase from Escherichia coli." J Mol Biol **330**(5): 1049-1059.

de Vries, S. J., Bonvin, M. J. J. (2008). "How proteins get in touch: interface prediction in the study of biomolecular complexes." Current Protein and Peptide Scence **9**: 394-406.

de Vries, S. J., Melquiond, A. S. J., Kastritis, P. L., Karaca, E., Bordogna, A., van Dijk, M., Rodrigues, J. P. G. L. M, Bonvin, A. M. J. J (2010). "Strenghts and weaknesses of data-driven docking in critical assessment of prediction of interactions." Proteins **78**(15): 3242-3249.

Delaglio, F., S. Grzesiek, G. W. Vuister, G. Zhu, J. Pfeifer and A. Bax (1995). "NMRPipe: a multidimensional spectral processing system based on UNIX pipes." J Biomol NMR **6**(3): 277-293.

di Maio, D., B. Chandramouli, R. Yan, G. Brancato and A. Pastore (2017). "Understanding the role of dynamics in the iron sulfur cluster molecular machine." Biochim Biophys Acta **1861**(1 Pt A): 3154-3163.

Ding, H. and R. J. Clark (2004). "Characterization of iron binding in IscA, an ancient iron-sulphur cluster assembly protein." Biochem J **379**(Pt 2): 433-440.

Ding, H., R. J. Clark and B. Ding (2004). "IscA mediates iron delivery for assembly of iron-sulfur clusters in IscU under the limited accessible free iron conditions." J Biol Chem **279**(36): 37499-37504.

Dominguez, C., R. Boelens and A. M. Bonvin (2003). "HADDOCK: a protein-protein docking approach based on biochemical or biophysical information." J Am Chem Soc **125**(7): 1731-1737.

Dominy, C. N. and D. W. Andrews (2003). "Site-directed mutagenesis by inverse PCR." Methods Mol Biol **235**: 209-223.

Faggianelli, N., R. Puglisi, L. Veneziano, S. Romano, M. Frontali, T. Vannocci, S. Fortuni, R. Testi and A. Pastore (2015). "Analyzing the Effects of a G137V Mutation in the FXN Gene." Front Mol Neurosci **8**: 66.

Finka, A., R. U. Mattoo and P. Goloubinoff (2016). "Experimental Milestones in the Discovery of Molecular Chaperones as Polypeptide Unfolding Enzymes." Annu Rev Biochem **85**: 715-742.

Fleischhacker, A. S., A. Stubna, K. L. Hsueh, Y. Guo, S. J. Teter, J. C. Rose, T. C. Brunold, J. L. Markley, E. Munck and P. J. Kiley (2012). "Characterization of the [2Fe-2S] cluster of Escherichia coli transcription factor IscR." Biochemistry **51**(22): 4453-4462.

Foury, F., A. Pastore and M. Trincal (2007). "Acidic residues of yeast frataxin have an essential role in Fe-S cluster assembly." EMBO Rep **8**(2): 194-199.

Frazzon, J. and D. R. Dean (2003). "Formation of iron-sulfur clusters in bacteria: an emerging field in bioinorganic chemistry." Curr Opin Chem Biol **7**(2): 166-173.

Fujii, T., M. Maeda, H. Mihara, T. Kurihara, N. Esaki and Y. Hata (2000). "Structure of a NifS homologue: X-ray structure analysis of CsdB, an Escherichia coli counterpart of mammalian selenocysteine lyase." Biochemistry **39**(6): 1263-1273.

Fuzery, A. K., J. J. Oh, D. T. Ta, L. E. Vickery and J. L. Markley (2011). "Three hydrophobic amino acids in Escherichia coli HscB make the greatest contribution to the stability of the HscB-IscU complex." BMC Biochem **12**: 3.

Fuzery, A. K., M. Tonelli, D. T. Ta, G. Cornilescu, L. E. Vickery and J. L. Markley (2008). "Solution structure of the iron-sulfur cluster cochaperone HscB and its binding surface for the iron-sulfur assembly scaffold protein IscU." Biochemistry **47**(36): 9394-9404.

Gakh, O., J. Adamec, A. M. Gacy, R. D. Twesten, W. G. Owen and G. Isaya (2002). "Physical evidence that yeast frataxin is an iron storage protein." Biochemistry **41**(21): 6798-6804.

Garcia-Serres, R., Clémancey, M., Oddou, JL., Pastore, A., Lesuisse, E., Latour, JM (2012). "Mössbauer studies of frataxin role in iron-sulfur cluster assembly and dysfunction-related disease." Hyperfine Interact **206**: 13-18.

Gerber, J., U. Muhlenhoff and R. Lill (2003). "An interaction between frataxin and Isu1/Nfs1 that is crucial for Fe/S cluster synthesis on Isu1." EMBO Rep **4**(9): 906-911.

Gibson, T. J., E. V. Koonin, G. Musco, A. Pastore and P. Bork (1996). "Friedreich's ataxia protein: phylogenetic evidence for mitochondrial dysfunction." Trends Neurosci **19**(11): 465-468.

Giel, J. L., A. D. Nesbit, E. L. Mettert, A. S. Fleischhacker, B. T. Wanta and P. J. Kiley (2013). "Regulation of iron-sulphur cluster homeostasis through transcriptional control of the Isc pathway by [2Fe-2S]-IscR in Escherichia coli." Mol Microbiol **87**(3): 478-492.

Glaser, T., B. Hedman, K. O. Hodgson and E. I. Solomon (2000). "Ligand K-edge X-ray absorption spectroscopy: a direct probe of ligand-metal covalency." Acc Chem Res **33**(12): 859-868.

Hentze, M. W., M. U. Muckenthaler and N. C. Andrews (2004). "Balancing acts: molecular control of mammalian iron metabolism." Cell **117**(3): 285-297.

Hoff, K. G., J. R. Cupp-Vickery and L. E. Vickery (2003). "Contributions of the LPPVK motif of the iron-sulfur template protein IscU to interactions with the Hsc66-Hsc20 chaperone system." J Biol Chem **278**(39): 37582-37589.

Hoff, K. G., J. J. Silberg and L. E. Vickery (2000). "Interaction of the iron-sulfur cluster assembly protein IscU with the Hsc66/Hsc20 molecular chaperone system of Escherichia coli." Proc Natl Acad Sci U S A **97**(14): 7790-7795.

Hoff, K. G., D. T. Ta, T. L. Tapley, J. J. Silberg and L. E. Vickery (2002). "Hsc66 substrate specificity is directed toward a discrete region of the iron-sulfur cluster template protein IscU." J Biol Chem **277**(30): 27353-27359.

Hwang, D. M., A. Dempsey, K. T. Tan and C. C. Liew (1996). "A modular domain of NifU, a nitrogen fixation cluster protein, is highly conserved in evolution." J Mol Evol **43**(5): 536-540.

Iametti, S., A. Barbiroli and F. Bonomi (2015). "Functional implications of the interaction between HscB and IscU in the biosynthesis of FeS clusters." J Biol Inorg Chem **20**(6): 1039-1048.

Iannuzzi, C., S. Adinolfi, B. D. Howes, R. Garcia-Serres, M. Clemancey, J. M. Latour, G. Smulevich and A. Pastore (2011). "The role of CyaY in iron sulfur cluster assembly on the E. coli IscU scaffold protein." PLoS One **6**(7): e21992.

Iannuzzi, C., M. Adrover, R. Puglisi, R. Yan, P. A. Temussi and A. Pastore (2014). "The role of zinc in the stability of the marginally stable IscU scaffold protein." Protein Sci **23**(9): 1208-1219.

Imlay, J. A. (2006). "Iron-sulphur clusters and the problem with oxygen." Mol Microbiol **59**(4): 1073-1082.

Jacobson, M. R., V. L. Cash, M. C. Weiss, N. F. Laird, W. E. Newton and D. R. Dean (1989). "Biochemical and genetic analysis of the nifUSVWZM cluster from Azotobacter vinelandii." Mol Gen Genet **219**(1-2): 49-57.

Jang, S. and J. A. Imlay (2010). "Hydrogen peroxide inactivates the Escherichia coli Isc iron-sulphur assembly system, and OxyR induces the Suf system to compensate." Mol Microbiol **78**(6): 1448-1467.

Jensen, L. T. and V. C. Culotta (2000). "Role of Saccharomyces cerevisiae ISA1 and ISA2 in iron homeostasis." Mol Cell Biol **20**(11): 3918-3927.

Jerabek-Willemsen, M., T. Andre, R. Wanner, H. M. Roth, S. Duhr, P. Baaske and D. Breitsprecher (2014). "MicroScale Thermophoresis: Interaction analysis and beyond." Journal of Molecular Structure **1077**: 101-113.

Jerabek-Willemsen, M., C. J. Wienken, D. Braun, P. Baaske and S. Duhr (2011). "Molecular interaction studies using microscale thermophoresis." Assay Drug Dev Technol **9**(4): 342-353.

Jervis, A. J., J. C. Crack, G. White, P. J. Artymiuk, M. R. Cheesman, A. J. Thomson, N. E. Le Brun and J. Green (2009). "The O2 sensitivity of the transcription factor FNR is controlled by Ser24 modulating the kinetics of [4Fe-4S] to [2Fe-2S] conversion." Proc Natl Acad Sci U S A **106**(12): 4659-4664.

Johnson, D. C., D. R. Dean, A. D. Smith and M. K. Johnson (2005). "Structure, function, and formation of biological iron-sulfur clusters." Annu Rev Biochem **74**: 247-281.

Johnson, M. K. (1998). "Iron-sulfur proteins: new roles for old clusters." Curr Opin Chem Biol **2**(2): 173-181.

Kambampati, R. and C. T. Lauhon (2000). "Evidence for the transfer of sulfane sulfur from IscS to ThiI during the in vitro biosynthesis of 4-thiouridine in Escherichia coli tRNA." J Biol Chem **275**(15): 10727-10730.

Kato, S., H. Mihara, T. Kurihara, Y. Takahashi, U. Tokumoto, T. Yoshimura and N. Esaki (2002). "Cys-328 of IscS and Cys-63 of IscU are the sites of disulfide bridge formation in a covalently bound IscS/IscU complex: implications for the mechanism of iron-sulfur cluster assembly." Proc Natl Acad Sci U S A **99**(9): 5948-5952.

Kim, J. H., J. R. Bothe, T. R. Alderson and J. L. Markley (2015). "Tangled web of interactions among proteins involved in iron-sulfur cluster assembly as unraveled by NMR, SAXS, chemical crosslinking, and functional studies." Biochim Biophys Acta **1853**(6): 1416-1428.

Kim, J. H., J. R. Bothe, R. O. Frederick, J. C. Holder and J. L. Markley (2014). "Role of IscX in iron-sulfur cluster biogenesis in Escherichia coli." J Am Chem Soc **136**(22): 7933-7942.

Kim, J. H., R. O. Frederick, N. M. Reinen, A. T. Troupis and J. L. Markley (2013). "[2Fe-2S]-ferredoxin binds directly to cysteine desulfurase and supplies an electron for iron-sulfur cluster assembly but is displaced by the scaffold protein or bacterial frataxin." J Am Chem Soc **135**(22): 8117-8120.

Kim, J. H., A. K. Fuzery, M. Tonelli, D. T. Ta, W. M. Westler, L. E. Vickery and J. L. Markley (2009). "Structure and dynamics of the iron-sulfur cluster assembly scaffold protein IscU and its interaction with the cochaperone HscB." Biochemistry **48**(26): 6062-6071.

Kim, J. H., M. Tonelli, R. O. Frederick, D. C. Chow and J. L. Markley (2012). "Specialized Hsp70 chaperone (HscA) binds preferentially to the disordered form, whereas J-protein (HscB) binds preferentially to the structured form of the iron-sulfur cluster scaffold protein (IscU)." J Biol Chem **287**(37): 31406-31413.

Kornhaber, G. J., D. Snyder, H. N. Moseley and G. T. Montelione (2006). "Identification of zinc-ligated cysteine residues based on 13Calpha and 13Cbeta chemical shift data." J Biomol NMR **34**(4): 259-269.

Koutnikova, H., V. Campuzano, F. Foury, P. Dolle, O. Cazzalini and M. Koenig (1997). "Studies of human, mouse and yeast homologues indicate a mitochondrial function for frataxin." Nat Genet **16**(4): 345-351.

Krebs, C., J. N. Agar, A. D. Smith, J. Frazzon, D. R. Dean, B. H. Huynh and M. K. Johnson (2001). "IscA, an alternate scaffold for Fe-S cluster biosynthesis." Biochemistry **40**(46): 14069-14080.

Lauhon, C. T. and R. Kambampati (2000). "The iscS gene in Escherichia coli is required for the biosynthesis of 4-thiouridine, thiamin, and NAD." J Biol Chem **275**(26): 20096-20103.

Layer, G., S. Ollagnier-de Choudens, Y. Sanakis and M. Fontecave (2006). "Iron-sulfur cluster biosynthesis: characterization of Escherichia coli CYaY as an iron donor for the assembly of [2Fe-2S] clusters in the scaffold IscU." J Biol Chem **281**(24): 16256-16263.

Lill, R. and G. Kispal (2000). "Maturation of cellular Fe-S proteins: an essential function of mitochondria." Trends Biochem Sci **25**(8): 352-356.

Liu, J., N. Oganesyan, D. H. Shin, J. Jancarik, H. Yokota, R. Kim and S. H. Kim (2005). "Structural characterization of an iron-sulfur cluster assembly protein IscU in a zinc-bound form." Proteins **59**(4): 875-881.

Mansour, A. N., C. Thompson, E. C. Theil, N. D. Chasteen and D. E. Sayers (1985). "Fe(III).ATP complexes. Models for ferritin and other polynuclear iron complexes with phosphate." J Biol Chem **260**(13): 7975-7979.

Markley, J. L., J. H. Kim, Z. Dai, J. R. Bothe, K. Cai, R. O. Frederick and M. Tonelli (2013). "Metamorphic protein IscU alternates conformations in the course of its role as the scaffold protein for iron-sulfur cluster biosynthesis and delivery." FEBS Lett **587**(8): 1172-1179.

Melquiond, A. S. J., Bonvin, A. J. J. (2010). Data-driven Docking: Using External Information to Spark the Biomolecular Rendez-vous, Imperial College Press.

Mihara, H. and N. Esaki (2002). "Bacterial cysteine desulfurases: their function and mechanisms." Appl Microbiol Biotechnol **60**(1-2): 12-23.

Musco, G., G. Stier, B. Kolmerer, S. Adinolfi, S. Martin, T. Frenkiel, T. Gibson and A. Pastore (2000). "Towards a structural understanding of Friedreich's ataxia: the solution structure of frataxin." Structure **8**(7): 695-707.

Nair, M., S. Adinolfi, G. Kelly, T. A. Frenkiel and A. Pastore (2003). "NMR assignment of the 1H, 15N and 13C resonances of the E. coli frataxin orthologue, CyaY." J Biomol NMR **27**(4): 403-404.

Nair, M., S. Adinolfi, C. Pastore, G. Kelly, P. Temussi and A. Pastore (2004). "Solution structure of the bacterial frataxin ortholog, CyaY: mapping the iron binding sites." Structure **12**(11): 2037-2048.

Ollagnier-de-Choudens, S., T. Mattioli, Y. Takahashi and M. Fontecave (2001). "Iron-sulfur cluster assembly: characterization of IscA and evidence for a specific and functional complex with ferredoxin." J Biol Chem **276**(25): 22604-22607.

Outten, F. W., O. Djaman and G. Storz (2004). "A suf operon requirement for Fe-S cluster assembly during iron starvation in Escherichia coli." Mol Microbiol **52**(3): 861-872.

Pandolfo, M. and A. Pastore (2009). "The pathogenesis of Friedreich ataxia and the structure and function of frataxin." J Neurol **256 Suppl 1**: 9-17.

Pastore, C., S. Adinolfi, M. A. Huynen, V. Rybin, S. Martin, M. Mayer, B. Bukau and A. Pastore (2006). "YfhJ, a molecular adaptor in iron-sulfur cluster formation or a frataxin-like protein?" Structure **14**(5): 857-867.

Pastore, C., M. Franzese, F. Sica, P. Temussi and A. Pastore (2007). "Understanding the binding properties of an unusual metal-binding protein--a study of bacterial frataxin." FEBS J **274**(16): 4199-4210.

Patchornik, G., R. Goldshleger and S. J. Karlish (2000). "The complex ATP-Fe(2+) serves as a specific affinity cleavage reagent in ATP-Mg(2+) sites of Na,K-ATPase: altered ligation of Fe(2+) (Mg(2+)) ions accompanies the E(1)-->E(2) conformational change." Proc Natl Acad Sci U S A **97**(22): 11954-11959.

Piotto, M., V. Saudek and V. Sklenar (1992). "Gradient-tailored excitation for single-quantum NMR spectroscopy of aqueous solutions." J Biomol NMR **2**(6): 661-665.

Prischi, F., P. V. Konarev, C. Iannuzzi, C. Pastore, S. Adinolfi, S. R. Martin, D. I. Svergun and A. Pastore (2010). "Structural bases for the interaction of frataxin with the central components of iron-sulphur cluster assembly." Nat Commun **1**: 95.

Prischi, F. and A. Pastore (2016). "Application of Nuclear Magnetic Resonance and Hybrid Methods to Structure Determination of Complex Systems." Adv Exp Med Biol **896**: 351-368.

Prischi, F., C. Pastore, M. Carroni, C. Iannuzzi, S. Adinolfi, P. Temussi and A. Pastore (2010). "Of the vulnerability of orphan complex proteins: the case study of the E. coli IscU and IscS proteins." Protein Expr Purif **73**(2): 161-166.

Puccio, H. and M. Koenig (2000). "Recent advances in the molecular pathogenesis of Friedreich ataxia." Hum Mol Genet **9**(6): 887-892.

Puglisi, R., R. Yan, S. Adinolfi and A. Pastore (2016). "A New Tessera into the Interactome of the isc Operon: A Novel Interaction between HscB and IscS." Front Mol Biosci **3**: 48.

Purcell, E. M. (1948). "Nuclear Magnetism in Relation to Problems of the Liquid and Solid States." Science **107**(2783): 433-440.

Py, B., P. L. Moreau and F. Barras (2011). "Fe-S clusters, fragile sentinels of the cell." Curr Opin Microbiol **14**(2): 218-223.

Ramelot, T. A., J. R. Cort, S. Goldsmith-Fischman, G. J. Kornhaber, R. Xiao, R. Shastry, T. B. Acton, B. Honig, G. T. Montelione and M. A. Kennedy (2004).

"Solution NMR structure of the iron-sulfur cluster assembly protein U (IscU) with zinc bound at the active site." J Mol Biol **344**(2): 567-583.

Rodger, A., Nordén, B. (1997). Circular Dichroism and Linear Dichroism.

Rouault, T. A. (2006). "The role of iron regulatory proteins in mammalian iron homeostasis and disease." Nat Chem Biol **2**(8): 406-414.

Sanfelice, D., R. Puglisi, S. R. Martin, L. Di Bari, A. Pastore and P. A. Temussi (2014). "Yeast frataxin is stabilized by low salt concentrations: cold denaturation disentangles ionic strength effects from specific interactions." PLoS One **9**(5): e95801.

Schmucker, S. and H. Puccio (2010). "Understanding the molecular mechanisms of Friedreich's ataxia to develop therapeutic approaches." Hum Mol Genet **19**(R1): R103-110.

Schwartz, C. J., J. L. Giel, T. Patschkowski, C. Luther, F. J. Ruzicka, H. Beinert and P. J. Kiley (2001). "IscR, an Fe-S cluster-containing transcription factor, represses expression of Escherichia coli genes encoding Fe-S cluster assembly proteins." Proc Natl Acad Sci U S A **98**(26): 14895-14900.

Seidel, S. A., P. M. Dijkman, W. A. Lea, G. van den Bogaart, M. Jerabek-Willemsen, A. Lazic, J. S. Joseph, P. Srinivasan, P. Baaske, A. Simeonov, I. Katritch, F. A. Melo, J. E. Ladbury, G. Schreiber, A. Watts, D. Braun and S. Duhr (2013). "Microscale thermophoresis quantifies biomolecular interactions under previously challenging conditions." Methods **59**(3): 301-315.

Shi, R., A. Proteau, M. Villarroya, I. Moukadiri, L. Zhang, J. F. Trempe, A. Matte, M. E. Armengod and M. Cygler (2010). "Structural basis for Fe-S cluster assembly and tRNA thiolation mediated by IscS protein-protein interactions." PLoS Biol **8**(4): e1000354.

Shimomura, Y., H. Kamikubo, Y. Nishi, T. Masako, M. Kataoka, Y. Kobayashi, K. Fukuyama and Y. Takahashi (2007). "Characterization and crystallization of an

IscU-type scaffold protein with bound [2Fe-2S] cluster from the hyperthermophile, aquifex aeolicus." J Biochem **142**(5): 577-586.

Shimomura, Y., Y. Takahashi, Y. Kakuta and K. Fukuyama (2005). "Crystal structure of Escherichia coli YfhJ protein, a member of the ISC machinery involved in assembly of iron-sulfur clusters." Proteins **60**(3): 566-569.

Silberg, J. J., K. G. Hoff, T. L. Tapley and L. E. Vickery (2001). "The Fe/S assembly protein IscU behaves as a substrate for the molecular chaperone Hsc66 from Escherichia coli." J Biol Chem **276**(3): 1696-1700.

Silberg, J. J., T. L. Tapley, K. G. Hoff and L. E. Vickery (2004). "Regulation of the HscA ATPase reaction cycle by the co-chaperone HscB and the iron-sulfur cluster assembly protein IscU." J Biol Chem **279**(52): 53924-53931.

Silberg, J. J. and L. E. Vickery (2000). "Kinetic characterization of the ATPase cycle of the molecular chaperone Hsc66 from Escherichia coli." J Biol Chem **275**(11): 7779-7786.

Stehling, O. and R. Lill (2013). "The role of mitochondria in cellular iron-sulfur protein biogenesis: mechanisms, connected processes, and diseases." Cold Spring Harb Perspect Biol **5**(8): a011312.

Takahashi, H., T. Nakanishi, K. Kami, Y. Arata and I. Shimada (2000). "A novel NMR method for determining the interfaces of large protein-protein complexes." Nat Struct Biol **7**(3): 220-223.

Tokumoto, U., S. Kitamura, K. Fukuyama and Y. Takahashi (2004). "Interchangeability and distinct properties of bacterial Fe-S cluster assembly systems: functional replacement of the isc and suf operons in Escherichia coli with the nifSU-like operon from Helicobacter pylori." J Biochem **136**(2): 199-209.

Tokumoto, U., S. Nomura, Y. Minami, H. Mihara, S. Kato, T. Kurihara, N. Esaki, H. Kanazawa, H. Matsubara and Y. Takahashi (2002). "Network of protein-protein interactions among iron-sulfur cluster assembly proteins in Escherichia coli." J Biochem **131**(5): 713-719.

Tokumoto, U. and Y. Takahashi (2001). "Genetic analysis of the isc operon in Escherichia coli involved in the biogenesis of cellular iron-sulfur proteins." J Biochem **130**(1): 63-71.

Tozzi, G., M. Nuccetelli, M. Lo Bello, S. Bernardini, L. Bellincampi, S. Ballerini, L. M. Gaeta, C. Casali, A. Pastore, G. Federici, E. Bertini and F. Piemonte (2002). "Antioxidant enzymes in blood of patients with Friedreich's ataxia." Arch Dis Child **86**(5): 376-379.

Tsai, C. L. and D. P. Barondeau (2010). "Human frataxin is an allosteric switch that activates the Fe-S cluster biosynthetic complex." Biochemistry **49**(43): 9132-9139.

Urbina, H. D., J. J. Silberg, K. G. Hoff and L. E. Vickery (2001). "Transfer of sulfur from IscS to IscU during Fe-S cluster assembly." J Biol Chem **276**(48): 44521-44526.

Vickery, L. E., J. J. Silberg and D. T. Ta (1997). "Hsc66 and Hsc20, a new heat shock cognate molecular chaperone system from Escherichia coli." Protein Sci **6**(5): 1047-1056.

Vranken, W. F., W. Boucher, T. J. Stevens, R. H. Fogh, A. Pajon, M. Llinas, E. L. Ulrich, J. L. Markley, J. Ionides and E. D. Laue (2005). "The CCPN data model for NMR spectroscopy: development of a software pipeline." Proteins **59**(4): 687-696.

Walsh, P., D. Bursac, Y. C. Law, D. Cyr and T. Lithgow (2004). "The J-protein family: modulating protein assembly, disassembly and translocation." EMBO Rep **5**(6): 567-571.

Watson, A. A., P. Mahajan, H. D. Mertens, M. J. Deery, W. Zhang, P. Pham, X. Du, T. Bartke, W. Zhang, C. Edlich, G. Berridge, Y. Chen, N. A. Burgess-Brown, T. Kouzarides, N. Wiechens, T. Owen-Hughes, D. I. Svergun, O. Gileadi and E. D. Laue (2012). "The PHD and chromo domains regulate the ATPase activity of the human chromatin remodeler CHD4." J Mol Biol **422**(1): 3-17.

Webb, M. R. (1992). "A continuous spectrophotometric assay for inorganic phosphate and for measuring phosphate release kinetics in biological systems." Proc Natl Acad Sci U S A **89**(11): 4884-4887.

Wu, S. P., S. S. Mansy and J. A. Cowan (2005). "Iron-sulfur cluster biosynthesis. Molecular chaperone DnaK promotes IscU-bound [2Fe-2S] cluster stability and inhibits cluster transfer activity." Biochemistry **44**(11): 4284-4293.

Yan, R., S. Adinolfi, C. Iannuzzi, G. Kelly, A. Oregioni, S. Martin and A. Pastore (2013). "Cluster and fold stability of E. coli ISC-type ferredoxin." PLoS One **8**(11): e78948.

Yan, R., S. Adinolfi and A. Pastore (2015). "Ferredoxin, in conjunction with NADPH and ferredoxin-NADP reductase, transfers electrons to the IscS/IscU complex to promote iron-sulfur cluster assembly." Biochim Biophys Acta **1854**(9): 1113-1117.

Yan, R., P. V. Konarev, C. Iannuzzi, S. Adinolfi, B. Roche, G. Kelly, L. Simon, S. R. Martin, B. Py, F. Barras, D. I. Svergun and A. Pastore (2013). "Ferredoxin competes with bacterial frataxin in binding to the desulfurase IscS." J Biol Chem **288**(34): 24777-24787.

Yoon, T. and J. A. Cowan (2003). "Iron-sulfur cluster biosynthesis. Characterization of frataxin as an iron donor for assembly of [2Fe-2S] clusters in ISU-type proteins." J Am Chem Soc **125**(20): 6078-6084.

Yoon, T. and J. A. Cowan (2004). "Frataxin-mediated iron delivery to ferrochelatase in the final step of heme biosynthesis." J Biol Chem **279**(25): 25943-25946.

Zhang, B., J. C. Crack, S. Subramanian, J. Green, A. J. Thomson, N. E. Le Brun and M. K. Johnson (2012). "Reversible cycling between cysteine persulfide-ligated [2Fe-2S] and cysteine-ligated [4Fe-4S] clusters in the FNR regulatory protein." Proc Natl Acad Sci U S A **109**(39): 15734-15739.

Zheng, L., V. L. Cash, D. H. Flint and D. R. Dean (1998). "Assembly of iron-sulfur clusters. Identification of an iscSUA-hscBA-fdx gene cluster from Azotobacter vinelandii." J Biol Chem **273**(21): 13264-13272.

Zheng, L., R. H. White, V. L. Cash and D. R. Dean (1994). "Mechanism for the desulfurization of L-cysteine catalyzed by the nifS gene product." Biochemistry **33**(15): 4714-4720.